

# On the role of circulation and mixing in the ventilation of oxygen minimum zones with a focus on the eastern tropical North Atlantic

P. Brandt<sup>1</sup>, H. W. Bange<sup>1</sup>, D. Banyte<sup>1</sup>, M. Dengler<sup>1</sup>, S.-H. Didwischus<sup>1</sup>, T. Fischer<sup>1</sup>, R. J. Greatbatch<sup>1</sup>, J. Hahn<sup>1</sup>, T. Kanzow<sup>1,\*</sup>, J. Karstensen<sup>1</sup>, A. Körtzinger<sup>1</sup>, G. Krahnemann<sup>1</sup>, S. Schmidtko<sup>1</sup>, L. Stramma<sup>1</sup>, T. Tanhua<sup>1</sup> and M. Visbeck<sup>1</sup>

[1] {GEOMAR Helmholtz-Zentrum für Ozeanforschung Kiel, Kiel, Germany}

[\*] {now at: Alfred-Wegener-Institut Helmholtz-Zentrum für Polar- und Meeresforschung, Bremerhaven, Germany}

Correspondence to: P. Brandt ([pbrandt@geomar.de](mailto:pbrandt@geomar.de))

Reply to reviewer #1

Reviewer #1: This article largely reviews recent results from the SFB 754 program designed to investigate the climate and biogeochemistry interactions in the oxygen minimum zones (OMZs) of the tropical oceans. It is very well written and gives a thorough and complete overview of the major results to date. Since it is primarily a review/progress article, it is difficult to find fault with any of the results since the article mainly reports and synthesizes the results rather than (re)interpret these results or present new results. So, consequently this review provides (hopefully) constructive comments rather than a scientific critique of the published record.

I very much liked the layout of the paper, and the discussion of the individual components of the oxygen budget and the main mechanisms that influence this budget in the eastern tropical Atlantic. An excellent approach. However I think in general there could have been more discussion of the error bars of the budget, particularly in the individual sections that discuss the processes. Most sections lacked any error bars on the estimates, other than to note that the mechanisms might be poorly constrained (a good reason to show or explicitly discuss the error bars and how they are comprised). Or perhaps error bars were presented in the accompanying figures (e.g. Figure 12, 13 showing the effect of diapycnal mixing) but there was little discussion of how these error bars were computed.

Answer to reviewer #1: We included more discussion on how the error bars were obtained particularly for diapycnal and lateral diffusive fluxes. The calculation of deep diapycnal mixing including error bars was repeated using more deep microstructure profiles that are now available. This leads to changes in Figures 11 to 13, and 21.

We included in section 4.1 “Error estimates are reported as 95% confidence limits and are based on standard errors of the mean of individual  $K_\rho$  and oxygen gradient profiles for each subregion. Subsequent error estimates for the mean total  $K_\rho$  profile (Fig. 12), flux profiles, and the mean supply profile (Fig. 13) were obtained from Gaussian error propagation (Ferrari and Polzin, 2005; Schafstall et al., 2010).”

Furthermore we included in section 4.2 the sentence “Hahn et al. (2014) estimated a meridional eddy diffusivity profile for the upper 1000 m with the range of uncertainty assumed as large as a factor 2 following Ferrari and Polzin (2005).” And “The corresponding error (i.e. of the eddy-driven meridional oxygen supply) was derived both from the error of the curvature of the meridional oxygen distribution (95% confidence) and the error of the eddy diffusivity (factor 2 assumed following Ferrari and Polzin (2005)).”

In section 6.3 we included: “Within this region, the diapycnal flux of oxygen from the mixed layer into the stratified ocean is  $73 \text{ mmol m}^{-2} \text{ d}^{-1}$ , with an upper and lower 95% confidence limit determined from Gaussian error propagation (Ferrari and Polzin, 2005; Schafstall et al., 2010) being  $105 \text{ mmol m}^{-2} \text{ d}^{-1}$  and  $44 \text{ mmol m}^{-2} \text{ d}^{-1}$ , respectively.”

Reviewer #1: In the section 4.3 Advection I kept wondering why there was no actual quantification of this component. It was not until the conclusions that it was reported that this component is so poorly resolved that it is actually represented as a (large!) residual in the budget. This information needs to be reported much earlier.

Answer to reviewer #1: Already in the last version of the manuscript, we stated right at the beginning of section 4.3 that “we are only able to quantify this term as a residual”.

We now include an explanation at the beginning of section 4.3 “A rigorous determination of the advection term would require mean sections around a closed box to fulfil mass balance within the box. This cannot be achieved with the present observing system. However, our measurements along  $23^\circ \text{ W}$  confirm that the

advection term is a major player in the ventilation of the OMZ, especially above 400 m depth.”

Reviewer #1: The reason this component cannot be resolved is because there are insufficient and/or inadequate measurements available to determine this component. This raises another issue. Given the disparate and large number of measurements collected as part of the SFB 754 program, it might also be worthwhile discussing what measurements might still be required and at what resolution. In other words, it is an ideal time to determine what legacy measurements might remain and what additional measurements (e.g. multiple glider transects crossing the deep tropical jets instrumented with O<sub>2</sub> sensors etc?) might be needed for monitoring the changes in the OMZ and the processes that lead to these changes.

Answer to reviewer #1: Thank you very much for this comment. Besides the difficulties of quantifying the mean advection, we now changed the wording and add sentences regarding the requirements for future observing systems.

In the summary and discussion we included: “Dedicated process studies using mooring arrays, shipboard and multiple glider observations may help to elucidate the role of different processes in the eastern boundary oxygen budget.” and we clarified: “Oxygen data from shipboard repeat hydrography and moored observations show substantial interannual variability (Fig. 8) and trend-like changes (Fig. 19). The continuation of such measurements is essential to be able to test different hypotheses for the driving mechanisms of oxygen changes in the ocean.”

Reviewer #1: Finally, given the length of the paper, I think that it’s probably best to only focus on the OMZ in the eastern tropical Atlantic Ocean and carve out the comparison with the Pacific for another paper later. It really is a very meaty paper already and there is a lot to digest!

Answer to reviewer #1 (same as answer to reviewer #2): Although removing the ETSP part would shorten the text and keep the focus on the ETNA, we like to keep the comparison of the ETNA OMZ with the ETSP OMZ in the text. The motivation here is similar as for the SFB 754 to compare a hypoxic system, i.e. the ETNA OMZ, with a suboxic system, i.e. the ETSP OMZ. Particularly the observed deoxygenation trend in the hypoxic ETNA OMZ might lead to a shift of the ETNA OMZ to suboxic conditions and hence the comparison of the two systems will lead to a better understanding of differences and similarities of both systems finally to investigate

possible consequences of such a possible regime shift in the future. This was not made clear in the earlier text and will be clarified in the revised manuscript.

We included in the introduction: “The Atlantic and Pacific OMZs have many similarities particularly regarding OMZ shape and circulation pattern. The ETNA and the eastern tropical South Pacific (ETSP) OMZs (Figs. 1, 2) are both located in the shadow zones of the ventilated thermocline and are ventilated by lateral and vertical mixing as well as by zonal advection in the equatorial band. However, the striking difference between both OMZs is that the ETNA OMZ is hypoxic (oxygen below ~60 to 120  $\mu\text{mol kg}^{-1}$ ) and the ETSP is suboxic (oxygen below about 10  $\mu\text{mol kg}^{-1}$ ). Karstensen et al. (2008) concluded that this difference is the result of reduced oxygen levels in the eastward current bands of the Pacific OMZs compared to the Atlantic OMZs, which they argue can be traced back to the larger ratio of the total volume of OMZ layer to the renewal or subduction rate in the Pacific compared to the Atlantic.” and

“The ETSP OMZ has been studied as well using a reduced observational program. However, the comparison between the hypoxic ETNA and the suboxic ETSP is of particular interest here, as the observed deoxygenation in the ETNA, or future climate change, might lead to a shift from hypoxic to suboxic conditions.”

At beginning of section 8 we included: “A continuation of the observed deoxygenation in the ETNA would turn the ETNA OMZ suboxic within a century, hence it is worth to look at differences and similarities of the ETNA and the ETSP with regard to a possible shift of a hypoxic system to a suboxic system.”

In the summary and discussion we included: “The relative importance of the different terms affecting the oxygen budgets of the ETNA und ETSP OMZs appear to be similar. For both OMZs the eastward advection of oxygen-rich waters from the well-ventilated western boundary was found to be a dominant ventilation process. As the zonal currents are of similar strength in the tropical Pacific and Atlantic, the difference in the basin width of both oceans consequently results in lower oxygen concentrations and larger water mass ages in the eastern tropical Pacific (Fig. 20) compared to the eastern tropical Atlantic (Fig. 6).”

Minor Comments by reviewer #1:

1. Page 12075: Is there any seasonal variation of the shallow OMZ?

We expect that there is a seasonal variation of the shallow OMZ. Unfortunately we don't have a good seasonal coverage of oxygen data in the eastern boundary upwelling region of Mauretania and Senegal and cannot give a clear statement.

2. Page 12077, line 6: I could not wrap my head around this first sentence of this paragraph. Is there a simpler way to write this?

We split the sentence into two: “The 23° W section (Fig. 6) cuts through the ETNA OMZ, which can be identified by low oxygen levels as well as by the high age of the water masses. The gradual change of salinity on density surfaces along this section defines the transition between low- and high-saline water masses of southern and northern origin, respectively.”

3. Page 12081: How good is the assumption that meridional advection is negligible? What about the possible significance of cross-equatorial exchanges via thermocline convergence, upwelling and Ekman divergence?

The thermocline convergence, upwelling and Ekman divergence describes the flow within the subtropical cell (STC). The water masses subducted in the eastern subtropics have to follow equatorward and westward pathways without a mean meridional flow into the OMZs, which is described by the ventilated thermocline theory (Luyten et al., 1983b) and observed geostrophic water mass pathways (Zhang et al., 2003). This is described in Sect. 3. So far there is no evidence of a significant mean meridional flow in the core of the open ocean OMZ.

4. Figure 3 caption needs more information about how these oxygen concentration estimates were determined.

We changed caption of Fig. 3: “Minimum oxygen concentration below 200 m (representing the deep oxygen minimum) as obtained from CTD station data taken during the period 2006 to 2013. Oxygen concentration at the deep oxygen minimum below 40  $\mu\text{mol kg}^{-1}$  is marked by purple dots.”

5. Figure 17. What causes the big spike at sigma-theta 26.1 in the AOUR values determined for the North Atlantic basin mean (black dots?)

The apparent “spike” that is seen for the density range 26.1 to 26.2 originates from the comparably young reservoir age of this density range (related to enhanced subduction rates). We added a statement to the text (also with a reference to the Figure 9 in

Karstensen et al. 2008 which nicely shows the enhanced subduction within the given density range).

# On the role of circulation and mixing in the ventilation of oxygen minimum zones with a focus on the eastern tropical North Atlantic

P. Brandt<sup>1</sup>, H. W. Bange<sup>1</sup>, D. Banyte<sup>1</sup>, M. Dengler<sup>1</sup>, S.-H. Didwischus<sup>1</sup>, T. Fischer<sup>1</sup>, R. J. Greatbatch<sup>1</sup>, J. Hahn<sup>1</sup>, T. Kanzow<sup>1,\*</sup>, J. Karstensen<sup>1</sup>, A. Körtzinger<sup>1</sup>, G. Krahnemann<sup>1</sup>, S. Schmidtke<sup>1</sup>, L. Stramma<sup>1</sup>, T. Tanhua<sup>1</sup> and M. Visbeck<sup>1</sup>

[1] {GEOMAR Helmholtz-Zentrum für Ozeanforschung Kiel, Kiel, Germany}

[\*] {now at: Alfred-Wegener-Institut Helmholtz-Zentrum für Polar- und Meeresforschung, Bremerhaven, Germany}

Correspondence to: P. Brandt ([pbrandt@geomar.de](mailto:pbrandt@geomar.de))

Reply to reviewer #2

Reviewer #2: This overview is an important contribution to the regional and global communities working on the ETNA and especially towards improving the way models reflect the climate sensitivities of the ETNA OMZ. It reflects a very significant and well coordinated effort by the community represented by the authors. The manuscript succeeds in assembling a description and steady state quantification of the oxygen ventilation and consumption processes but it does so in a manner which is dense and hard to read and make the connections. While there is an attempt to "integrate" the processes in Fig 21 the text has the sense of a number of almost standalone parts of study.

One easy gain to simplify the text would be to remove the section on the ETSP which interrupts the coherence of the ETNA focus. It is also not clear how and where this study adds to what was already known. In this respect a focus in the introduction not just on the gaps in the ETNA that this study set out to investigate but also a brief comparison of the Atlantic and Pacific OMZs to put some context to the relatively well ventilated ETNA.

Answer to reviewer #2 (same as answer to reviewer #1): Although removing the ETSP part would shorten the text and keep the focus on the ETNA, we like to keep the comparison of the ETNA OMZ with the ETSP OMZ in the text. The motivation here is similar as for the SFB 754 to compare a hypoxic system, i.e. the ETNA OMZ, with

a suboxic system, i.e. the ETSP OMZ. Particularly the observed deoxygenation trend in the hypoxic ETNA OMZ might lead to a shift of the ETNA OMZ to suboxic conditions and hence the comparison of the two systems will lead to a better understanding of differences and similarities of both systems finally to investigate possible consequences of such a possible regime shift in the future. This was not made clear in the earlier text and will be clarified in the revised manuscript.

We included in the introduction: “The Atlantic and Pacific OMZs have many similarities particularly regarding OMZ shape and circulation pattern. The ETNA and the eastern tropical South Pacific (ETSP) OMZs (Figs. 1, 2) are both located in the shadow zones of the ventilated thermocline and are ventilated by lateral and vertical mixing as well as by zonal advection in the equatorial band. However, the striking difference between both OMZs is that the ETNA OMZ is hypoxic (oxygen below ~60 to 120  $\mu\text{mol kg}^{-1}$ ) and the ETSP is suboxic (oxygen below about 10  $\mu\text{mol kg}^{-1}$ ). Karstensen et al. (2008) concluded that this difference is the result of reduced oxygen levels in the eastward current bands of the Pacific OMZs compared to the Atlantic OMZs, which they argue can be traced back to the larger ratio of the total volume of OMZ layer to the renewal or subduction rate in the Pacific compared to the Atlantic.”

and

“The ETSP OMZ has been studied as well using a reduced observational program. However, the comparison between the hypoxic ETNA and the suboxic ETSP is of particular interest here, as the observed deoxygenation in the ETNA, or future climate change, might lead to a shift from hypoxic to suboxic conditions.”

At beginning of section 8 we included: “A continuation of the observed deoxygenation in the ETNA would turn the ETNA OMZ suboxic within a century, hence it is worth to look at differences and similarities of the ETNA and the ETSP with regard to a possible shift of a hypoxic system to a suboxic system.”

In the summary and discussion we included: “The relative importance of the different terms affecting the oxygen budgets of the ETNA und ETSP OMZs appear to be similar. For both OMZs the eastward advection of oxygen-rich waters from the well-ventilated western boundary was found to be a dominant ventilation process. As the zonal currents are of similar strength in the tropical Pacific and Atlantic, the difference in the basin width of both oceans consequently results in lower oxygen concentrations



and larger water mass ages in the eastern tropical Pacific (Fig. 20) compared to the eastern tropical Atlantic (Fig. 6).”

Reviewer #2: Much modelling and observational work has been undertaken on the role of planetary wave systems and dynamics to explain O<sub>2</sub> variability and trends in the tropical OMZs but this is not really reflected in this study. Given that these dynamics appear to explain a significant part of the variability in the ETSP and the ETSA it seem that the study should explain why these are under-represented in the ETNA.

Answer to reviewer #2: We are not sure, what is exactly meant with the role of planetary wave systems and dynamics. However, we identified an under-representation of the role of remote forcing via equatorial Kelvin and coastal-trapped waves for the variability in the coastal upwelling regions in the previous version of our manuscript. Thus, we included in section 6.1 a paragraph regarding the role of intraseasonal coastal-trapped waves: “Besides the seasonal cycle, the flow variability off Mauretania and Senegal is influenced by intraseasonal coastal-trapped waves partly originating in the equatorial wave-guide (Polo et al., 2008). However, associated sea level anomalies are substantially weaker in the North Atlantic compared to the same latitude band in the South Atlantic. A strong influence of coastal-trapped waves on the oxygen distribution on the shelf of the ETNA as evidenced for the eastern boundary upwelling systems of the South Pacific and South Atlantic (Gutierrez et al., 2008;Monteiro et al., 2011) could so far not be shown.”

And in section 8.2 we included “Eddies are mainly generated by coastal flow instabilities that are influenced by remote equatorial forcing via coastal-trapped waves (Belmadani et al., 2012).”

Reviewer #2: The time series data in Figs 8 and 9 indicate that there are seasonal and intra-seasonal modes which warrant consideration in this context.

Answer to reviewer #2: The time series at 5°N show weak annual and semi-annual variability that might be associated with planetary wave propagation on these timescales. Similarly, intraseasonal variability at 5° N might result from Rossby wave propagation associated with the instability of the NECC. We included in section 4 explicitly planetary waves in the list of processes affecting time series shown in Figs. 8 and 9.

Reviewer #2: Given that one of the major scientific benefits of such a synthesis is a better understanding of the climate sensitivities of the ETNA, it would have been useful to see some

discussion on where models may look to improve the way they reflect the climate sensitivity of the OMZ.

Answer to reviewer #2: In the summary and discussion, we suggest directions for model improvements: “The increase in resolution of ocean circulation models improves the tropical circulation and associated oxygen distribution in the Atlantic (Duteil et al., 2014) and the Pacific OMZs (Montes et al., 2014), suggesting that model physics largely contribute to the oxygen bias in coarser-resolution models. However, particularly the intermediate circulation (below 250 m) is still underestimated by these high-resolution simulations in realistic settings.”

“Such a regional pattern is most likely due to changes in the circulation pattern associated with forced ocean dynamics as well as with internal ocean dynamics. [...] Improvements of model ventilation physics by increased resolution and/or improved parameterizations will reduce errors in the simulated mean oxygen distribution and its variability, but at the same time will help to better understand the climate sensitivity of OMZs with regard to anthropogenic climate change.”

Reviewer #2: The meridional negative anomaly of the oxygen trend (Fig. 18) between 10 - 30N and 100 - 500m would seem a good basis to examine where the imbalance may be emerging in the proposed budgets Fig. 13 and 14.

Answer to reviewer #2: We are so far not able to conclude from the budget calculation about the trend pattern (Fig. 18). However, we included in Sect. 7: “Changes in the strength and location of the wind-driven gyres are a possible explanation for the long-term oxygen trends observed between 15° and 30° N in Fig. 18.”

Reviewer #2: Finally, the summary is again too long and much of the discussion points are repeating the text. Overall, an effort to clarify the objectives and context of the study as well as removal of non critical parts will help further highlight the strengths of this otherwise comprehensive excellent study.

Answer to reviewer #2: We removed repeating parts of the discussion and also streamlined the text in many places in the main body of the manuscript, which hopefully helps to clarify its main points.

1 **On the role of circulation and mixing in the ventilation of**  
2 **oxygen minimum zones with a focus on the eastern**  
3 **tropical North Atlantic**

4  
5 P. Brandt<sup>1</sup>, [H. W. Bange<sup>1</sup>](#), D. Banyte<sup>1</sup>, M. Dengler<sup>1</sup>, S.-H. Didwischus<sup>1</sup>, T. Fischer<sup>1</sup>, R.  
6 J. Greatbatch<sup>1</sup>, J. Hahn<sup>1</sup>, T. Kanzow<sup>1,\*</sup>, J. Karstensen<sup>1</sup>, A. Körtzinger<sup>1</sup>, G.  
7 Krahmhann<sup>1</sup>, S. Schmidtko<sup>1</sup>, L. Stramma<sup>1</sup>, T. Tanhua<sup>1</sup> and M. Visbeck<sup>1</sup>

8 <sup>1</sup>GEOMAR Helmholtz-Zentrum für Ozeanforschung Kiel, Kiel, Germany

9 \*now at: Alfred-Wegener-Institut Helmholtz-Zentrum für Polar- und Meeresforschung,  
10 Bremerhaven, Germany

11 Correspondence to: P. Brandt ([pbrandt@geomar.de](mailto:pbrandt@geomar.de))

12  
13 **Abstract**

14 Ocean observations [are analysed](#) in the framework of the Collaborative Research Center 754  
15 (SFB 754) "Climate-Biogeochemistry Interactions in the Tropical Ocean" [to study 1](#)) the  
16 structure of tropical oxygen minimum zones (OMZs), 2) the processes that contribute to the  
17 oxygen budget, and 3) long-term changes in the oxygen distribution. The OMZ of the eastern  
18 tropical North Atlantic (ETNA), located between the well-ventilated subtropical gyre and the  
19 equatorial oxygen maximum, is composed of a deep OMZ at about 400 m depth with its core  
20 region centred at about 20° W, 10° N and a shallow OMZ at about 100 m depth with lowest  
21 oxygen concentrations in proximity to the coastal upwelling region off Mauritania and  
22 Senegal. The oxygen budget of the deep OMZ is given by oxygen consumption mainly  
23 balanced by the oxygen supply due to meridional eddy fluxes (about 60 %) and vertical  
24 mixing (about 20 %, locally up to 30 %). Advection by zonal jets is crucial for the  
25 establishment of the equatorial oxygen maximum. In the latitude range of the deep OMZ, it  
26 dominates the oxygen supply in the upper 300 to 400 m and generates the intermediate  
27 oxygen maximum between deep and shallow OMZs. Water mass ages from transient tracers  
28 indicate substantially older water masses in the core of the deep OMZ (about 120-180 years)  
29 compared to regions north and south of it. The deoxygenation of the ETNA OMZ during  
30 recent decades suggests a substantial imbalance in the oxygen budget: about 10 % of the

Peter Brandt 28.10.2014 18:59

Gelöscht: carried out

Peter Brandt 28.10.2014 18:59

Gelöscht: are used

33 oxygen consumption during that period was not balanced by ventilation. Long-term oxygen  
34 observations show variability on interannual, decadal and multidecadal time scales that can  
35 partly be attributed to circulation changes. In comparison to the ETNA OMZ the eastern  
36 tropical South Pacific OMZ shows a similar structure including an equatorial oxygen  
37 maximum driven by zonal advection, but overall much lower oxygen concentrations  
38 approaching zero in extended regions. As the shape of the OMZs is set by ocean circulation,  
39 the widespread misrepresentation of the intermediate circulation in ocean circulation models  
40 substantially contributes to their oxygen bias, which might have significant impacts on  
41 predictions of future oxygen levels.

42

## 43 1 Introduction

44 The oceanic oxygen distribution is generally characterized by slightly supersaturated oxygen  
45 levels in the surface layer, an intermediate oxygen minimum, and higher oxygen levels at  
46 depth. This vertical structure is a consequence of the delicate balance between the supply of  
47 oxygen through ventilation and circulation, [oxygen production by photosynthesis](#), and oxygen  
48 consumption by remineralization of sinking organic matter. The horizontal distribution of  
49 oxygen shows major large scale open ocean subsurface oxygen minimum zones (OMZs) in  
50 the eastern parts of the tropical Atlantic and Pacific Oceans as well as in the northern Indian  
51 Ocean. By analysing a combination of historical and modern observations, an expansion and  
52 intensification of OMZs in the tropical oceans has been detected (Stramma et al., 2008b).  
53 However, numerical simulations with global or regional models are not able to consistently  
54 reproduce such trends and thus up to now fail to provide an explanation of the observed  
55 oxygen trends in the tropical ocean (Stramma et al., 2012).

56 OMZs in the tropical Atlantic were first identified by analysing hydrographic data from the  
57 German Meteor Expedition during 1925 to 1927 (Wattenberg, 1938). This dataset revealed  
58 the existence of OMZs in both hemispheres of the eastern tropical Atlantic at a depth between  
59 300 and 700 m, situated equatorward of the subtropical gyres and separated by an equatorial  
60 oxygen maximum. Based on data, including those from the German Meteor Expedition, and  
61 theoretical considerations, Wyrтки (1962) concluded that the boundaries of these OMZs are set  
62 by advection with the lowest oxygen levels occurring in almost stagnant water bodies. A  
63 plausible theory of thermocline ventilation was delivered by Luyten et al. (1983b). The basis  
64 of their theory is of an ocean forced by subtropical Ekman pumping and otherwise obeying  
65 circulation pathways that are governed by potential vorticity conservation. This theory

Peter Brandt 27.10.2014 22:44

Gelöscht: s well as

67 explains the existence of non-ventilated, near-stagnant shadow zones in the eastern tropics.  
68 The remaining slow ventilation of such shadow zones, which under the assumption of steady  
69 state is required to balance oxygen consumption, is expected to be the consequence of lateral  
70 fluxes of oxygen from oxygen-rich water masses of the subtropics as well as due to diapycnal  
71 oxygen fluxes from oxygen-rich layers above and below the thermocline of the OMZs.

Peter Brandt 27.10.2014 22:46  
Gelöscht: in

72 The near-surface layers (upper ~250 m) of the tropical oceans are characterized by the  
73 presence of energetic zonal current bands. In the Atlantic below that layer, substantial mean  
74 zonal currents are also found particularly in the depth range of the OMZs (Fig. 1). Close to the  
75 equator, the strongest intermediate currents are observed with eastward flow at 2° N and 2° S  
76 and westward flow in between. The eastward current bands have been found to ventilate the  
77 central and eastern equatorial region with oxygen-rich waters from the western boundary  
78 (Tsuchiya et al., 1992;Schott et al., 1995;Schott et al., 1998). Together with time-varying  
79 equatorial jets they produce an equatorial oxygen maximum at intermediate depths (Brandt et  
80 al., 2012). Further poleward alternating zonal jets are present at intermediate depths including  
81 the latitude range of the OMZs. Their strengths have been quantified using subsurface drift  
82 trajectories from floats (Maximenko et al., 2005;Ollitrault et al., 2006) and repeated shipboard  
83 sections (Brandt et al., 2010). Such currents have been reproduced by idealized process  
84 modelling (Ménesguen et al., 2009;Ascani et al., 2010;Qiu et al., 2013) but are typically not  
85 found (or are unrealistically weak) in ocean circulation models. They contribute to the  
86 ventilation of the eastern tropical North Atlantic (ETNA) at intermediate depth, and decadal  
87 to multidecadal changes in the strengths of these jets might play a significant role in  
88 modulating long-term oxygen changes in the ETNA OMZ (Brandt et al., 2010).

Peter Brandt 27.10.2014 22:56  
Gelöscht: well-ventilated

Peter Brandt 27.10.2014 22:57  
Gelöscht: and

Peter Brandt 27.10.2014 22:57  
Gelöscht: together

89 The Atlantic and Pacific OMZs have many similarities particularly regarding OMZ shape and  
90 circulation pattern. The ETNA and eastern tropical South Pacific (ETSP) OMZs (Figs. 1, 2)  
91 are both located in the shadow zones of the ventilated thermocline and are ventilated by  
92 lateral and vertical mixing as well as by zonal advection in the equatorial band. However, the  
93 striking difference between both OMZs is that the ETNA OMZ is hypoxic (oxygen below ~60  
94 to 120  $\mu\text{mol kg}^{-1}$ ) and the ETSP is suboxic (oxygen below about 10  $\mu\text{mol kg}^{-1}$ ). Karstensen et  
95 al. (2008) concluded that this difference is the result of reduced oxygen levels in the eastward  
96 current bands of the Pacific OMZs compared to the Atlantic OMZs, which can be traced back  
97 to the larger ratio of the total volume of OMZ layer to the renewal or subduction rate in the  
98 Pacific compared to the Atlantic.

103 As part of the Collaborative Research Center 754 (Sonderforschungsbereich, SFB 754)  
104 "Climate-Biogeochemistry Interactions in the Tropical Ocean" (first phase 2008-2011 and  
105 second phase 2012-2015) physical processes responsible for the ventilation of the ETNA  
106 OMZ have been studied using an extended observational program including repeat  
107 hydrography by shipboard and glider measurements, an array of subsurface moorings,  
108 microstructure measurements and two tracer release experiments. The goals of the research  
109 program are to deliver an improved understanding of the ventilation physics of the ETNA  
110 OMZ, to come up with a quantitative understanding of the functioning of the OMZs, to  
111 monitor regional oxygen variability and trends and to analyse their causes. The ETSP OMZ  
112 have been studied as well using a reduced observational program. However, the comparison  
113 between the hypoxic ETNA and the suboxic ETSP is of particular interest here, as the  
114 observed deoxygenation in the ETNA, or future climate change, might lead to a shift from  
115 hypoxic to suboxic conditions. The present paper provides an overview of the current status of  
116 the science regarding these topics. The paper is organized as follows: In Sect. 2, data and  
117 methods used in this study are described. In Sect. 3, the current system and the OMZ structure  
118 in the ETNA are characterized. Results for the quantification of the strength of different  
119 ventilation processes, i.e. vertical mixing, lateral mixing, and advection, are presented in Sect.  
120 4. In Sect. 5, the current knowledge on oxygen consumption estimates is presented. The OMZ  
121 structure and processes at the continental margin are presented in Sect. 6. Long-term oxygen  
122 variability with a special focus on the period of enhanced data coverage is presented in Sect.  
123 7. The results obtained for the ETNA OMZ are then compared to results obtained for the  
124 ETSP in Sect. 8 and finally, in Sect. 9, the results are summarized and discussed.

125

## 126 **2 Ocean Observations,**

127 A major focus of the observational work presented here has been on circulation, ventilation  
128 physics, and water mass distribution. In the tropical North Atlantic, observations concentrated  
129 on the 23° W section with repeat hydrography, microstructure measurements, velocity  
130 measurements (Table 1), and moored observations (Table 2). The 23° W section cuts through  
131 the ETNA OMZ from south of the Cape Verde archipelago to slightly south of the equator  
132 (Fig. 1). Along the 23° W section, moorings with instrumentation to continuously observe  
133 temperature, salinity, oxygen and velocity were deployed at different latitudes (8° N, 5° N, 0°)  
134 delivering multi-year time series. Additionally, oxygen sensors were installed at 300 m and  
135 500 m depth at selected moorings (23° W, 4° N and 11.5° N) of the Prediction and Research

Peter Brandt 1.11.2014 11:28

**Gelöscht:** al work within the SFB 754

Peter Brandt 1.11.2014 11:28

**Gelöscht:** The SFB 754 addresses climate induced ocean deoxygenation, with a focus on tropical OMZ in the Atlantic and Pacific, and its implications for the global marine biogeochemical system.

141 moored Array in the Tropical Atlantic (PIRATA; Bourles et al. (2008)) and at a subsurface  
142 mooring at 23° W, 2° N (Fig. 1). For the analysis of hydrographic and velocity data acquired  
143 along 23° W, we used the measurements given in Table 1. Besides the 23° W section, we  
144 shall present here also data acquired along 18° N at the northern boundary of the ETNA OMZ  
145 (Fig. 1, Table 1). Moreover, two tracer release experiments (TREs) were carried out in the  
146 ETNA OMZ. During the first TRE, GUTRE (Guinea Upwelling Tracer Release Experiment),  
147 in April 2008, 92 kg of the halocarbon tracer trifluoromethyl sulfur pentafluoride (CF<sub>3</sub>SF<sub>5</sub>)  
148 were released at 23° W, 8° N on the potential density surface,  $\sigma_{\theta}=26.88 \text{ kg m}^{-3}$ . The depth of  
149 release, of about 330 m, corresponds to the depth of the oxycline above the deep oxygen  
150 minimum. During the following 2.5 years, three tracer surveys were carried out to measure  
151 the vertical and horizontal spreading of the tracer (Banyte et al. (2012), Table 1). During the  
152 second TRE, OSTRE (Oxygen Supply Tracer Release Experiment), in November 2012, 88.5  
153 kg of the same tracer were released at 21° W, 11° N on the potential density surface  $\sigma_{\theta}=27.03$   
154  $\text{kg m}^{-3}$  corresponding to about 500 m depth which is in the core region of the ETNA OMZ.

155 In the ETSP OMZ a particular focus was on the ~86° W section (section located at 85°50'W  
156 north of 15° S with a westward shift to 88° W south of 20° S, called ~86° W section in the  
157 following) with hydrographic and current measurements from 2° N to about 22° S (Fig. 2).  
158 Two recent cruises covered that section repeating measurements taken during the RV Knorr  
159 cruise in March 1993 (Table 1). Additionally, four cruises were carried out along the  
160 continental margin of Peru (Table 1) to investigate the circulation along the continental slope  
161 and shelf off Peru as well as the physical processes contributing to the redistribution of  
162 oxygen, nutrients and other solutes.

163

### 164 3 Structure of the ETNA OMZ

165 The subtropical gyre circulation of the northern hemisphere is, to first order, determined by  
166 the negative wind stress curl associated with mid-latitude westerlies and northeast trade  
167 winds. The resulting Ekman pumping drives subduction of oxygen-rich surface water masses  
168 in the subtropics. According to theory, equatorward and westward propagation of subducted  
169 water masses forms the northern boundary of the shadow zone of the ventilated thermocline  
170 (Luyten et al., 1983b). Within the shadow zone, which is characterized by a weak mean  
171 circulation, the ETNA OMZ with a core depth at about 400 m is found. Lowest oxygen  
172 concentrations at the core depth are found away from the continental margin at about 20° W,  
173 10° N (Fig. 3). North of the ETNA OMZ is the North Equatorial Current (NEC) flowing

Peter Brandt 4.11.2014 11:50

Gelöscht: , in addition to

Peter Brandt 4.11.2014 11:50

Gelöscht: , data from other German, US, and French cruises carried out during 1999 to 2011 as listed in

Peter Brandt 4.11.2014 11:50

Gelöscht: Hahn et al. (2014)

Peter Brandt 4.11.2014 11:51

Gelöscht: The 18° N section was, in addition to two cruises listed in Table 1, covered several times during 2005 to 2010 by research cruises (RV Poseidon cruises 320/1, 347/1, 348/1, 399/2, RV Meteor cruise 68/3).

Peter Brandt 27.10.2014 23:11

Gelöscht: 0

Peter Brandt 4.11.2014 11:53

Gelöscht: (Table 1)

Peter Brandt 4.11.2014 11:58

Gelöscht: three

Peter Brandt 14.11.2014 17:03

Gelöscht: positive

188 southwestward along the Cape Verde Frontal Zone. It transports oxygen-rich Central Water  
189 (CW) formed by subduction in the subtropics as well as intermediate water masses in the  
190 deeper layers having their origin mainly in the Labrador Sea and the Mediterranean outflow.  
191 To the south, the ETNA OMZ is bounded by the energetic zonal flows near the equator  
192 forming the equatorial oxygen maximum (Brandt et al., 2012). Above the main deep OMZ, at  
193 a depth of about 100 m, a shallow OMZ is situated, defined as the secondary oxygen  
194 minimum below the surface mixed layer and above 200 m (Fig. 4). It is characterized by  
195 generally higher oxygen levels compared to the deep OMZ, while occasionally extremely low  
196 oxygen levels are possible, and is most pronounced in the northeastern part of the shadow  
197 zone close to the highly productive eastern boundary upwelling region off Mauritania and  
198 Senegal (Fischer et al., 2013). The mean 18° N section shows shallow mixed layer depths at  
199 the continental margin typical for coastal upwelling regions as well as lower salinities in the  
200 CW layer that are a consequence of the northward transport of southern hemisphere water  
201 along the continental slope within the Poleward Undercurrent (Barton, 1989) and the surface  
202 flow associated with the Mauritania Current (Mittelstaedt, 1983) (Fig. 5).

203 The western boundary of the Atlantic Ocean is associated with relatively high oxygen levels  
204 at all latitudes (Fig. 1). At the density of the OMZ layer, the North Brazil Undercurrent  
205 (NBUC) / North Brazil Current (NBC) (Schott et al., 2005) transports central and intermediate  
206 water masses of southern hemisphere origin northward. The high oxygen concentrations in the  
207 CW layer of the NBUC can be traced back along the different branches of the South  
208 Equatorial Current (SEC) to the subduction region in the eastern subtropical gyre (Tsuchiya,  
209 1986; Stramma and England, 1999). The CW also includes water from the Indian Ocean that  
210 are brought into the Atlantic by eddy shedding from the Agulhas retroflexion.

211 The Antarctic Intermediate Water (AAIW) below the CW originates mainly from the Drake  
212 Passage and is transported around the southern hemisphere subtropical gyre to feed into the  
213 NBUC (Suga and Talley, 1995). Of importance for the ventilation of the ETNA OMZ is the  
214 northward flow of CW and AAIW across the equator. The northward penetration of southern  
215 hemisphere water masses at the western boundary changes with depth: AAIW dominates as  
216 far as 15° N, the upper CW only as far as 10° N because of the presence of water masses of  
217 northern hemisphere origin (Kirchner et al., 2009).

218 A substantial part of the water masses transported northward within the NBUC forms the  
219 upper branch of the Atlantic Meridional Overturning Circulation (AMOC), a circulation  
220 known since the German Meteor cruises in the 1920's, as documented by Wüst (1935). The



221 presence of the AMOC under present climate conditions is identified as the main reason for  
 222 the dominance of southern hemisphere water masses in the tropical North Atlantic discussed  
 223 above. It contributes to the asymmetric shallow overturning circulations in both hemispheres  
 224 as well: the subtropical cell (STC) of the northern hemisphere being much weaker than its  
 225 counterpart in the southern hemisphere (Schott et al., 2004). The STC connects the subduction  
 226 regions of the eastern subtropical gyres to the equatorial and coastal upwelling regions. In the  
 227 northern hemisphere, the subducted water masses mostly do not reach the equator. Instead,  
 228 they contribute to the eastward flow within the North Equatorial Counter Current  
 229 (NECC)/North Equatorial Undercurrent (NEUC) at about 5° N (Zhang et al., 2003). A  
 230 particular feature in the ETNA is the presence of an open ocean upwelling regime within the  
 231 cyclonic circulation of the Guinea Dome south of the Cape Verde archipelago. Associated  
 232 with the presence of the Guinea Dome are changes in the potential vorticity distribution that  
 233 further limit the flow of newly subducted water masses from the northern hemisphere  
 234 subtropics toward the equator within the STC (Malanotte-Rizzoli et al., 2000).

235 The 23° W section (Fig. 6) cuts through the ETNA OMZ, which can be identified by low  
 236 oxygen levels as well as by the high age of the water masses. The gradual change of salinity  
 237 on density surfaces along this section defines the transition between low- and high-saline  
 238 water masses of southern and northern origin, respectively. Along this section mean eastward  
 239 and westward flow is typically identified by positive and negative oxygen anomalies relative  
 240 to the background oxygen distribution (Brandt et al., 2010).

241 Ventilation time scales of the interior ocean can be quantified by analysing transient tracer  
 242 distributions. A comprehensive set of CFC-12 and SF<sub>6</sub> measurements in the ETNA (these  
 243 tracers were measured in parallel to the deliberately released tracer CF<sub>3</sub>SF<sub>5</sub>), has been explored  
 244 in detail by Schneider et al. (2012) using the concept of transit time distributions (TTDs) (e.g.  
 245 Waugh et al. (2004)). The mean age in the centre of the OMZ ( $\sigma_\theta=27.0 \text{ kg m}^{-3}$ ) is in the range  
 246 of 120 to 180 years (Fig. 7). The mean age refers to the average time it takes for a water  
 247 parcel to reach a certain location in the interior ocean from the time it was last in contact with  
 248 the surface ocean and hence atmosphere (see Sect. 5 for more discussion on the TTD  
 249 concept). In contrast to waters in the OMZ centre, water south of about 5° N is significantly  
 250 better ventilated with mean ages close to 100 years, reflecting the more energetic circulation  
 251 in the equatorial region. Roughly the same age is found north of about 13° N close to the  
 252 Cape Verde Islands despite lower oxygen values in the northern compared to the southern  
 253 region. Below the poorly ventilated OMZ, the even older AAIW ( $\sigma_\theta=27.3 \text{ kg m}^{-3}$ ) with

- Peter Brandt 26.10.2014 17:30  
Gelöscht: Along t
- Peter Brandt 26.10.2014 17:30  
Gelöscht: ting
- Peter Brandt 26.10.2014 17:32  
Gelöscht: (defined, beside
- Peter Brandt 26.10.2014 17:33  
Gelöscht: ,
- Peter Brandt 26.10.2014 17:33  
Gelöscht: , see e.g.
- Peter Brandt 26.10.2014 17:33  
Gelöscht: Schneider et al. (2012)
- Peter Brandt 26.10.2014 17:33  
Gelöscht: ),
- Peter Brandt 26.10.2014 17:35  
Gelöscht: the meridional
- Peter Brandt 26.10.2014 17:38  
Gelöscht: and temperature
- Peter Brandt 26.10.2014 17:35  
Gelöscht: gradient
- Peter Brandt 26.10.2014 17:36  
Gelöscht: can be observed
- Peter Brandt 26.10.2014 17:36  
Gelöscht: ing
- Peter Brandt 26.10.2014 17:39  
Gelöscht: (Fig. 6)
- Peter Brandt 26.10.2014 16:58  
Gelöscht: high and low
- Peter Brandt 26.10.2014 16:58  
Gelöscht: levels
- Peter Brandt 1.11.2014 11:34  
Gelöscht: Observational work during the SFB 754 included a
- Peter Brandt 1.11.2014 11:34  
Gelöscht: a
- Peter Brandt 1.11.2014 11:35  
Gelöscht: . This data set

273 ventilation times in excess of 500 years is found (close to the detection limit of the CFCs, and  
274 thus difficult to accurately quantify), although this water mass has high oxygen concentration.  
275 Again, at this density layer the area south of 5° N is significantly better ventilated than north  
276 of 5° N (Schneider et al., 2012).

277

## 278 4 Ventilation processes

279 The oxygen budget of the OMZ takes account of consumption, advection, and diffusion of  
280 oxygen. Any imbalance of these terms results in decreasing or increasing oxygen  
281 concentration. While consumption is an oxygen sink, advection and diffusion might be  
282 sources or sinks depending on the background conditions. Mean advection of oxygen  
283 manifests itself in the mean oxygen and velocity distributions: along 23° W, mean eastward  
284 current bands are generally associated with elevated oxygen content (Fig. 6) representing an  
285 advective ventilation pathway from the western boundary toward the OMZ (Brandt et al.,  
286 2010). Horizontal and vertical diffusion act on the mean horizontal and vertical oxygen  
287 gradients, respectively. The associated variance production by mesoscale eddy stirring and  
288 small-scale turbulence (Ferrari and Polzin, 2005) results in locally elevated oxygen variance.  
289 The Eulerian variance along 23° W, as obtained from ship sections, might additionally result  
290 from lateral meandering of zonal currents or from vertical movements of isopycnals  
291 associated with internal waves and eddies. Moored time series reflect this variability pattern.  
292 There is generally higher oxygen variance at 300 m depth close to the oxycline above the  
293 deep OMZ core compared to 500 m depth (cf. Figs. 8, 9). Time scales of processes driving the  
294 variance in moored time series cover a wide range from those associated with internal waves  
295 and tides, inertial oscillations, the mesoscale eddy field to seasonal and interannual variability,  
296 including planetary waves (Hahn et al., 2014). Using repeat ship sections, the effect of  
297 vertical motion of isopycnals can be removed by calculating oxygen variance on potential  
298 density surfaces and projecting back onto depth space (Fig. 10). The remaining oxygen  
299 variance in regions of weak mean flow surrounding the ETNA OMZ might be associated with  
300 processes responsible for vertical and lateral mixing that is discussed in the following  
301 subsections.

### 302 4.1 Vertical mixing

303 Vertical mixing acts on the vertical oxygen gradients and leads to an oxygen supply to the  
304 OMZ via down-gradient oxygen fluxes. In order to estimate the vertical or diapycnal oxygen  
305 supply, the diapycnal diffusivity  $K_p$  as a measure for diapycnal mixing is required. From the

Peter Brandt 27.10.2014 23:14

Gelöscht: an

Peter Brandt 27.10.2014 23:14

Gelöscht: tendency

Peter Brandt 26.10.2014 16:59

Gelöscht: of oxygen

Peter Brandt 2.11.2014 18:39

Gelöscht:

Peter Brandt 14.11.2014 17:04

Gelöscht: ,

311 diapycnal spread of the deliberately released tracer during GUTRE, a mean diapycnal  
 312 diffusivity of  $(1.2\pm 0.2)\times 10^{-5} \text{ m}^2 \text{ s}^{-1}$  was derived (Banyte et al., 2012). The tracer was injected  
 313 on the isopycnal  $\sigma_\theta=26.88 \text{ kg m}^{-3}$  (about 330 m), corresponding to the oxycline above the  
 314 deep OMZ. GUTRE was accompanied by extensive microstructure and finescale shear  
 315 measurements that delivered an estimate of  $(1.0\pm 0.2)\times 10^{-5} \text{ m}^2 \text{ s}^{-1}$  for  $K_\rho$  for the depth range  
 316 between 150 and 500 m (Fischer et al., 2013). The value inferred from microstructure  
 317 measurements only considers diapycnal mixing due to small-scale turbulence. However,  
 318 double diffusive enhancement was found to be small ( $\sim 0.1\times 10^{-5} \text{ m}^2 \text{ s}^{-1}$ ) in this depth interval  
 319 (Fischer et al., 2013), so the total diffusivities estimated by the two independent methods  
 320 agree within the error bars. This estimate of diapycnal mixing is considerably larger than the  
 321 expected background mixing at this latitude (e.g. Gregg et al. (2003)), probably due to the  
 322 presence of rough topography (e.g. the Sierra Leone Rise) in the southern part of the OMZ.  
 323 Combining  $K_\rho$  with simultaneous profiles of the vertical oxygen gradient allows  
 324 determination of the profile of the diapycnal oxygen flux. Its divergence represents the  
 325 oxygen supply to the OMZ and amounted to about  $1 \mu\text{mol kg}^{-1} \text{ yr}^{-1}$  in the OMZ core, with the  
 326 required oxygen transported downwards from the upper CW (Fischer et al., 2013).

327 Deeper ranging microstructure profiles acquired during the most recent cruises to the ETNA  
 328 OMZ (Table 1), allowed us to extend the analysis into the deeper water column down to 800 m  
 329 depth; i.e. allowed us to estimate the diapycnal oxygen flux from the AAIW below as well. In  
 330 total 200 microstructure profiles, 40 of them down to 800 m, were about equally partitioned to  
 331 three subregions of the OMZ: a seamount subregion (7 % of OMZ area), an abyssal plain  
 332 subregion (80 % of OMZ area), and a transition subregion (13 % of OMZ area). They served  
 333 to estimate subregional mean profiles of the turbulent part of diapycnal diffusivity (Fig. 11).  
 334 Double diffusive enhancement of  $K_\rho$  from simultaneous CTD profiles for each subregion  
 335 following St Laurent and Schmitt (1999) was accounted for to obtain subregional total  $K_\rho$   
 336 profiles (Fig. 11) and an area-weighted mean total  $K_\rho$  profile (Fig. 12). The mean diapycnal  
 337 supply, (Fig. 13) that, in the following, will be used in the oxygen budget was then derived as  
 338 the divergence of the low-pass filtered mean diapycnal flux. The mean flux profile was  
 339 calculated as the area-weighted mean of the three flux profiles from the three subregions,  
 340 which in turn were obtained by combining mean  $K_\rho$  with vertical oxygen gradient profiles  
 341 from the three subregions. Error estimates are reported as 95% confidence limits and are  
 342 based on standard errors of the mean of individual  $K_\rho$  and oxygen gradient profiles for each  
 343 subregion. Subsequent error estimates for the mean total  $K_\rho$  profile (Fig. 12), flux profiles,

Peter Brandt 2.11.2014 18:39  
 Gelösch:   
 Peter Brandt 4.11.2014 14:22  
 Gelösch: (Fischer et al., 2013)

Peter Brandt 4.11.2014 14:25  
 Gelösch: ly  
 Peter Brandt 2.11.2014 18:37  
 Gelösch: 20 deep

Peter Brandt 26.10.2014 17:02  
 Gelösch: They served to estimate the relative shape of the  $K_\rho$  profiles between 500 and 800 m for each subregion, in relation to their 150-500 m average  $K_\rho$ . The absolute scaling of  $K_\rho$  at 500-800 m for each subregion was then achieved by multiplying with the mean  $K_\rho$  between 150 and 500 m from all available microstructure profiles.

Peter Brandt 4.11.2014 15:08  
 Gelösch: was estimated

Peter Brandt 4.11.2014 14:50  
 Gelösch: ,

Peter Brandt 4.11.2014 14:50  
 Gelösch: and finally the three  $K_\rho$  profiles (Fig. 11) were averaged using area-weighting allowing the comparison with the mean diapycnal diffusivity from the TRE (Fig. 12).

Peter Brandt 4.11.2014 14:41  
 Gelösch: profile

Peter Brandt 4.11.2014 15:05  
 Gelösch: was

Peter Brandt 4.11.2014 14:52  
 Gelösch: supply

Peter Brandt 4.11.2014 15:43  
 Gelösch: the

Peter Brandt 4.11.2014 15:42  
 Gelösch: profiles

Peter Brandt 8.11.2014 11:52  
 Gelösch: and

Peter Brandt 4.11.2014 15:42  
 Gelösch: profiles of the mean

368 and the mean supply profile (Fig. 13) were obtained from Gaussian error propagation (Ferrari  
369 and Polzin, 2005; Schafstall et al., 2010).

370

## 371 4.2 Lateral Mixing

372 Lateral mixing is induced to first order by oceanic mesoscale activity, which dominantly acts  
373 along isopycnal surfaces. It effectively mixes oxygen in regions with strong isopycnal oxygen  
374 gradients, thus substantially contributing to the ventilation of an OMZ across its lateral  
375 boundaries (Luyten et al., 1983a; McCreary et al., 2013; Gnanadesikan et al., 2013; Hahn et al.,  
376 2014). For the ETNA OMZ the eddy-driven meridional oxygen flux could be quantified along  
377 23° W both by a diffusive flux parameterization and by eddy correlation (Hahn et al., 2014).

378 The diffusive flux parameterization as the first method rests on the idea that the eddy-driven  
379 along-isopycnal oxygen flux can be expressed as a diffusive flux  $F^d = K_e \nabla O_2$  which is down  
380 the mean oxygen gradient  $\nabla O_2$  with a horizontal eddy diffusivity  $K_e$ . Two independent  
381 estimates of the meridional component of  $K_e$  for the ETNA regime were derived. On the one  
382 hand, Banyte et al. (2013) analysed the lateral spreading of the tracer released at 330 m during  
383 GUTRE. On the other hand, Hahn et al. (2014) used hydrographic and velocity observations  
384 in the upper 1000 m from research vessels and moorings along 23° W during the last 15 years.  
385 Fundamentally, Hahn et al. (2014) based their analysis on the mixing length theory (as  
386 applied in Ferrari and Polzin (2005)) as well as on the theory of two-dimensional mesoscale  
387 turbulence on a  $\beta$ -plane (Eden, 2007).

388 By comparing observed and simulated tracer distributions, Banyte et al. (2013) estimated a  
389 meridional eddy diffusivity of  $500 \text{ m}^2 \text{ s}^{-1}$  at about 300 m with an uncertainty of  $200 \text{ m}^2 \text{ s}^{-1}$   
390 (Fig. 14). Hahn et al. (2014) estimated a meridional eddy diffusivity profile for the upper  
391 1000 m with the range of uncertainty assumed as large as a factor 2 following Ferrari and  
392 Polzin (2005). The profile shows maximum eddy diffusivity close to the surface and  
393 decreasing values with depth (Fig. 14). At 300 m, it yields  $580 \text{ m}^2 \text{ s}^{-1}$  which is in good  
394 agreement with the estimate from Banyte et al. (2013). Together with the mean oxygen  
395 distribution, the obtained meridional eddy diffusivity was applied to derive the eddy-driven  
396 meridional oxygen flux along 23° W.

397 As a second method the eddy correlation was used to directly calculate the eddy-driven  
398 meridional oxygen flux along isopycnal surfaces using mooring time series of oxygen and  
399 meridional velocity acquired at 5° N, 23° W and 8° N, 23° W in the years 2009-2012 and

Peter Brandt 4.11.2014 14:51

Gelösch: Fischer et al. (2013)

Peter Brandt 4.11.2014 16:24

Gelösch: (Fischer et al., 2013)

Peter Brandt 2.11.2014 19:11

Gelösch: The estimates from

Peter Brandt 2.11.2014 19:13

Gelösch: and

Peter Brandt 2.11.2014 19:30

Gelösch: are in good agreement (Fig. 14). The average profile of  $K_e$  shows maximum eddy diffusivity close to the surface and decreasing values with depth

Peter Brandt 8.11.2014 12:12

Gelösch: estimate of

Peter Brandt 8.11.2014 12:12

Gelösch:  $K_e$

410 2011-2012, respectively (see Hahn et al. (2014) for details). Although both estimation  
411 methods are accompanied by large uncertainties, a comparison of the results at the mooring  
412 sites reveals coherent profiles of the meridional oxygen flux (100-800 m). At the depth of the  
413 OMZ they yield a northward oxygen flux towards the centre of the OMZ.

414 The oxygen that is meridionally supplied to the ETNA OMZ regime by lateral mixing can  
415 then be derived as the divergence of the eddy-driven meridional oxygen flux. The average  
416 profile of this eddy-driven meridional oxygen supply (6°-14° N, 23° W) obtained using the  
417 diffusive flux parameterization shows a substantial gain of oxygen at the depth of the OMZ  
418 and a loss of oxygen above (Fig. 14). The corresponding error was derived both from the error  
419 of the curvature of the meridional oxygen distribution (95% confidence) and the error of the  
420 eddy diffusivity (factor 2 assumed following (Ferrari and Polzin, 2005)).

421 The tropical and subtropical oceans are generally assumed to be associated with an  
422 anisotropic horizontal eddy diffusivity (Banyte et al., 2013; Eden, 2007; Eden and Greatbatch,  
423 2009; Kamenkovich et al., 2009) with larger horizontal eddy diffusivities in the zonal than in  
424 the meridional direction. Nevertheless, at the depth of the OMZ core, we consider the zonal  
425 eddy flux divergence small compared to the meridional eddy flux divergence, since the 2<sup>nd</sup>  
426 derivative of oxygen is an order of magnitude smaller in the zonal than the meridional  
427 direction.

### 428 4.3 Advection

429 We now turn to the remaining ventilation term in the budget; that is, the term associated with  
430 zonal advection (meridional advection is assumed to be negligible). We are only able to  
431 quantify this term as a residual. A rigorous determination of the advection term would require  
432 mean sections around a closed box to fulfil mass balance within the box. This cannot be  
433 achieved with the present observing system. However, our measurements along 23° W  
434 confirm that the advection term is a major player in the ventilation of the OMZ, especially  
435 above 400 m depth.

436 The key factor for carrying the relatively oxygen-rich waters eastwards from the western  
437 boundary is the presence of a series of latitudinally stacked zonal jets that are now known to  
438 be an ubiquitous feature of the tropical oceans (e.g. Maximenko et al. (2005), Qiu et al.  
439 (2013)). Near the equator in the Atlantic, these jets are confined below the Equatorial  
440 Undercurrent (EUC), but away from the equator they extend to the surface, and at all latitudes  
441 they tend to have a strong depth-independent (barotropic) structure (Fig. 6). Brandt et al.  
442 (2010) suggested that a reduction in the strength of these jets north of the equator was a factor

Peter Brandt 2.11.2014 19:37

Gelöscht: e

Peter Brandt 2.11.2014 19:41

Gelöscht: derived from

Peter Brandt 26.10.2014 17:16

Gelöscht: but

Peter Brandt 26.10.2014 17:18

Gelöscht: is

447 in the recent reduction in oxygen within the OMZ. The influence these jets have on the  
448 meridional oxygen distribution can clearly be seen in Figure 13 of Hahn et al. (2014) showing  
449 the eddy-driven meridional oxygen supply. The red and blue alternating bands above 400 m  
450 depth in that figure indicate a latitudinal redistribution of oxygen by mesoscale eddies, i.e. a  
451 oxygen gain for westward jets and an oxygen loss for eastward jets. It is clear from this figure  
452 that the zonal jets must play an important role in ventilating the upper 400 m of the water  
453 column in the latitude band (north of 6° N) of the OMZ. Looking at the equatorial region, the  
454 oxygen source (shown in blue) associated with the eastward jets, centred near 2° N and 2° S  
455 below 350 m depth, can also be seen in Figure 13 of Hahn et al. (2014). These so-called  
456 “flanking jets” are clearly an important ventilation pathway for maintaining the oxygen  
457 maximum at the equator, as discussed further below.

458 The ventilation of the equatorial region, where there is a local oxygen maximum, has been  
459 studied by Brandt et al. (2012) using an advection-diffusion model. The role of the equatorial  
460 deep jets (EDJ; see Brandt et al. (2008) and Brandt et al. (2011)) was also discussed in that  
461 paper. As can be seen from Fig. 6, the “flanking jets” are much stronger than the off-  
462 equatorial zonal jets noted earlier. Ascani et al. (2010) have suggested that these jets are  
463 maintained by Yanai waves, generated at the surface (possibly by instability of the energetic  
464 near-surface flow field forming tropical instability waves (von Schuckmann et al.,  
465 2008; Jochum et al., 2004)), which break at depth. The jets show considerable variability (see  
466 Fig. 15) on monthly time scales but are almost always unidirectional (especially in the  
467 northern hemisphere); their longitudinal dependence along the equator is currently uncertain.  
468 The EDJ are also thought to be generated by downward propagating Yanai waves, in this case  
469 by barotropic instability of these waves as discussed by Hua et al. (2008) (see also d'Orgeville  
470 et al. (2007) and Ménesguen et al. (2009)). The EDJ show downward phase propagation but  
471 upward energy propagation, consistent with the above theory, and lead to variability with a  
472 roughly 4.5-year period throughout the water column within 2 degrees latitude on either side  
473 of the equator and above about 3000 m depth (Brandt et al., 2011). As shown by Brandt et al.  
474 (2012), there is evidence of a corresponding 4.5-year variability in oxygen levels in the same  
475 region (Fig. 8, equator) with variability at 300 m depth at 23° W on the equator having a  
476 range comparable to the range of the mean oxygen level along the equator across the whole  
477 Atlantic.

478

## 479 **5 Consumption**

480 Oxygen consumption is a key mechanism for the formation of OMZs (Sverdrup,  
481 1938;Wyrтки, 1962) and, although being a prominent part of the local oxygen budget of the  
482 OMZs, it is among the poorest constrained ones. We will consider here only the net  
483 consumption that is the combined effect of removal and production of oxygen. Removal of  
484 oxygen is related to the metabolism of marine life as well as to elementary chemical reactions,  
485 whereas production of oxygen is related to photosynthesis and as such confined to the  
486 euphotic zone (e.g. Martz et al. (2008)). We will focus in this section on pelagic oxygen  
487 consumption; removal of oxygen from the water column by uptake at the sediment-water  
488 interface will be discussed in Sect. 6.

489 Direct observations of oxygen in-situ respiration are rare, primarily due to technical  
490 difficulties (e.g. Holtappels et al. (2014)). The most commonly applied approach to quantify  
491 time and space integrated oxygen removal and production processes is through an *apparent*  
492 *oxygen utilization rate* (AOUR; e.g. Riley (1951);Jenkins (1982, 1998);Karstensen et al.  
493 (2008);Martz et al. (2008);Stanley et al. (2012)). The AOURL is calculated as the ratio between  
494 the apparent oxygen utilization (AOU) and age ( $\tau$ ). Hereby AOU is determined as the  
495 difference between the air saturation value of dissolved oxygen (e.g. Weiss (1970)) at a given  
496 temperature and salinity (surface water saturation is commonly assumed to be 100 %) and the  
497 observed in-situ oxygen concentration. The *aging* of the water starts when a water parcel  
498 leaves the surface mixed layer ( $\tau=0$ ) and enters the ocean interior. As the aging is closely  
499 linked to the ventilation process the age is also called *ventilation age*. In many cases the  
500 ventilation age is calculated from transient tracers (e.g. CFC-11, CFC-12, CCl<sub>4</sub>, SF<sub>6</sub>). Under  
501 the assumption of a given surface saturation (typically 100 %), the observed in-situ tracer  
502 concentration is converted back to an equivalent atmospheric mixing ratio via its solubility  
503 function. The comparison with the respective tracer atmospheric time history finally yields the  
504 *tracer age*. For radioactive tracers (e.g. <sup>3</sup>He/<sup>3</sup>H, <sup>39</sup>Ar) a slightly different approach is used but  
505 still requires the knowledge of surface concentrations or surface input functions (e.g. Roether  
506 et al. (2013);Lu et al. (2014)). AOURL calculated using the tracer age follows an exponential  
507 decay with depth, at least for oceanic regions dominated by advection (Riley, 1951;Jenkins,  
508 1982, 1998;Karstensen et al., 2008;Martz et al., 2008;Stanley et al., 2012). Such a structure  
509 supports the view that consumption is primarily a function of downward sinking particles  
510 (Martin et al., 1987).

511 The basic concept behind a ratio of along pathway oxygen removal and along pathway age  
512 increase assumes that the two quantities are consistently altered by ocean transport processes,

513 e.g. it is assumed that as age increases so does AOU (Thiele and Sarmiento, 1990). While this  
514 seems to be a reasonable assumption for the ventilated gyre it is questionable for the shadow  
515 zone where the OMZs are located. Here diapycnal mixing (Fischer et al., 2013) and complex  
516 advection/lateral mixing patterns (Brandt et al., 2010;Hahn et al., 2014) have a strong  
517 influence on the local oxygen transport and water parcels from multiple source regions with  
518 different ventilation ages and along-path integrated oxygen consumption meet and mix.

519 Water mass composition and water ages can also be considered in a TTD approach (Haine  
520 and Hall, 2002), but limitations exist for non-steady state tracers (such as transient tracers).  
521 The TTD concept acknowledges the shortcomings in age calculations, which assign a single  
522 tracer age to a water parcel, and provides a framework to more realistically characterize the  
523 ventilation age (e.g. Waugh et al. (2004)) by providing a mean age of the TTD. In a study  
524 using transient tracer data set (up to 2009), Schneider et al. (2012) showed for the ETNA that  
525 the TTD obeys an inverse Gaussian function with the two moments  $\Gamma$  and  $\Delta$  being equal  
526 ( $\Delta/\Gamma=1$ ), where  $\Gamma$  is the mean age and  $\Delta$  defines the width of the TTD. In the limit of  $\Delta/\Gamma=0$ ,  
527 the mean age of the TTD equals the single tracer age.

528 Here an extended set of CFC-12, SF<sub>6</sub> and oxygen data collected in the ETNA OMZ is used to  
529 apply the TTD approach for exploring the oxygen consumption rate. Using CFC-12 and SF<sub>6</sub>  
530 data (SF<sub>6</sub> preferentially used if available and CFC-12 if CFC-12>450 ppt, i.e. corresponding  
531 to atmospheric mixing ratios at about the end of the near-linear atmospheric increase) the  
532 AOUR is calculated using two different  $\Delta/\Gamma$  ratios (Fig. 16). Note that the AOUR for  $\Delta/\Gamma=0$  is  
533 larger than values reported previously (Fig. 16) that were obtained by using a single tracer age  
534 concept applied to data collected in the ventilated gyre (e.g. Karstensen et al. (2008)).

535 The two estimates for  $\Delta/\Gamma=0$  and  $\Delta/\Gamma=1$  represent an upper and lower limit of the AOUR  
536 within the ETNA OMZ, respectively. A shortcoming of the TTD concept in this region is its  
537 one-dimensionality (single water mass), i.e. it only considers the along-isopycnal mixing of  
538 parcels of a single source water mass, which might have encountered different advection and  
539 diffusion pathways and thus differ in age and AOU. The influence of diapycnal mixing  
540 (Fischer et al., 2013) and the mixing of two or more source waters (e.g. North and South  
541 Atlantic Central Water) (Kirchner et al., 2009;Brandt et al., 2010) is not considered by TTD  
542 concept, which probably leads to a bias of the resulting AOUR. In fact our AOUR values for  
543  $\Delta/\Gamma=1$  are lower than those calculated by Stanley et al. (2012) for the ventilated gyre region  
544 of the western North Atlantic close to Bermuda, where they used the TTD approach with  
545  $\Delta/\Gamma=1$  on tritium (<sup>3</sup>H) and <sup>3</sup>He measurements. They derived AOUR values close to 5  $\mu\text{mol kg}^{-1}$



546  $\text{yr}^{-1}$  for the potential density level of  $27.0 \text{ kg m}^{-3}$  that were similar to AOUR values obtained  
547 by Karstensen et al. (2008) using CFC-11 ages. For the same density level that is close to the  
548 OMZ core depth at roughly 400 m, we derived AOUR values of only about  $1.5 \mu\text{mol kg}^{-1} \text{ yr}^{-1}$   
549 using the TTD approach with  $\Delta/\Gamma=1$ . The main differences are that the waters off Bermuda  
550 are much better represented by a single water mass and that they are significantly younger  
551 with a TTD derived mean age of a few tens of years. Waters in the ETNA OMZ instead are a  
552 mixture of water masses from multiple sources, some of which might be rather old resulting  
553 in a mean TTD age of 120-180 years (Fig. 7).

554 Another approach to estimate the large scale AOUR is based on the *reservoir age* (Bolin and  
555 Rodhe, 1973), which is derived as the ratio of the total volume of the reservoir for an  
556 isopycnal range and the corresponding ventilating flux (that is the subduction rate). The  
557 AOUR based on the reservoir age is then given by the ratio of the mean AOU of the isopycnal  
558 volume and the corresponding reservoir age. For the ETNA OMZ, the AOUR obtained using  
559 obtained reservoir ages of Karstensen et al. (2008), is for some density classes rather similar to  
560 the TTD approach with  $\Delta/\Gamma=0$ , while for the well-ventilated isopycnal volumes (26.1 to 26.2  
561  $\text{kg m}^{-3}$ ; see also Fig. 9 in Karstensen et al. (2008)) it is closer to the AOUR from the tracer age  
562 approach (Fig. 17).

## 563 6 Processes at the continental margin

564 Processes contributing to the ventilation of the OMZ at the continental margin are, advective  
565 oxygen transport within the eastern boundary current system, upper-ocean diapycnal oxygen  
566 supply due to increased turbulent mixing on the continental slope and shelf, and, eddy-driven  
567 isopycnal oxygen transport. In comparison to the open ocean OMZs, the consumption of  
568 oxygen at the continental margin, is generally enhanced, due to high pelagic primary  
569 production, which in turn, results in an increased respiration associated with sinking particles  
570 in the water column and at the sediment-water interface. These processes are largely  
571 responsible for the regional oxygen distribution particularly defining the shape of the shallow  
572 OMZ. Along the eastern boundary, oxygen concentrations within the shallow OMZ decrease  
573 towards the north reaching a minimum at about  $20^\circ \text{ N}$  (Fig. 4). For the deep OMZ, minimum  
574 oxygen levels at the continental margin are found south of  $16^\circ \text{ N}$  (Machin and Pelegri, 2009).

### 575 6.1 Upwelling and circulation

576 The continental margin off Mauritania and Senegal is part of the Canary eastern boundary  
577 upwelling system that extends from the northern tip of the Iberia peninsula at  $43^\circ \text{ N}$  to south  
578 of Dakar at about  $10^\circ \text{ N}$  (e.g. Mittelstaedt (1991)). Due to changes in wind forcing associated

Peter Brandt 27.10.2014 17:31

Gelöscht: for

Peter Brandt 27.10.2014 17:46

Gelöscht: (after

Peter Brandt 27.10.2014 17:46

Gelöscht: )

Peter Brandt 27.10.2014 17:48

Gelöscht: (Fig. 17).

Peter Brandt 27.10.2014 17:40

Gelöscht: However, on average it is between the upper and lower bounds of AOUR values as resulting from the TTD approach with  $\Delta/\Gamma=0$  and  $\Delta/\Gamma=1$ , respectively. . ... [1]

Peter Brandt 28.10.2014 15:22

Gelöscht: consist of

Peter Brandt 28.10.2014 15:23

Gelöscht: s well as

Peter Brandt 28.10.2014 15:25

Gelöscht: T

Peter Brandt 28.10.2014 15:29

Gelöscht: in these regions

Peter Brandt 28.10.2014 15:26

Gelöscht: increased

Peter Brandt 28.10.2014 15:31

Gelöscht: a

Peter Brandt 28.10.2014 15:32

Gelöscht:

Peter Brandt 28.10.2014 15:32

Gelöscht: ing

596 with the migration of the Intertropical Convergence Zone, coastal upwelling off Mauritania  
597 and Senegal exhibits a pronounced seasonality. Here winds favorable to upwelling prevail  
598 primarily from December to April. The seasonality in upwelling and associated primary  
599 production must be reflected in oxygen consumption and thus in water-column oxygen  
600 concentrations at the continental margin.

601 The ventilation of the waters above the continental margin occurs primarily through the  
602 Mauritania Current in the surface layer and the Poleward Undercurrent below. Both currents,  
603 transport relatively oxygen-rich South Atlantic Central Water, which is supplied by the  
604 eastward flowing NECC and NEUC (Figs. 1, 4), northward into the upwelling region. Often,  
605 these two currents are not distinct from each other (e.g. Peña-Izquierdo et al. (2012)). Usually,  
606 the Poleward Undercurrent is found attached to the continental slope between 50 and 300 m  
607 depth, but it may extend as deep as 1000 m (Mittelstaedt, 1983; Barton, 1989; Hagen,  
608 2001; Peña-Izquierdo et al., 2012). Average along-shore velocities from 18° N (Fig. 5) show  
609 dominantly poleward flow in the upper 300 m at the continental slope of Mauritania  
610 exceeding  $0.05 \text{ m s}^{-1}$ . However, the effect of the eddy field and other variability on the mean  
611 flow is clearly not averaged out due to the small number of available ship sections.

612 Previous studies showed that the Mauritania Current exhibits a seasonal behavior  
613 (Mittelstaedt, 1991), which was found to be associated with the seasonality of the NECC,  
614 suggesting that the ventilation of the water masses above the continental margin also varies  
615 seasonally. In boreal winter and early boreal spring, when the NECC is weak, the Mauritania  
616 Current only reaches latitudes of about 14° N, while in boreal summer and early boreal  
617 autumn, due to the strengthening of the NECC and the relaxation of the northeast trade winds,  
618 the Mauritania Current reaches latitudes of about 20° N (Mittelstaedt, 1991; Stramma et al.,  
619 2008a). Besides the seasonal cycle, the flow variability off Mauretania and Senegal is  
620 influenced by intraseasonal coastal-trapped waves partly originating in the equatorial wave-  
621 guide (Polo et al., 2008). However associated sea level anomalies are substantially weaker  
622 compared to the same latitude band in the South Atlantic. A strong influence of coastal-  
623 trapped waves on the oxygen distribution on the shelf of the ETNA as evidenced for the  
624 eastern boundary upwelling system of the South Pacific and South Atlantic (Gutierrez et al.,  
625 2008; Monteiro et al., 2011) could so far not be shown.

626 Several studies have indicated that most of the water carried northward at the continental  
627 margin of Mauritania recirculates in the region off Cape Blanc at about 21° N within a  
628 cyclonic gyre (Mittelstaedt, 1983; Peña-Izquierdo et al., 2012). This circulation pattern is in

Peter Brandt 28.10.2014 15:49

**Gelösch:** flows

Peter Brandt 28.10.2014 15:56

**Gelösch:** , which is carried

Peter Brandt 28.10.2014 15:57

**Gelösch:** within the

Peter Brandt 28.10.2014 15:59

**Gelösch:** 6

Peter Brandt 28.10.2014 15:49

**Gelösch:** flows

Peter Brandt 27.10.2014 09:47

**Gelösch:** that can be associated with the Mauritania Current and the Poleward Undercurrent

636 agreement with the regional distribution of oxygen levels within the shallow oxygen  
637 minimum that exhibits lowest oxygen concentrations at the continental margin and offshore  
638 just south of Cape Blanc (Peña-Izquierdo et al., 2012).

## 639 **6.2 Benthic oxygen uptake**

640 Oxygen uptake within the benthic region (i.e., the sediment and the immediately overlying  
641 water) is largely controlled by sediment oxygen consumption and can be a significant sink for  
642 oxygen from the water column above. In contrast to the difficulties of direct measurement of  
643 pelagic oxygen consumption, local measurements of sediment oxygen uptake are relatively  
644 straightforward to perform with a variety of techniques. Recent developments in measurement  
645 techniques include the use of benthic chambers, eddy-correlation techniques, multi-sensor  
646 microprofilers and benthic observatories (e.g. Glud (2008)). Total benthic oxygen uptake  
647 (TOU), which includes all processes consuming oxygen within the benthic region, is  
648 commonly measured by enclosure techniques such as benthic chambers. With these systems,  
649 the initial oxygen decrease of an overlying well-mixed water phase is approximately linear.  
650 TOU is then calculated based on the rate of oxygen decrease, accounting for the enclosed area  
651 and water volume. TOU rates have recently been measured in the upper 1000 m on the  
652 continental slope and shelf off Mauritania using benthic chambers attached to landers (Dale et  
653 al., 2014). The reported TOU rates that are quantified in terms of oxygen fluxes into the  
654 sediments were as high as  $10 \text{ mmol m}^{-2} \text{ d}^{-1}$  in depths between 50 and 100 m and decreased  
655 quasi-exponentially to about  $3 \text{ mmol m}^{-2} \text{ d}^{-1}$  in a depth of 1000 m. To compare TOU rates to  
656 pelagic oxygen consumption, we have to apply the TOU to a water volume with a given in-  
657 situ density: the consumption within a 1 m thick layer above the bottom due to TOU is three  
658 orders of magnitudes larger when compared to pelagic oxygen consumption occurring at  
659 similar depths. This is due to the volume-specific production and degradation of organic  
660 material in surface sediments, which supports high densities of microbes and metazoans  
661 (Glud, 2008). In shelf areas, it is estimated that 10 to 50 % of the pelagic primary production  
662 reaches the sediment (Canfield, 1993; Wollast, 1998) and benthic remineralization plays a key  
663 role in this region for the recycling of nutrients and burial of carbon.

664 Although the benthic oxygen consumption due to TOU at the shelf strongly exceeds pelagic  
665 oxygen consumption, benthic processes play a minor role for oxygen depletion within larger  
666 volumes as that of the deep OMZ. To illustrate this, we assume that oxygen depleted water  
667 masses are laterally exchanged between the shelf and the open ocean. Between 300 and 600 m  
668 depth the continental margin has a typical average topographic slope of about 4 %

Peter Brandt 27.10.2014 12:21

Gelöscht: characterizes

670 corresponding to 25 m shelf width per 1 m depth change. Assuming a TOU of  $5 \text{ mmol m}^{-2} \text{ d}^{-1}$   
 671 results in an oxygen depletion by the sediments of  $125 \text{ mmol d}^{-1}$  per 1 m depth range and 1 m  
 672 along-shelf distance. Using the range of pelagic oxygen consumption determined in Sect. 5 (1  
 673 to  $5 \text{ } \mu\text{mol kg}^{-1} \text{ yr}^{-1}$ ) and corresponding in-situ density, the equivalent water volume **resulting**  
 674 **in an oxygen depletion of**  $125 \text{ mmol d}^{-1}$  would be  $44 \times 10^3 \text{ m}^3$  to  $9 \times 10^3 \text{ m}^3$ , corresponding to a  
 675 distance from the shelf, where both processes have comparable influence, of 44 km to 9 km.  
 676 In other words, pelagic oxygen consumption within the deep OMZ, typically extending about  
 677 1000 km offshore, is 1 to 2 orders of magnitude larger than benthic oxygen consumption due  
 678 to oxygen fluxes into the continental slope sediments. Reduced topographic slopes at  
 679 shallower depths suggest a more important role of benthic oxygen uptake for the shallow  
 680 OMZ, which is characterized by minimum oxygen concentration close to the continental  
 681 margin and is not as widespread as its deeper counterpart (cf. Figs. 3, 4).

### 682 6.3 Diapycnal oxygen fluxes at the continental margin

683 Diapycnal mixing on continental slopes and shelf is often found to be elevated due to tides  
 684 interacting with topographic boundaries that accelerate an energy cascade from large scale  
 685 open ocean tides to small-scale turbulence (e.g. Sandstrom and Oakey (1995)). As shown by  
 686 Schafstall et al. (2010), diapycnal mixing along the upper continental slope and lower shelf  
 687 region off Mauritania is strongly elevated due to the presence of nonlinear internal waves that  
 688 are boosted by the interaction of the barotropic tide with critically sloping topography (e.g.  
 689 Holloway (1985)). Diapycnal nutrient fluxes calculated for the upwelling region are amongst  
 690 the highest reported to date (Schafstall et al., 2010).

691 To assess the role of diapycnal mixing for ventilating the upper layer of the ocean above the  
 692 continental slope, the diapycnal oxygen flux was calculated from 112 microstructure profiles  
 693 collected the continental slope between 500 m and 100 m water depth at  $18^\circ \text{ N}$  along with  
 694 CTD- $\text{O}_2$  profiles from two boreal winter cruises on the shelf of Mauritania (for details of the  
 695 data set used see Schafstall et al. (2010)). **Elevated mixing was found in a region with water**  
 696 **depths shallower than 500 m** (Schafstall et al., 2010). Within this region, the diapycnal flux of  
 697 oxygen from the mixed layer into the stratified ocean is  $73 \text{ mmol m}^{-2} \text{ d}^{-1}$ , **with an upper and**  
 698 **lower 95% confidence limit determined from Gaussian error propagation** (Ferrari and Polzin,  
 699 2005; Schafstall et al., 2010) **being  $105 \text{ mmol m}^{-2} \text{ d}^{-1}$  and  $44 \text{ mmol m}^{-2} \text{ d}^{-1}$ , respectively. The**  
 700 **diapycnal oxygen flux thus exceeds** the benthic oxygen uptake by about a factor of 7. The  
 701 diapycnal flux profile exponentially decays with depth and the downward oxygen flux is  
 702 reduced to less than  $10 \text{ mmol m}^{-2} \text{ d}^{-1}$  at a depth of 60 m below the mixed layer, **which has an**

Peter Brandt 27.10.2014 12:21

Gelöscht: consuming

Peter Brandt 2.11.2014 18:39

Gelöscht:

Peter Brandt 27.10.2014 12:25

Gelöscht: the

Peter Brandt 27.10.2014 12:25

Gelöscht: n upwelling

Peter Brandt 8.11.2014 13:02

Gelöscht: collected during

Peter Brandt 27.10.2014 12:26

Gelöscht: Mixing

Peter Brandt 27.10.2014 12:26

Gelöscht: on the continental slope and shelf off Mauritania is elevated

Peter Brandt 27.10.2014 12:26

Gelöscht: the

Peter Brandt 8.11.2014 13:38

Gelöscht: a

Peter Brandt 8.11.2014 13:04

Gelöscht: above

Peter Brandt 8.11.2014 13:04

Gelöscht: 80

Peter Brandt 8.11.2014 13:07

Gelöscht: thus exceeding

Peter Brandt 8.11.2014 13:07

Gelöscht: 8

717 | average thickness of about 20 m. Diapycnal mixing is thus able to fully supply the oxygen  
718 | that is required by the benthic oxygen uptake for water depths shallower than, about 80 m. At  
719 | about 150 m depth, however, the diapycnal flux changes sign due to the presence of the  
720 | shallow OMZ and oxygen here is essentially fluxed upward, although at small rates. Thus,  
721 | oxygen from the sea surface cannot contribute to ventilating the deeper water column via  
722 | diapycnal mixing.

723 | It should be noted that the diapycnal oxygen flux divergence from the mixed layer to 60 m  
724 | below the mixed layer yields a diapycnal oxygen supply of about  $400 \mu\text{mol kg}^{-1} \text{yr}^{-1}$ . In steady  
725 | state other oxygen transport processes and consumption are required to balance this  
726 | substantial oxygen supply. While vertical advection during the upwelling season might  
727 | contribute to the balance, the oxygen supply due to other transport processes should be at least  
728 | an order of magnitude lower in this region. The diapycnal oxygen supply to the upper  
729 | thermocline can thus be used to define an upper limit of the oxygen consumption below the  
730 | mixed layer. Such a consumption rate is, however, two orders of magnitude larger than the  
731 | one estimated for the deep ocean as discussed above.

732 | The results suggest that the high oxygen demand of the water column and the sediments  
733 | within the upwelling region at shallow depths above the shallow OMZ may well be supplied  
734 | from the surface via diapycnal mixing. At larger, depths however, the continental slope must  
735 | be ventilated via advective processes or isopycnal mixing. Nevertheless, although benthic  
736 | oxygen uptake is an important local process decreasing oxygen levels in the bottom waters  
737 | along the continental slope, it is negligible for the overall oxygen balance of the deep open  
738 | ocean OMZ.

739

## 740 | **7 Long-term variability in ETNA OMZ**

741 | OMZs of the tropical oceans expanded and intensified during the last 50 years. Decreasing  
742 | oxygen trends were found for the 300-700 m layers of selected regions with the strongest  
743 | decrease in the ETNA of  $-0.34 \pm 0.13 \mu\text{mol kg}^{-1} \text{yr}^{-1}$  for the region  $10\text{-}14^\circ \text{N}$ ,  $20\text{-}30^\circ \text{W}$   
744 | (Stramma et al., 2008b). The global analysis of observed changes in the oxygen content  
745 | between 1960-1974 and 1990-2008 indicates a widespread and significant deoxygenation at  
746 | about 200 m depth in the tropical oceans (Stramma et al., 2010b). In the ETNA, this depth  
747 | level corresponds to the intermediate oxygen maximum between the deep and shallow OMZs  
748 | that is mainly ventilated by advection via zonal jets. A similar regional pattern of

Peter Brandt 8.11.2014 13:16

Gelösch: As the mixed layer depth averages to about 20 m

Peter Brandt 8.11.2014 13:21

Gelösch: , the d

Peter Brandt 8.11.2014 13:31

Gelösch: oxygen flux

Peter Brandt 8.11.2014 13:21

Gelösch: completely

Peter Brandt 8.11.2014 13:39

Gelösch: at

Peter Brandt 27.10.2014 12:27

Gelösch: below

Peter Brandt 8.11.2014 13:34

Gelösch: 10

Peter Brandt 27.10.2014 12:28

Gelösch: Below that

758 deoxygenation as for the 200 m level was found when vertically averaging oxygen changes  
759 over 200-700 m, albeit with a smaller amplitude (Stramma et al., 2010b).

760 One of the main questions regarding the observed oxygen trend is its possible relation to  
761 anthropogenic forcing that was suggested in a number of recent studies (Bopp et al.,  
762 2002;Keeling and Garcia, 2002;Plattner et al., 2002;Matear and Hirst, 2003;Oschlies et al.,  
763 2008;Schmittner et al., 2008;Frölicher et al., 2009;Keeling et al., 2010;Helm et al., 2011).  
764 Different mechanisms were suggested. Global warming results in decreasing oxygen  
765 solubility in surface waters, and due to the increasing upper ocean stratification, it might  
766 impact ocean circulation, subduction, and vertical mixing. Increased CO<sub>2</sub> levels and ocean  
767 acidification might impact biogeochemistry and oxygen consumption as well. However, up to  
768 now, current coupled climate-biogeochemistry models fail to reproduce the observed regional  
769 patterns of the oxygen trend, thus prohibiting a solid conclusion to be drawn about driving  
770 mechanisms of the observed on-going deoxygenation (Stramma et al., 2012).

771 Similarly it remains an open question, how much of the observed oxygen changes are related  
772 to internal variability of the ocean and the climate system and what the dominant mechanisms  
773 are. The analysis of dissolved oxygen concentrations at 300 m depth in the tropical and South  
774 Atlantic Ocean south of 20° N obtained from stations collected during the 1925-to-1927  
775 Meteor Expedition and the period 1990-2008 showed different and sometimes reversed trends  
776 compared to the mean oxygen trends found for the last 50 years, which indicates that the trend  
777 is not continuous but multidecadal variations are superimposed (Stramma et al., 2012). The  
778 oxygen trend along 23° W for the period 1972 to 2013 indicates a widespread oxygen decline  
779 with the strongest oxygen reduction above the core of the deep OMZ and north of the Cape  
780 Verde archipelago (Fig. 18). However, oxygen anomalies within two boxes covering the  
781 region of relatively high oxygen above the deep oxycline (150-300 m) and the core region of  
782 the deep OMZ (350-700 m) (Fig. 19) show varying trends over the extended period (1900-  
783 2013) and the more recent period of enhanced measurements from 2006 to 2013. Note that the  
784 trend over the extended period is dominated by data taken during the 1970's, 1980's and the  
785 period 2006-2013. For the intermediate oxygen maximum (150-300 m) there is only a weak  
786 oxygen decline during the period 1900-2013 of  $-0.8 \pm 0.5 \mu\text{mol kg}^{-1} \text{decade}^{-1}$ , while during the  
787 period 2006-2013 a much stronger decline of  $-14.3 \pm 6.9 \mu\text{mol kg}^{-1} \text{decade}^{-1}$  was observed. For  
788 the deep oxygen minimum (350-700 m) the long-term trend for the period 1900-2013 is  
789  $-1.8 \pm 0.3 \mu\text{mol kg}^{-1} \text{decade}^{-1}$ , while during the period 2006-2013 oxygen increased by  $2.7 \pm 1.9$   
790  $\mu\text{mol kg}^{-1} \text{decade}^{-1}$ . These variations in the obtained trends that are related to different time

791 scales and depth ranges may help to understand underlying mechanism of long-term oxygen  
792 changes.

793 Different mechanisms might contribute to decadal to multidecadal oxygen variability: 1)  
794 Decadal to multidecadal AMOC changes would result in changes of the water mass  
795 distribution in the tropical North Atlantic as identified for example in simulations with ocean-  
796 atmosphere general circulation models (Chang et al., 2008). Shifts of the boundary between  
797 northern and southern hemisphere water masses would likely affect oxygen distribution as  
798 well. 2) The transport of Indian Ocean CW toward the Atlantic via the Agulhas leakage might  
799 have increased during the last decades due to a poleward shift of the southern hemisphere  
800 westerlies. Such a change was observable in the NBUC as an increase in CW salinity  
801 (Biaostoch et al., 2009) and might be associated with changes in the oxygen distribution as  
802 well. 3) Changes in the strength of latitudinally stacked zonal jets as derived by Brandt et al.  
803 (2010) result in changes in the advective pathways to the ETNA OMZ with likely strongest  
804 impact in the upper 300-400 m of the water column (Hahn et al., 2014). 4) Changes in the  
805 strength and location of the wind-driven gyres are a possible explanation for the long-term  
806 oxygen trends observed between 15° and 30° N in Fig. 18. 5) The variability of ventilation  
807 efficiency, either through dynamics (subduction) or saturation (warming) is able to produce  
808 oxygen anomalies that propagate into the ocean's interior (Karstensen et al., 2008).

809 In the North Atlantic, indications exist of a North Atlantic Oscillation (NAO) influence on  
810 multidecadal oxygen variations (Stendardo and Gruber, 2012). A similar influence of the  
811 NAO (e.g. due to associated changes in the northeast trade winds) on the water masses of the  
812 ETNA OMZ has not yet been shown. However, multidecadal changes in the strength of  
813 Atlantic STCs were detected in assimilation model runs. These changes include a minimum  
814 STC-layer (about 50-300 m) convergence in the early 1970's and a maximum in the early  
815 1990's (Rabe et al., 2008), which would affect the supply of newly subducted oxygen-rich  
816 water masses from the subtropics to the tropics.

817

## 818 **8 Similarities and differences between ETNA and ETSP OMZs**

819 Similar to the hypoxic ETNA OMZ, the suboxic ETSP OMZ is located in the shadow zone  
820 equatorward of the subtropical gyre with lowest oxygen levels near the shelf-break. The most  
821 prominent difference between both OMZs is that the ETSP OMZ covers a much wider region  
822 and that oxygen values in its core region are close to zero (Karstensen et al., 2008) while the  
823 typical large scale oxygen minimum in the ETNA only recently reached values slightly below

824 40  $\mu\text{mol kg}^{-1}$  (Stramma et al., 2009). A continuation of the observed deoxygenation in the  
825 ETNA would turn the ETNA OMZ suboxic within a century, hence it is worth to look at  
826 differences and similarities of the ETNA and the ETSP with regard to a possible shift of a  
827 hypoxic system to a suboxic system.

## 828 8.1 The large scale distribution

829 Different to the ETNA with its Guinea Dome, and the eastern tropical South Atlantic and  
830 eastern tropical North Pacific with similar domes there is no dome in the ETSP (Kessler,  
831 2006). Similar to the equatorial Atlantic, the equatorial Pacific is characterized by a local  
832 oxygen maximum and a system of eastward and westward currents (Figs. 2, 20). Near the  
833 equator, the EUC, the NICC and SICC all carry water richer in oxygen than the adjacent  
834 westward flows (Stramma et al., 2010a). In the eastern Pacific, the Northern and Southern  
835 Subsurface Countercurrents (NSCC and SSCC) are already low in oxygen and, different from  
836 the corresponding current bands in the Atlantic, do not provide oxygen-rich water to the  
837 OMZ. Near the Peruvian shelf, poleward and equatorward currents exist which supply  
838 equatorial and subtropical water to the eastern near shelf regions (Fig. 2). The Chile-Peru  
839 Coastal Current (CPCC) and the Peru-Chile Current (PCC) flow equatorward in the near-  
840 surface layer close to the coast and farther than ~150 km from the coast, respectively, while  
841 the Peru-Chile Undercurrent (PCUC) flows poleward in subsurface layers along the outer  
842 continental shelf and inner slope (Chaigneau et al., 2013). Based on a hydrographic survey off  
843 Peru in January and February 2009 and in combination with float data and model results,  
844 Czeschel et al. (2011) prepared a schematic on the intermediate circulation of the ETSP and  
845 its link to the OMZ. The centre of the OMZ is a stagnant flow area and the mean currents at  
846 400 m depth in the open ocean ETSP are weak. Along the ~86° W section, lowest oxygen is  
847 observed between 6° S and 10° S centred at about 400 m depth and on the isopycnal  $\sigma_\theta=26.8$   
848  $\text{kg m}^{-3}$ . Along this isopycnal the mean age is increased in the region of the low oxygen core  
849 with maximum mean age of about 300 yr at about 11° S, slightly poleward of the lowest  
850 oxygen concentration, and reduced near the equator with a mean age of about 200 yr (Fig.  
851 20).

## 852 8.2 Mesoscale processes

853 Mesoscale variability dominantly occurs as propagating Rossby waves and as nonlinear  
854 vortices or eddies. In particular, nonlinear vortices can trap and transport momentum, heat,  
855 mass and the chemical constituents of seawater, and therefore contribute to the large scale  
856 water mass distribution (Chelton et al., 2007). Eddies are mainly generated by coastal flow

Peter Brandt 8.11.2014 17:03

Gelösch: the

Peter Brandt 8.11.2014 17:03

Gelösch: in

Peter Brandt 8.11.2014 17:02

Gelösch: the ETNA

Peter Brandt 8.11.2014 17:03

Gelösch: similar domes in

Peter Brandt 1.11.2014 11:38

Gelösch: T

Peter Brandt 8.11.2014 17:06

Gelösch: the

Peter Brandt 14.11.2014 17:08

Gelösch: linear

Peter Brandt 14.11.2014 17:09

Gelösch: contrast to linear waves

Peter Brandt 8.11.2014 17:26

Gelösch:



866 | instabilities that are influenced by remote equatorial forcing via coastal-trapped waves  
867 | (Belmadani et al., 2012). They move from the coastal upwelling regions westward and hence  
868 | transport shelf waters offshore. These eddies affect the regions' biogeochemical budgets, but  
869 | also the primary productivity of the regions (Lachkar and Gruber, 2012) and seem to play a  
870 | important role for the oxygen distribution on the poleward side of the OMZ's. In global  
871 | satellite observations of nonlinear mesoscale eddies by Chelton et al. (2011) it turned out that  
872 | in the ETNA south and east of the Cape Verde Islands almost no eddies with a lifetime of  $\geq 16$   
873 | weeks were present, while in the ETSP a large number of such eddies could be identified,  
874 | their occurrence extends close to the equator and the Peruvian shelf as can be seen in Figure  
875 | 4a of Chelton et al. (2011). Despite the inferred weak eddy activity in the ETNA, water mass  
876 | anomalies including local oxygen minima at shallow depth just below the mixed layer have  
877 | been found in cyclonic as well as in anticyclonic mode water eddies in this region (see Fig. 4,  
878 | showing few profiles with oxygen concentration below  $40 \mu\text{mol kg}^{-1}$ ). In the ETSP, a region  
879 | of high eddy production is located just off the shelf at  $15\text{-}16^\circ \text{ S}$  and strong eddies were  
880 | described from a survey in November 2012. A strong anticyclonic mode water eddy located  
881 | near the shelf of Peru at about  $16^\circ \text{ S}$  showed a heat anomaly of  $17.7 \times 10^{18} \text{ J}$ , a salt anomaly of  
882 |  $36.5 \times 10^{10} \text{ kg}$  (Stramma et al., 2013) and an oxygen anomaly of  $-10.0 \times 10^{16} \mu\text{mol}$  (Stramma et  
883 | al., 2014). Even in a mooring at  $\sim 20^\circ \text{ S}$ ,  $85^\circ \text{ W}$  some 1500 km offshore the passage of an  
884 | anticyclonic mode water eddy carrying an oxygen anomaly of  $-10.5 \times 10^{16} \mu\text{mol}$  could be  
885 | observed (Stramma et al., 2014). As eddies fall apart at the end of their lifetime the anomalous  
886 | hydrographic and biogeochemistry anomalies are redistributed in the ocean.

### 887 | **8.3 Oxygen budgets**

888 | A quantitative evaluation of the different terms of the oxygen budget of the tropical Pacific  
889 | OMZ could not be performed so far. A rough estimate of the oxygen budget was instead given  
890 | by Stramma et al. (2010a). They estimated the advective oxygen supply to the tropical Pacific  
891 | OMZ from oxygen concentrations at, and zonal mass transport across, the  $125^\circ \text{ W}$  meridian.  
892 | The eastward mass transport associated with the EUC, SCC's and ICCs was estimated to be  
893 | about  $30 \times 10^9 \text{ kg s}^{-1}$ . It was assumed that this mass transport is returned by the adjacent  
894 | westward currents with a typical relative oxygen difference between eastward and westward  
895 | currents of about  $20 \mu\text{mol kg}^{-1}$ . The resulting net advective molar oxygen supply across  $125^\circ$   
896 | W is  $0.6 \times 10^6 \text{ mol s}^{-1}$  (Stramma et al., 2010a). The diffusive supply was estimated through the  
897 | climatological  $60 \mu\text{mol kg}^{-1}$  surface surrounding the tropical Pacific OMZ. Vertical and lateral  
898 | oxygen gradients were evaluated at this surface and multiplied with a diapycnal diffusivity of

900 |  $1 \times 10^{-5} \text{ m}^2 \text{ s}^{-1}$  (Ledwell et al., 1998) and a horizontal eddy diffusivity of  $500 \text{ m}^2 \text{ s}^{-1}$   
901 characteristic for the off-equatorial regions (Davis, 2005), respectively. Integrating these  
902 products over the surface area resulted in a vertical diffusive molar oxygen supply of  $0.4 \times 10^6$   
903  $\text{mol s}^{-1}$  mostly through the upper surface, where the gradients are large, and in a lateral  
904 diffusive molar oxygen supply of  $0.8 \times 10^6 \text{ mol s}^{-1}$  (Stramma et al., 2010a). The mass of the  
905 tropical Pacific OMZs between  $30^\circ \text{ N}$  and  $30^\circ \text{ S}$  with oxygen concentrations  $< 60 \mu\text{mol kg}^{-1}$  is  
906 about  $16 \times 10^{18} \text{ kg}$ . Dividing the estimates of molar supply by the mass leads to an advective  
907 oxygen supply of about  $1.2 \mu\text{mol kg}^{-1} \text{ yr}^{-1}$ , a lateral diffusive oxygen supply of  $1.6 \mu\text{mol kg}^{-1}$   
908  $\text{yr}^{-1}$  and a vertical diffusive oxygen supply of  $0.8 \mu\text{mol kg}^{-1} \text{ yr}^{-1}$ . The oxygen utilization rate  
909 calculated to balance the net oxygen supply resulted in about  $3.6 \mu\text{mol kg}^{-1} \text{ yr}^{-1}$ . These rough  
910 estimates of the oxygen budget are far from being a reliable result, however it points to an  
911 allocation of about 33 % by advection, 45 % by eddy mixing and 22 % by vertical mixing.  
912 The calculation of the tropical Pacific oxygen budget differs from the calculation of the  
913 ETNA oxygen budget presented above: While advection along the equator is included in the  
914 oxygen supply to the tropical Pacific OMZ, it is not in the ETNA OMZ. The budget of the  
915 ETNA OMZ included only the advective supply by zonal jets in the latitude range of the  
916 ETNA OMZ, while eddy mixing meridionally fluxes oxygen from the subtropical gyre in the  
917 north and the well-ventilated equatorial region in the south into the ETNA OMZ.

#### 918 **8.4 Trends in oxygen**

919 As the ETSP OMZ is extremely low in oxygen a decreasing trend is much more difficult to  
920 determine. Furthermore, data are sparse to investigate the trend. However, for the eastern  
921 Pacific equatorial region ( $5^\circ \text{ S}$  to  $5^\circ \text{ N}$ ,  $105\text{-}115^\circ \text{ W}$ ) a decrease of  $0.13 \pm 0.32 \mu\text{mol kg}^{-1} \text{ yr}^{-1}$   
922 was described (Stramma et al., 2008b) for the 300-700 m depth layer for the last 50 years. The  
923 stronger decrease in oxygen in the ETNA compared to the ETSP is also visible from a global  
924 compilation of the trends of the last 50 years at 300 m depth (Stramma et al., 2012).

925 On interannual to multidecadal times scales oxygen variability in the ETSP is expected to be  
926 influenced by similar processes as those influencing the ETNA (see end of Sect. 7), but likely  
927 differ due to the different climate signals influencing these ocean basins. In the Pacific, the  
928 multidecadal variability of the Pacific Decadal Oscillation (PDO) has the strongest influence  
929 on long time scales, while El Niño/Southern Oscillation (ENSO), that mainly influences the  
930 upper 350 m of the ETSP, is superimposed on long-term changes (Czeschel et al., 2012). The  
931 variability of the Pacific STCs exhibits an ENSO signature with strong meridional transport  
932 occurring during La Niña and weak meridional transport during El Niño and hence is a

Peter Brandt 8.11.2014 18:00

Gelöscht: n isopycnal

Peter Brandt 8.11.2014 18:00

Gelöscht: on coefficient

Peter Brandt 8.11.2014 18:05

Gelöscht: while

Peter Brandt 14.11.2014 17:11

Gelöscht: ETNA and

937 possible mechanism for oxygen variability (Zilberman et al., 2013). Model runs indicate a  
938 control of decadal and bidecadal climate variability in the tropical Pacific by the off-  
939 equatorial South Pacific Ocean triggered by changes of wind stress curl in the South Pacific  
940 extratropics (Tatebe et al., 2013) as an additional mechanism for oxygen variability. Besides  
941 decadal to multidecadal changes in the ventilation processes, variations in the oxygen  
942 consumption have been suggested to result in changes of the suboxic and hypoxic volume of  
943 the tropical and subtropical Pacific on similar timescales (Deutsch et al., 2011; Ito and  
944 Deutsch, 2013). From 3 sediment cores along the North American margin Deutsch et al.  
945 (2014) proposed that centennial changes in the North Pacific anoxia are linked to changes of  
946 tropical trade winds and their effect on upwelling and biological production.

947

## 948 **9 Summary and discussion**

949 The aim of the present paper is to provide a synthesis of the results from recent efforts to  
950 understand the physical mechanisms underpinning the functioning of the OMZs in the eastern  
951 tropical oceans with a focus on the ETNA. The paper is mainly based on observations in the  
952 ETNA and the ETSP. The ETNA was selected to perform a dedicated observational program  
953 consisting of a large number of research cruises, continuous moored observations, and TREs  
954 to better understand the role of circulation and mixing in the ventilation of the OMZ. Results  
955 are summarized in the schematic Fig. 21. The ETSP was selected to allow a comparison of a  
956 hypoxic and a suboxic OMZ.

957 One of the main results of these efforts is a first quantification of the oxygen budget of the  
958 deep ETNA OMZ (Brandt et al., 2010; Fischer et al., 2013; Hahn et al., 2014) that is here  
959 extended to 800 m depth (Fig. 21). Integrating the different terms of the oxygen budget of the  
960 ETNA OMZ (Hahn et al., 2014) in the depth range below the deep oxycline from 350 m to  
961 570 m yields a consumption (after Karstensen et al. (2008)) mainly balanced by the  
962 divergence of the meridional eddy flux (about 60 %) and the divergence of the diapycnal flux  
963 (20 %). The obtained residual of about 20 % can be ascribed in equal parts to the zonal  
964 advection and the long-term oxygen tendency as taken from Brandt et al. (2010). However,  
965 these are rough estimates. Most of the terms in the oxygen budget are associated with  
966 significant error, which particularly is the case for consumption and meridional eddy flux.  
967 Due to the TRE (Banyte et al., 2012) and repeated microstructure measurements (Fischer et  
968 al., 2013) the error in the diapycnal oxygen supply is comparatively small. The diapycnal  
969 oxygen supply is strongest slightly above the deep OMZ core, where it accounts for about one

Peter Brandt 1.11.2014 13:39

Gelöscht: esent

Peter Brandt 1.11.2014 13:45

Gelöscht: in the framework of the SFB 754

972 third of the oxygen supply required to balance consumption. There are, however, indications  
973 of regional variations in the diapycnal eddy diffusivity with higher values over the seamount  
974 region (up to one order of magnitude) compared to the abyssal plains (Fig. 11) resulting also  
975 in a general increase of the diapycnal eddy diffusivity with depth (Fig. 12).

976 The contribution of the mean advection to the oxygen budget of the OMZ cannot yet be  
977 quantified from observational data. Instead, idealized advection-diffusion models were used  
978 to estimate this contribution (Brandt et al., 2010; Brandt et al., 2012). For these calculations a  
979 basin-wide mean velocity field has to be prescribed based mainly on our knowledge of the  
980 mean flow along 23°W. However, the zonal extent of the zonal jets, their deviation from a  
981 purely zonal flow, and their connection to the well-ventilated western boundary regime are  
982 crucial in this calculation, but are not well constrained by observations, which leads again to a  
983 large uncertainty of the contribution of the mean advection to the oxygen budget of the ETNA  
984 OMZ.

985 Consumption as the main oxygen sink in the oxygen budget of the OMZ is currently best  
986 estimated as the net consumption along a water mass path from the subduction region toward  
987 the OMZ (Haine and Hall, 2002; Karstensen et al., 2008; Schneider et al., 2012). The different  
988 methods presented here yield a range of possible net consumption rates differing by a factor  
989 of 2 to 4 (Fig. 17). Besides this uncertainty, AOUR represents a large scale net consumption  
990 rate that cannot account for the regional inhomogeneity in consumption for example due to  
991 higher productivity in coastal, equatorial or open ocean upwelling regions compared to the  
992 oligotrophic ocean. For a local oxygen budget as presented here, the local oxygen  
993 consumption within the OMZ is required which could substantially differ from values  
994 representing an integrated oxygen consumption along pathways from the subduction regions,  
995 through the oligotrophic ocean (often including the western boundary regime) into the OMZs.  
996 Additionally, the assumption of a consumption profile decreasing exponentially with depth  
997 (Martin et al., 1987) might be invalid. Lutz et al. (2002) noted the inability to fit sediment trap  
998 data to a single exponential function. Due to vertical changes in lability of organic matter,  
999 sinking rate, and mineral ballast effect, they therefore suggested to use the sum of two  
1000 exponential functions with different decay. Processes that would also contribute to a deviation  
1001 from a single exponential profile include respiration associated with the daily vertical  
1002 migration cycle of zooplankton (Bianchi et al., 2013) or oxygen consumption at the sediment-  
1003 ocean interface and associated lateral spreading of low oxygen waters. To tackle the problem  
1004 of regional and temporal consumption variability new targeted data/model approaches are

Peter Brandt 4.11.2014 16:21

**Gelösch:** The presence of seamounts in extended parts of ETNA OMZ might explain the observed smaller equatorward reduction of the diapycnal diffusivity than expected from internal wave-wave interaction theory (Heney et al., 1986; Gregg et al., 2003; Banyte et al., 2012). It might also be responsible for an increased diapycnal oxygen supply from below (Figs. 11, 13).

Peter Brandt 14.11.2014 17:13

**Gelösch:** The strength of the zonal jets penetrating into the ETNA OMZ (as well as into the ETSP OMZ) is of the order of a few cm/s and generally smaller than the characteristic eddy velocity (Hahn et al., 2014); the contribution of the zonal mean advection calculated from the currently available number of repeated ship sections remains thus uncertain. Note that the few moorings in the ETNA OMZ do not resolve the meridional structure of latitudinally stacked zonal jets.

Peter Brandt 14.11.2014 17:14

**Gelösch:** e

Peter Brandt 14.11.2014 17:14

**Gelösch:** of mean advection to the oxygen budget of the OMZ

Peter Brandt 27.10.2014 17:59

**Gelösch:** . The TTD concept additionally accounts for mixing between water masses following different paths

Peter Brandt 27.10.2014 18:46

**Gelösch:** Obtained net consumption estimates strongly depend on the water mass age and the comparison of different methods to derive such ages

Peter Brandt 27.10.2014 18:46

**Gelösch:** s

Peter Brandt 27.10.2014 18:48

**Gelösch:** these estimates

Peter Brandt 27.10.2014 18:49

**Gelösch:** s

1035 required including observations of sinking particles or incubations for estimating pelagic  
1036 oxygen consumption.

1037 The relative importance of the different terms affecting the oxygen budgets of the ETNA and  
1038 ETSP OMZs appear to be similar. For both OMZs the eastward advection of oxygen-rich  
1039 waters from the well-ventilated western boundary was found to be a dominant ventilation  
1040 process. As the zonal currents are of similar strength in the tropical Pacific and Atlantic, the  
1041 difference in the basin width of both oceans consequently results in lower oxygen  
1042 concentrations and larger water mass ages in the eastern tropical Pacific (Fig. 20) compared to  
1043 the eastern tropical Atlantic (Fig. 6).

1044 Processes contributing to the oxygen budget at the eastern boundary include diapycnal mixing,  
1045 locally elevated due to tide-topography interaction, advective oxygen supply associated with  
1046 (seasonally varying) eastern boundary circulation and coastal-trapped waves, mesoscale  
1047 eddies favouring and redistributing oxygen anomalies, pelagic consumption and consumption  
1048 at the sediment-ocean interface. Due to high variability of most of these processes both in  
1049 space and time, the mean oxygen budget at the shelf is much less constrained compared to the  
1050 open ocean. Often these processes are characterized by strong physical-biogeochemical  
1051 interaction. For example the downward oxygen flux from the mixed layer due to elevated  
1052 diapycnal mixing at the shelf (Schafstall et al., 2010) must be balanced at least partly by local  
1053 consumption. The extremely large vertical oxygen gradients at the shelf in the ETSP (from  
1054 saturated oxygen levels in the mixed layer to zero oxygen within few meters below) suggest  
1055 extremely high consumptions rates just below the mixed layer. Another example are isolated  
1056 eddies generated by the instability of the eastern boundary current. Such eddies transfer shelf  
1057 water properties toward the open ocean while transforming these properties (particularly  
1058 oxygen) by enhanced physical-biogeochemical interactions during their westward migration  
1059 (Stramma et al., 2014). Their influence on the mean distribution of the shallow and deep  
1060 OMZ could so far not be quantified. Dedicated process studies using mooring arrays,  
1061 shipboard and multiple glider observations may help to elucidate the role of different  
1062 processes in the eastern boundary oxygen budget.

1063 The increase in resolution of ocean circulation models improves the tropical circulation and  
1064 associated oxygen distribution in the Atlantic (Duteil et al., 2014) and the Pacific OMZs  
1065 (Montes et al., 2014), suggesting that deficiencies in model physics largely contribute to the  
1066 oxygen bias in coarser-resolution models. However, particularly the intermediate circulation  
1067 (below 250 m) is still underestimated by these high-resolution simulations in realistic settings.

Peter Brandt 27.10.2014 14:26

Gelöscht: ,

Peter Brandt 1.11.2014 10:53

[1] verschoben (Einfügung)

Peter Brandt 1.11.2014 10:53

Gelöscht: Nevertheless, t

Peter Brandt 1.11.2014 10:51

Gelöscht: Ocean circulation is the main factor setting the OMZ boundaries.

Peter Brandt 1.11.2014 10:53

[1] nach oben verschoben: Nevertheless, the increase in resolution of ocean circulation models improves the tropical circulation and associated oxygen distribution (Duteil et al., 2014), suggesting that model physics largely contribute to the oxygen bias in coarser-resolution models.

Peter Brandt 1.11.2014 10:40

Gelöscht: (Duteil et al., 2014) Poleward of the tropical Atlantic and Pacific OMZs are the well-ventilated subtropical gyres. The OMZs of both hemispheres are separated by an equatorial oxygen maximum (Figs. 1, 2) that is generated by the energetic flow composed of narrow zonal jets along the equator (Stramma et al., 2010a; Brandt et al., 2012). In the vertical the ETNA OMZ is characterized by an intermediate oxygen maximum at about 200-300 m separating the shallow from the deep oxygen minimum (Fig. 21). From the residual of the oxygen budget it could be concluded that this intermediate oxygen maximum can be ascribed to the oxygen supply by advection associated with latitudinally stacked zonal jets (Hahn et al., 2014) [2]

Peter Brandt 1.11.2014 10:56

Gelöscht: Duteil et al. (2014)

Peter Brandt 1.11.2014 10:56

Gelöscht: ).

1096 | To identify the physical mechanism responsible for the mean and variable zonal jets, idealized  
1097 high-resolution models have been employed (Ménesguen et al., 2009;Ascani et al., 2010;Qiu  
1098 et al., 2013). Such idealized models could further be used, by including oxygen in the  
1099 simulations, to study the roles of mean and variable advection in maintaining the tropical  
1100 OMZs and to identify the mechanisms driving oxygen variability on interannual to  
1101 multidecadal timescales.

Peter Brandt 2.11.2014 18:30

Gelöscht:

1102 The oxygen decline in the ETNA OMZ during the last decades corresponds to about 10 % of  
1103 the oxygen sink due to consumption not balanced by ventilation processes. This is a  
1104 substantial imbalance in the oxygen budget of the ETNA OMZ. The regional pattern along the  
1105 23° W section indicates strongest oxygen reduction above the core of the deep OMZ and  
1106 north of the Cape Verde archipelago (Fig. 18). Such a regional pattern is most likely due to  
1107 changes in the circulation pattern associated with forced ocean dynamics as well as with  
1108 internal ocean dynamics. Time series of all available oxygen data of the ETNA OMZ (Fig.  
1109 19) indicate variations on interannual, decadal, and multidecadal time scales; the long-term  
1110 trend of deoxygenation associated with anthropogenic climate changes might not be the  
1111 dominant signal on such a regional scale. Improvements of model ventilation physics by  
1112 increased resolution and/or improved parameterizations will reduce errors in the simulated  
1113 mean oxygen distribution and its variability, but at the same time will help to better  
1114 understand the climate sensitivity of OMZ with regard to anthropogenic climate change.

Peter Brandt 8.11.2014 22:35

Gelöscht: associated with

1115 Oxygen data from shipboard repeat hydrography and moored observations show substantial  
1116 interannual variability (Fig. 8) and trend-like changes (Fig. 19). The continuation of such  
1117 measurements is essential to be able to test different hypotheses for the driving mechanisms  
1118 of oxygen changes in the ocean. Using idealized or process models, distinct observed  
1119 variability patterns might be reproduced and attributed to circulation changes and/or changes  
1120 in the water mass distribution associated with the AMOC, STCs, PDO, or ENSO. For ocean  
1121 circulation models the acquired data provide the basis for improving the physical system in  
1122 coupled climate-biogeochemistry simulations to make projection of future oxygen evolution  
1123 more reliable.

Peter Brandt 8.11.2014 22:43

Gelöscht: Up to now, the regional pattern of observed oxygen changes cannot be reproduced by coupled climate-biogeochemistry models (Stramma et al., 2012), which could be the result of biases in the simulated mean circulation and oxygen distribution. Today it remains an open question how such biases influence the evolution of the oceanic oxygen content under on-going anthropogenic climate change in coupled climate-biogeochemistry simulations.

Peter Brandt 8.11.2014 22:11

Gelöscht: -

... [3]

Peter Brandt 1.11.2014 13:55

Gelöscht: during the period 2006-2013

Peter Brandt 1.11.2014 13:55

Gelöscht: but also substantial interannual variability as for example associated with the EDJ (Fig. 8)

Peter Brandt 1.11.2014 13:56

Gelöscht: extension

Peter Brandt 1.11.2014 16:32

Gelöscht: these

Peter Brandt 1.11.2014 13:56

Gelöscht: time series

## 1124 Acknowledgments

1125 This study was funded by the Deutsche Forschungsgemeinschaft as part of the  
1126 Sonderforschungsbereich 754 "Climate-Biogeochemistry Interactions in the Tropical Ocean",  
1127 through several research cruises with RV *Meteor* and RV *Maria S. Merian* and by the  
1128 Deutsche Bundesministerium für Bildung und Forschung (BMBF) as part of the projects

1150 | NORDATLANTIK ([03F0605B](#), 03F0443B), RACE (03F0651B), SOPRAN ([03F0462A](#),  
1151 | [03F0662A](#)), and AWA (01DG12073E). Moored velocity and oxygen observations were partly  
1152 | acquired in cooperation with the PIRATA project and we would like to thank B. Bourlès, R.  
1153 | Lumpkin, C. Schmid, and G. Foltz for their help with mooring work and data sharing. We  
1154 | also thank J. Lübbecke, L. D. Bryant, and [B. Dewitte](#) for helpful discussions and comments  
1155 | on an earlier version of the manuscript. We thank the captains and crew of the RV *Maria S.*  
1156 | *Merian*, RV *Meteor*, [RV Poseidon](#), and RV *L'Atalante* as well as our technical group for their  
1157 | help with the fieldwork.

Peter Brandt 28.10.2014 16:08

**Gelöscht:** and

1159 **References**

- 1160 Ascani, F., Firing, E., Dutrieux, P., McCreary, J. P., and Ishida, A.: Deep equatorial ocean circulation  
1161 induced by a forced-dissipated Yanai beam, *J Phys Oceanogr*, 40, 1118-1142, 10.1175/2010jpo4356.1,  
1162 2010.
- 1163 Banyte, D., Tanhua, T., Visbeck, M., Wallace, D. W. R., Karstensen, J., Krahnmann, G., Schneider, A.,  
1164 Stramma, L., and Dengler, M.: Diapycnal diffusivity at the upper boundary of the tropical North  
1165 Atlantic oxygen minimum zone, *J Geophys Res-Oceans*, 117, 10.1029/2011jc007762, 2012.
- 1166 Banyte, D., Visbeck, M., Tanhua, T., Fischer, T., Krahnmann, G., and Karstensen, J.: Lateral diffusivity  
1167 from tracer release experiments in the tropical North Atlantic thermocline, *J Geophys Res-Oceans*,  
1168 118, 2719-2733, 10.1002/Jgrc.20211, 2013.
- 1169 Barton, E. D.: The poleward undercurrent on the eastern boundary of the subtropical North Atlantic,  
1170 in: *Poleward flows along Eastern Ocean Boundaries*, Lecture Note Series ed., edited by: Neshyba, S.  
1171 J., Smith, R. L., and Mooers, C. N. K., Springer-Verlag, 82-95, 1989.
- 1172 Belmadani, A., Echevin, V., Dewitte, B., and Colas, F.: Equatorially forced intraseasonal propagations  
1173 along the Peru-Chile coast and their relation with the nearshore eddy activity in 1992-2000: A  
1174 modeling study, *J Geophys Res-Oceans*, 117, 10.1029/2011jc007848, 2012.
- 1175 Bianchi, D., Galbraith, E. D., Carozza, D. A., Mislán, K. A. S., and Stock, C. A.: Intensification of  
1176 open-ocean oxygen depletion by vertically migrating animals, *Nat Geosci*, 6, 545-548,  
1177 10.1038/Ngeo1837, 2013.
- 1178 Biastoch, A., Böning, C. W., Schwarzkopf, F. U., and Lutjeharms, J. R. E.: Increase in Agulhas  
1179 leakage due to poleward shift of Southern Hemisphere westerlies, *Nature*, 462, 495-498,  
1180 10.1038/nature08519, 2009.
- 1181 Bolin, B., and Rodhe, H.: Note on Concepts of Age Distribution and Transit-Time in Natural  
1182 Reservoirs, *Tellus*, 25, 58-62, 1973.
- 1183 Bopp, L., Le Quere, C., Heimann, M., Manning, A. C., and Monfray, P.: Climate-induced oceanic  
1184 oxygen fluxes: Implications for the contemporary carbon budget, *Global Biogeochem Cy*, 16,  
1185 10.1029/2001gb001445, 2002.
- 1186 Bourles, B., Lumpkin, R., McPhaden, M. J., Hernandez, F., Nobre, P., Campos, E., Yu, L. S., Planton,  
1187 S., Busalacchi, A., Moura, A. D., Servain, J., and Trotte, J.: The PIRATA program: History,  
1188 accomplishments, and future directions, *B Am Meteorol Soc*, 89, 1111-1125,  
1189 10.1175/2008bams2462.1, 2008.
- 1190 Brandt, P., Hormann, V., Bourles, B., Fischer, J., Schott, F. A., Stramma, L., and Dengler, M.: Oxygen  
1191 tongues and zonal currents in the equatorial Atlantic, *J Geophys Res-Oceans*, 113,  
1192 10.1029/2007jc004435, 2008.
- 1193 Brandt, P., Hormann, V., Körtzinger, A., Visbeck, M., Krahnmann, G., Stramma, L., Lumpkin, R., and  
1194 Schmid, C.: Changes in the ventilation of the oxygen minimum zone of the tropical North Atlantic, *J*  
1195 *Phys Oceanogr*, 40, 1784-1801, 10.1175/2010jpo4301.1, 2010.
- 1196 Brandt, P., Funk, A., Hormann, V., Dengler, M., Greatbatch, R. J., and Toole, J. M.: Interannual  
1197 atmospheric variability forced by the deep equatorial Atlantic Ocean, *Nature*, 473, 497-500,  
1198 10.1038/Nature10013, 2011.
- 1199 Brandt, P., Greatbatch, R. J., Claus, M., Didwischus, S. H., Hormann, V., Funk, A., Hahn, J.,  
1200 Krahnmann, G., Fischer, J., and Körtzinger, A.: Ventilation of the equatorial Atlantic by the equatorial  
1201 deep jets, *J Geophys Res-Oceans*, 117, 10.1029/2012jc008118, 2012.
- 1202 Canfield, D. E.: Organic Matter Oxidation in Marine Sediments, in: *Interactions of C, N, P and S*  
1203 *Biogeochemical Cycles and Global Change*, edited by: Wollast, R., Mackenzie, F. T., and Chou, L.,  
1204 NATO ASI Series, Springer Berlin Heidelberg, 333-363, 1993.
- 1205 Chaigneau, A., Dominguez, N., Eldin, G., Vasquez, L., Flores, R., Grados, C., and Echevin, V.: Near-  
1206 coastal circulation in the Northern Humboldt Current System from shipboard ADCP data, *J Geophys*  
1207 *Res-Oceans*, 118, 5251-5266, 10.1002/Jgrc.20328, 2013.
- 1208 Chang, P., Zhang, R., Hazeleger, W., Wen, C., Wan, X. Q., Ji, L., Haarsma, R. J., Breugem, W. P.,  
1209 and Seidel, H.: Oceanic link between abrupt changes in the North Atlantic Ocean and the African  
1210 monsoon, *Nat Geosci*, 1, 444-448, 10.1038/Ngeo218, 2008.
- 1211 Chelton, D. B., Schlax, M. G., Samelson, R. M., and de Szoeke, R. A.: Global observations of large  
1212 oceanic eddies, *Geophys Res Lett*, 34, 10.1029/2007gl030812, 2007.



1213 Chelton, D. B., Schlax, M. G., and Samelson, R. M.: Global observations of nonlinear mesoscale  
 1214 eddies, *Prog Oceanogr*, 91, 167-216, 10.1016/J.Pocean.2011.01.002, 2011.  
 1215 Czeschel, R., Stramma, L., Schwarzkopf, F. U., Giese, B. S., Funk, A., and Karstensen, J.: Middepth  
 1216 circulation of the eastern tropical South Pacific and its link to the oxygen minimum zone, *J Geophys  
 1217 Res-Oceans*, 116, 10.1029/2010jc006565, 2011.  
 1218 Czeschel, R., Stramma, L., and Johnson, G. C.: Oxygen decreases and variability in the eastern  
 1219 equatorial Pacific, *J Geophys Res-Oceans*, 117, 10.1029/2012jc008043, 2012.  
 1220 d'Orgeville, M., Hua, B. L., and Sasaki, H.: Equatorial deep jets triggered by a large vertical scale  
 1221 variability within the western boundary layer, *J Mar Res*, 65, 1-25, 10.1357/002224007780388720,  
 1222 2007.  
 1223 Dale, A. W., Sommer, S., Ryabenko, E., Noffke, A., Bohlen, L., Wallmann, K., Stolpovsky, K.,  
 1224 Greinert, J., and Pfannkuche, O.: Benthic nitrogen fluxes and fractionation of nitrate in the  
 1225 Mauritanian oxygen minimum zone (Eastern Tropical North Atlantic), *Geochim Cosmochim Acta*, 134,  
 1226 234-256, 10.1016/J.Gca.2014.02.026, 2014.  
 1227 Davis, R. E.: Intermediate-depth circulation of the Indian and South Pacific Oceans measured by  
 1228 autonomous floats, *J Phys Oceanogr*, 35, 683-707, 10.1175/Jpo2702.1, 2005.  
 1229 Deutsch, C., Brix, H., Ito, T., Frenzel, H., and Thompson, L.: Climate-Forced Variability of Ocean  
 1230 Hypoxia, *Science*, 333, 336-339, 10.1126/Science.1202422, 2011.  
 1231 Deutsch, C., Berelson, W., Thunell, R., Weber, T., Tems, C., McManus, J., Crusius, J., Ito, T.,  
 1232 Baumgartner, T., Ferreira, V., Mey, J., and van Geen, A.: Centennial changes in North Pacific anoxia  
 1233 linked to tropical trade winds, *Science*, 345, 665-668, 10.1126/Science.1252332, 2014.  
 1234 Duteil, O., Schwarzkopf, F. U., Böning, C. W., and Oschlies, A.: Major role of the equatorial current  
 1235 system in setting oxygen levels in the eastern tropical Atlantic Ocean: A high-resolution model study,  
 1236 *Geophys Res Lett*, 41, 2033-2040, 10.1002/2013gl058888, 2014.  
 1237 Eden, C.: Eddy length scales in the North Atlantic Ocean, *J Geophys Res-Oceans*, 112,  
 1238 10.1029/2006jc003901, 2007.  
 1239 Eden, C., and Greatbatch, R. J.: A diagnosis of isopycnal mixing by mesoscale eddies, *Ocean Model*,  
 1240 27, 98-106, 10.1016/j.ocemod.2008.12.002, 2009.  
 1241 Ferrari, R., and Polzin, K. L.: Finescale structure of the T-S relation in the eastern North Atlantic, *J  
 1242 Phys Oceanogr*, 35, 1437-1454, 10.1175/Jpo2763.1, 2005.  
 1243 Fischer, T., Banyte, D., Brandt, P., Dengler, M., Krahnemann, G., Tanhua, T., and Visbeck, M.:  
 1244 Diapycnal oxygen supply to the tropical North Atlantic oxygen minimum zone, *Biogeosciences*, 10,  
 1245 5079-5093, 10.5194/Bg-10-5079-2013, 2013.  
 1246 Frölicher, T. L., Joos, F., Plattner, G. K., Steinacher, M., and Doney, S. C.: Natural variability and  
 1247 anthropogenic trends in oceanic oxygen in a coupled carbon cycle-climate model ensemble, *Global  
 1248 Biogeochem Cy*, 23, 10.1029/2008gb003316, 2009.  
 1249 Glud, R. N.: Oxygen dynamics of marine sediments, *Mar Biol Res*, 4, 243-289,  
 1250 10.1080/17451000801888726, 2008.  
 1251 Gnanadesikan, A., Bianchi, D., and Pradal, M. A.: Critical role for mesoscale eddy diffusion in  
 1252 supplying oxygen to hypoxic ocean waters, *Geophys Res Lett*, 40, 5194-5198, 10.1002/Grl.50998,  
 1253 2013.  
 1254 Gregg, M. C., Sanford, T. B., and Winkel, D. P.: Reduced mixing from the breaking of internal waves  
 1255 in equatorial waters, *Nature*, 422, 513-515, 10.1038/Nature01507, 2003.  
 1256 Gutierrez, D., Enriquez, E., Purca, S., Quipuzcoa, L., Marquina, R., Flores, G., and Graco, M.:  
 1257 Oxygenation episodes on the continental shelf of central Peru: Remote forcing and benthic ecosystem  
 1258 response, *Prog Oceanogr*, 79, 177-189, 10.1016/J.Pocean.2008.10.025, 2008.  
 1259 Hagen, E.: Northwest African upwelling scenario, *Oceanol Acta*, 24, 113-128, 10.1016/S0399-  
 1260 1784(00)01110-5, 2001.  
 1261 Hahn, J., Brandt, P., Greatbatch, R. J., Krahnemann, G., and Körtzinger, A.: Oxygen variance and  
 1262 meridional oxygen supply in the Tropical North East Atlantic oxygen minimum zone, *Clim Dynam*, 1-  
 1263 26, 10.1007/s00382-014-2065-0, 2014.  
 1264 Haine, T. W. N., and Hall, T. M.: A generalized transport theory: Water-mass composition and age, *J  
 1265 Phys Oceanogr*, 32, 1932-1946, 10.1175/1520-0485(2002)032<1932:Agttwm>2.0.Co;2, 2002.  
 1266 Helm, K. P., Bindoff, N. L., and Church, J. A.: Observed decreases in oxygen content of the global  
 1267 ocean, *Geophys Res Lett*, 38, 10.1029/2011gl049513, 2011.

1268 Henyey, F. S., Wright, J., and Flatte, S. M.: Energy and Action Flow through the Internal Wave Field -  
 1269 an Eikonal Approach, *J Geophys Res-Oceans*, 91, 8487-8495, 10.1029/Jc091ic07p08487, 1986.  
 1270 Holloway, P. E.: A comparison of semidiurnal internal tides from different bathymetric locations on  
 1271 the Australian North-West Shelf, *J Phys Oceanogr*, 15, 240-251, 10.1175/1520-  
 1272 0485(1985)015<0240:Acosit>2.0.Co;2, 1985.  
 1273 Holtappels, M., Tiano, L., Kalvelage, T., Lavik, G., Revsbech, N. P., and Kuypers, M. M. M.: Aquatic  
 1274 Respiration Rate Measurements at Low Oxygen Concentrations, *Plos One*, 9,  
 1275 10.1371/journal.pone.0089369, 2014.  
 1276 Hua, B. L., d'Orgeville, M., Fruman, M. D., Menesguen, C., Schopp, R., Klein, P., and Sasaki, H.:  
 1277 Destabilization of mixed Rossby gravity waves and the formation of equatorial zonal jets, *J Fluid*  
 1278 *Mech*, 610, 311-341, 10.1017/S0022112008002656, 2008.  
 1279 Ito, T., and Deutsch, C.: Variability of the oxygen minimum zone in the tropical North Pacific during  
 1280 the late twentieth century, *Global Biogeochem Cy*, 27, 1119-1128, 10.1002/2013gb004567, 2013.  
 1281 Jenkins, W. J.: Oxygen Utilization Rates in North-Atlantic Sub-Tropical Gyre and Primary Production  
 1282 in Oligotrophic Systems, *Nature*, 300, 246-248, 10.1038/300246a0, 1982.  
 1283 Jenkins, W. J.: Studying subtropical thermocline ventilation and circulation using tritium and He-3, *J*  
 1284 *Geophys Res-Oceans*, 103, 15817-15831, 10.1029/98jc00141, 1998.  
 1285 Jochum, M., Malanotte-Rizzoli, P., and Busalacchi, A.: Tropical instability waves in the Atlantic  
 1286 ocean, *Ocean Model*, 7, 145-163, 10.1016/S1463-5003(03)00042-8, 2004.  
 1287 Kamenkovich, I., Berloff, P., and Pedlosky, J.: Anisotropic material transport by eddies and eddy-  
 1288 driven currents in a model of the North Atlantic, *J Phys Oceanogr*, 39, 3162-3175,  
 1289 10.1175/2009jpo4239.1, 2009.  
 1290 Karstensen, J., Stramma, L., and Visbeck, M.: Oxygen minimum zones in the eastern tropical Atlantic  
 1291 and Pacific oceans, *Prog Oceanogr*, 77, 331-350, 10.1016/J.Pocean.2007.05.009, 2008.  
 1292 Keeling, R. F., and Garcia, H. E.: The change in oceanic O-2 inventory associated with recent global  
 1293 warming, *P Natl Acad Sci USA*, 99, 7848-7853, 10.1073/Pnas.122154899, 2002.  
 1294 Keeling, R. F., Körtzinger, A., and Gruber, N.: Ocean deoxygenation in a warming world, *Annu Rev*  
 1295 *Mar Sci*, 2, 199-229, 10.1146/Annurev.Marine.010908.163855, 2010.  
 1296 Kessler, W. S.: The circulation of the eastern tropical Pacific: A review, *Prog Oceanogr*, 69, 181-217,  
 1297 10.1016/J.Pocean.2006.03.009, 2006.  
 1298 Kirchner, K., Rhein, M., Hüttl-Kabus, S., and Böning, C. W.: On the spreading of South Atlantic  
 1299 Water into the Northern Hemisphere, *J Geophys Res-Oceans*, 114, 10.1029/2008JC005165, 2009.  
 1300 Lachkar, Z., and Gruber, N.: A comparative study of biological production in eastern boundary  
 1301 upwelling systems using an artificial neural network, *Biogeosciences*, 9, 293-308, 10.5194/Bg-9-293-  
 1302 2012, 2012.  
 1303 Ledwell, J. R., Watson, A. J., and Law, C. S.: Mixing of a tracer in the pycnocline, *J Geophys Res-*  
 1304 *Oceans*, 103, 21499-21529, 10.1029/98jc01738, 1998.  
 1305 Lu, Z. T., Schlosser, P., Smethie Jr, W. M., Sturchio, N. C., Fischer, T. P., Kennedy, B. M., Purtschert,  
 1306 R., Severinghaus, J. P., Solomon, D. K., Tanhua, T., and Yokochi, R.: Tracer applications of noble gas  
 1307 radionuclides in the geosciences, *Earth-Science Reviews*, 10.1016/j.earscirev.2013.09.002, 2014.  
 1308 Lutz, M., Dunbar, R., and Caldeira, K.: Regional variability in the vertical flux of particulate organic  
 1309 carbon in the ocean interior, *Global Biogeochem Cy*, 16, 10.1029/2000gb001383, 2002.  
 1310 Luyten, J., Pedlosky, J., and Stommel, H.: Climatic Inferences from the Ventilated Thermocline,  
 1311 *Climatic Change*, 5, 183-191, 10.1007/Bf00141269, 1983a.  
 1312 Luyten, J. R., Pedlosky, J., and Stommel, H.: The ventilated thermocline, *J Phys Oceanogr*, 13, 292-  
 1313 309, 10.1175/1520-0485(1983)013<0292:Tvt>2.0.Co;2, 1983b.  
 1314 Machin, F., and Pelegri, J. L.: Northward penetration of Antarctic Intermediate Water off Northwest  
 1315 Africa, *J Phys Oceanogr*, 39, 512-535, 10.1175/2008jpo3825.1, 2009.  
 1316 Malanotte-Rizzoli, P., Hedstrom, K., Arango, H., and Haidvogel, D. B.: Water mass pathways  
 1317 between the subtropical and tropical ocean in a climatological simulation of the North Atlantic ocean  
 1318 circulation, *Dynam Atmos Oceans*, 32, 331-371, 10.1016/S0377-0265(00)00051-8, 2000.  
 1319 Martin, J. H., Knauer, G. A., Karl, D. M., and Broenkow, W. W.: Vertex - carbon cycling in the  
 1320 Northeast Pacific, *Deep-Sea Research Part a-Oceanographic Research Papers*, 34, 267-285,  
 1321 10.1016/0198-0149(87)90086-0, 1987.

1322 Martz, T. R., Johnson, K. S., and Riser, S. C.: Ocean metabolism observed with oxygen sensors on  
 1323 profiling floats in the South Pacific, *Limnol Oceanogr*, 53, 2094-2111,  
 1324 10.4319/Lo.2008.53.5\_Part\_2.2094, 2008.  
 1325 Matear, R. J., and Hirst, A. C.: Long-term changes in dissolved oxygen concentrations in the ocean  
 1326 caused by protracted global warming, *Global Biogeochem Cy*, 17, 10.1029/2002gb001997, 2003.  
 1327 Maximenko, N. A., Bang, B., and Sasaki, H.: Observational evidence of alternating zonal jets in the  
 1328 world ocean, *Geophys Res Lett*, 32, 10.1029/2005gl022728, 2005.  
 1329 McCreary, J. P., Yu, Z. J., Hood, R. R., Vinayachandran, P. N., Furue, R., Ishida, A., and Richards, K.  
 1330 J.: Dynamics of the Indian-Ocean oxygen minimum zones, *Prog Oceanogr*, 112, 15-37,  
 1331 10.1016/J.Pocean.2013.03.002, 2013.  
 1332 Ménesguen, C., Hua, B. L., Fruman, M. D., and Schopp, R.: Dynamics of the combined extra-  
 1333 equatorial and equatorial deep jets in the Atlantic, *J Mar Res*, 67, 323-346,  
 1334 10.1357/002224009789954766, 2009.  
 1335 Mittelstaedt, E.: The upwelling area off Northwest Africa - a description of phenomena related to  
 1336 coastal upwelling, *Prog Oceanogr*, 12, 307-331, 10.1016/0079-6611(83)90012-5, 1983.  
 1337 Mittelstaedt, E.: The ocean boundary along the Northwest African Coast - circulation and  
 1338 oceanographic properties at the sea-surface, *Prog Oceanogr*, 26, 307-355, 10.1016/0079-  
 1339 6611(91)90011-A, 1991.  
 1340 Monteiro, P. M. S., Dewitte, B., Scranton, M. I., Paulmier, A., and van der Plas, A. K.: The role of  
 1341 open ocean boundary forcing on seasonal to decadal-scale variability and long-term change of natural  
 1342 shelf hypoxia, *Environ Res Lett*, 6, 10.1088/1748-9326/6/2/025002, 2011.  
 1343 Montes, I., Dewitte, B., Gutknecht, E., Paulmier, A., Dadou, I., Oschlies, A., and Garçon, V.: High-  
 1344 resolution modeling of the Eastern Tropical Pacific oxygen minimum zone: Sensitivity to the tropical  
 1345 oceanic circulation, *J Geophys Res-Oceans*, 119, 5515-5532, 10.1002/2014jc009858, 2014.  
 1346 Ollitrault, M., Lankhorst, M., Fratantoni, D., Richardson, P., and Zenk, W.: Zonal intermediate  
 1347 currents in the equatorial Atlantic Ocean, *Geophys Res Lett*, 33, 10.1029/2005gl025368, 2006.  
 1348 Oschlies, A., Schulz, K. G., Riebesell, U., and Schmittner, A.: Simulated 21st century's increase in  
 1349 oceanic suboxia by CO<sub>2</sub>-enhanced biotic carbon export, *Global Biogeochem Cy*, 22,  
 1350 10.1029/2007gb003147, 2008.  
 1351 Peña-Izquierdo, J., Pelegri, J. L., Pastor, M. V., Castellanos, P., Emelianov, M., Gasser, M., Salvador,  
 1352 J., and Vazquez-Dominguez, E.: The continental slope current system between Cape Verde and the  
 1353 Canary Islands, *Sci Mar*, 76, 65-78, 10.3989/Scimar.03607.18c, 2012.  
 1354 Plattner, G. K., Joos, F., and Stocker, T. F.: Revision of the global carbon budget due to changing air-  
 1355 sea oxygen fluxes, *Global Biogeochem Cy*, 16, 10.1029/2001gb001746, 2002.  
 1356 Polo, I., Lazar, A., Rodriguez-Fonseca, B., and Arnault, S.: Oceanic Kelvin waves and tropical  
 1357 Atlantic intraseasonal variability: 1. Kelvin wave characterization, *J Geophys Res-Oceans*, 113,  
 1358 10.1029/2007jc004495, 2008.  
 1359 Qiu, B., Chen, S. M., and Sasaki, H.: Generation of the North Equatorial Undercurrent jets by triad  
 1360 baroclinic Rossby wave interactions, *J Phys Oceanogr*, 43, 2682-2698, 10.1175/Jpo-D-13-099.1, 2013.  
 1361 Rabe, B., Schott, F. A., and Kohl, A.: Mean circulation and variability of the tropical Atlantic during  
 1362 1952-2001 in the GECCO assimilation fields, *J Phys Oceanogr*, 38, 177-192, 10.1175/2007jpo3541.1,  
 1363 2008.  
 1364 Riley, G. A.: Oxygen, phosphate, and nitrate in the Atlantic Ocean, *Bull. Bingham. oceanogr. Coll.*,  
 1365 12, 1-126, 1951.  
 1366 Roether, W., Jean-Baptiste, P., Fourre, E., and Sultenfuss, J.: The transient distributions of nuclear  
 1367 weapon-generated tritium and its decay product He-3 in the Mediterranean Sea, 1952-2011, and their  
 1368 oceanographic potential, *Ocean Sci*, 9, 837-854, 10.5194/Os-9-837-2013, 2013.  
 1369 Sandstrom, H., and Oakey, N. S.: Dissipation in internal tides and solitary waves, *J Phys Oceanogr*,  
 1370 25, 604-614, 10.1175/1520-0485(1995)025<0604:Diitas>2.0.Co;2, 1995.  
 1371 Schafstall, J., Dengler, M., Brandt, P., and Bange, H.: Tidal-induced mixing and diapycnal nutrient  
 1372 fluxes in the Mauritanian upwelling region, *J Geophys Res-Oceans*, 115, 10.1029/2009jc005940,  
 1373 2010.  
 1374 Schmidtko, S., Johnson, G. C., and Lyman, J. M.: MIMOC: A global monthly isopycnal upper-ocean  
 1375 climatology with mixed layers, *J Geophys Res-Oceans*, 118, 1658-1672, 10.1002/Jgrc.20122, 2013.

1376 Schmittner, A., Oschlies, A., Matthews, H. D., and Galbraith, E. D.: Future changes in climate, ocean  
1377 circulation, ecosystems, and biogeochemical cycling simulated for a business-as-usual CO<sub>2</sub> emission  
1378 scenario until year 4000 AD, *Global Biogeochem Cy*, 22, 10.1029/2007gb002953, 2008.

1379 Schneider, A., Tanhua, T., Körtzinger, A., and Wallace, D. W. R.: An evaluation of tracer fields and  
1380 anthropogenic carbon in the equatorial and the tropical North Atlantic, *Deep-Sea Res Pt I*, 67, 85-97,  
1381 10.1016/J.Dsr.2012.05.007, 2012.

1382 Schott, F. A., Stramma, L., and Fischer, J.: The warm water inflow into the western tropical Atlantic  
1383 boundary regime, spring 1994, *J Geophys Res-Oceans*, 100, 24745-24760, 10.1029/95jc02803, 1995.

1384 Schott, F. A., Fischer, J., and Stramma, L.: Transports and pathways of the upper-layer circulation in  
1385 the western tropical Atlantic, *J Phys Oceanogr*, 28, 1904-1928, 10.1175/1520-  
1386 0485(1998)028<1904:TAPOTU>2.0.CO;2, 1998.

1387 Schott, F. A., McCreary, J. P., and Johnson, G. C.: Shallow overturning circulations of the tropical-  
1388 subtropical oceans, in: *Earth Climate: The Ocean-Atmosphere Interaction*, edited by: Wang, C., Xie,  
1389 S.-P., and Carton, J. A., *Geophysical Monograph 147*, American Geophysical Union, Washington,  
1390 DC, 261-304, 2004.

1391 Schott, F. A., Dengler, M., Zantopp, R., Stramma, L., Fischer, J., and Brandt, P.: The shallow and  
1392 deep western boundary circulation of the South Atlantic at 5°-11°S, *J Phys Oceanogr*, 35, 2031-2053,  
1393 10.1175/JPO2813.1, 2005.

1394 St Laurent, L., and Schmitt, R. W.: The contribution of salt fingers to vertical mixing in the North  
1395 Atlantic Tracer Release Experiment, *J Phys Oceanogr*, 29, 1404-1424, 10.1175/1520-  
1396 0485(1999)029<1404:Tcosft>2.0.Co;2, 1999.

1397 Stanley, R. H. R., Doney, S. C., Jenkins, W. J., and Lott, D. E.: Apparent oxygen utilization rates  
1398 calculated from tritium and helium-3 profiles at the Bermuda Atlantic Time-series Study site,  
1399 *Biogeosciences*, 9, 1969-1983, 10.5194/Bg-9-1969-2012, 2012.

1400 Stendardo, I., and Gruber, N.: Oxygen trends over five decades in the North Atlantic, *J Geophys Res-*  
1401 *Oceans*, 117, 10.1029/2012jc007909, 2012.

1402 Stramma, L., and England, M. H.: On the water masses and mean circulation of the South Atlantic  
1403 Ocean, *J Geophys Res-Oceans*, 104, 20863-20883, 10.1029/1999JC900139, 1999.

1404 Stramma, L., Brandt, P., Schafstall, J., Schott, F., Fischer, J., and Körtzinger, A.: Oxygen minimum  
1405 zone in the North Atlantic south and east of the Cape Verde Islands, *J Geophys Res-Oceans*, 113,  
1406 10.1029/2007jc004369, 2008a.

1407 Stramma, L., Johnson, G. C., Sprintall, J., and Mohrholz, V.: Expanding oxygen-minimum zones in  
1408 the tropical oceans, *Science*, 320, 655-658, 10.1126/Science.1153847, 2008b.

1409 Stramma, L., Visbeck, M., Brandt, P., Tanhua, T., and Wallace, D.: Deoxygenation in the oxygen  
1410 minimum zone of the eastern tropical North Atlantic, *Geophys Res Lett*, 36, 10.1029/2009gl039593,  
1411 2009.

1412 Stramma, L., Johnson, G. C., Firing, E., and Schmidtko, S.: Eastern Pacific oxygen minimum zones:  
1413 Supply paths and multidecadal changes, *J Geophys Res-Oceans*, 115, 10.1029/2009jc005976, 2010a.

1414 Stramma, L., Schmidtko, S., Levin, L. A., and Johnson, G. C.: Ocean oxygen minima expansions and  
1415 their biological impacts, *Deep-Sea Res Pt I*, 57, 587-595, 10.1016/J.Dsr.2010.01.005, 2010b.

1416 Stramma, L., Oschlies, A., and Schmidtko, S.: Mismatch between observed and modeled trends in  
1417 dissolved upper-ocean oxygen over the last 50 yr, *Biogeosciences*, 9, 4045-4057, 10.5194/Bg-9-4045-  
1418 2012, 2012.

1419 Stramma, L., Bange, H. W., Czeschel, R., Lorenzo, A., and Frank, M.: On the role of mesoscale eddies  
1420 for the biological productivity and biogeochemistry in the eastern tropical Pacific Ocean off Peru,  
1421 *Biogeosciences*, 10, 7293-7306, 10.5194/Bg-10-7293-2013, 2013.

1422 Stramma, L., Weller, R. A., Czeschel, R., and Bigorre, S.: Eddies and an extreme water mass anomaly  
1423 observed in the eastern south Pacific at the Stratus mooring, *J. Geophys. Res. Oceans*, 119, 2169-9291,  
1424 10.1002/2013JC009470, 2014.

1425 Suga, T., and Talley, L. D.: Antarctic intermediate water circulation in the tropical and subtropical  
1426 South-Atlantic, *J Geophys Res-Oceans*, 100, 13441-13453, 10.1029/95jc00858, 1995.

1427 Sverdrup, H. U.: On the Explanation of the Oxygen Minima and Maxima in the Oceans, *Journal du*  
1428 *Conseil*, 13, 163-172, 10.1093/icesjms/13.2.163, 1938.

1429 Tatebe, H., Imada, Y., Mori, M., Kimoto, M., and Hasumi, H.: Control of Decadal and Bidecadal  
 1430 Climate Variability in the Tropical Pacific by the Off-Equatorial South Pacific Ocean, *J Climate*, 26,  
 1431 6524-6534, 10.1175/Jcli-D-12-00137.1, 2013.  
 1432 Thiele, G., and Sarmiento, J. L.: Tracer Dating and Ocean Ventilation, *J Geophys Res-Oceans*, 95,  
 1433 9377-9391, 10.1029/Jc095ic06p09377, 1990.  
 1434 Tsuchiya, M.: Thermostats and circulation in the upper layer of the Atlantic Ocean, *Prog Oceanogr*,  
 1435 16, 235-267, 1986.  
 1436 Tsuchiya, M., Talley, L. D., and McCartney, M. S.: An eastern Atlantic section from Iceland  
 1437 southward across the equator, *Deep-Sea Research Part a-Oceanographic Research Papers*, 39, 1885-  
 1438 1917, 10.1016/0198-0149(92)90004-D, 1992.  
 1439 von Schuckmann, K., Brandt, P., and Eden, C.: Generation of tropical instability waves in the Atlantic  
 1440 Ocean, *J Geophys Res-Oceans*, 113, 10.1029/2007jc004712, 2008.  
 1441 Wattenberg, H.: Die Verteilung des Sauerstoffs im Atlantischen Ozean, *Wissenschaftliche Ergebnisse*  
 1442 *der Deutschen Atlantischen Expedition auf dem Forschungs- und Vermessungsschiff Meteor 1925-*  
 1443 *1927*, 9.1, edited by: Defant, A., de Gruyter, Berlin, Leipzig, 132 pp., 1938.  
 1444 Waugh, D. W., Haine, T. W. N., and Hall, T. M.: Transport times and anthropogenic carbon in the  
 1445 subpolar North Atlantic Ocean, *Deep-Sea Res Pt I*, 51, 1475-1491, 10.1016/J.Dsr.2004.06.011, 2004.  
 1446 Weiss, R. F.: Solubility of Nitrogen, Oxygen and Argon in Water and Seawater, *Deep-Sea Res*, 17,  
 1447 721-735, 10.1016/0011-7471(70)90037-9, 1970.  
 1448 Wollast, R.: Evaluation and comparison of the global carbon cycle in the coastal zone and in the open  
 1449 ocean, in: *The Sea*, edited by: Robinson, A., Brink, K. H., Wiley, New York, 213-252, 1998.  
 1450 Wüst, G.: Die Stratosphäre des Atlantischen Ozeans, *Deutsche Atlantische Exped. Meteor 1925-1927*,  
 1451 *Wiss. Erg.*, 6(2), 288 pp., 1935.  
 1452 Wyrski, K.: The oxygen minima in relation to ocean circulation, *Deep-Sea Res*, 9, 11-23,  
 1453 10.1016/0011-7471(62)90243-7, 1962.  
 1454 Zhang, D. X., McPhaden, M. J., and Johns, W. E.: Observational evidence for flow between the  
 1455 subtropical and tropical Atlantic: The Atlantic subtropical cells, *J Phys Oceanogr*, 33, 1783-1797,  
 1456 10.1175/2408.1, 2003.  
 1457 Zilberman, N. V., Roemmich, D. H., and Gille, S. T.: The Mean and the Time Variability of the  
 1458 Shallow Meridional Overturning Circulation in the Tropical South Pacific Ocean, *J Climate*, 26, 4069-  
 1459 4087, 10.1175/Jcli-D-12-00120.1, 2013.

1460

1461 Table 1. Research cruises to the tropical eastern Atlantic and Pacific oceans. Depending on  
 1462 the measurements carried out and the geographical area covered on the different cruises up to  
 1463 22 sections were used to determine the mean 23° W section, 7 sections for the mean 18° N  
 1464 sections and 3 sections for the mean ~86° W section.

<u>Vessel and Cruise (Date)</u>	<u>Main Work</u>	<u>Region</u>
<b>Tropical Atlantic, 5° S-14° N / ~23° W and OMZ area</b>		
<u>Thalassa (Jul-Aug 1999)</u>	<u>23° W section</u>	<u>5° S-6° N</u>
<u>Seaward Johnson (Jan 2000)</u>	<u>23° W section</u>	<u>5° S-4° N</u>
<u>Meteor 47/1 (Apr 2000)</u>	<u>23° W section</u>	<u>5° S-4° N</u>
<u>Meteor 55 (Oct 2002)</u>	<u>24° W section</u>	<u>0-10° N</u>
<u>Polarstern Ant XXII/5 (Jun 2005)</u>	<u>23° W section</u>	<u>5° S-14° N</u>
<u>Meteor 68/1 (May 2006)</u>	<u>23° W section</u>	<u>2° S-0.5° N</u>
<u>Ron Brown (Jun 2006)</u>	<u>23° W section</u>	<u>5° S-14° N</u>
<u>Meteor 68/2 (Jun-Jul 2006)</u>	<u>23° W section, moorings</u>	<u>4° S-14° N</u>
<u>Ron Brown (May 2007)</u>	<u>23° W section</u>	<u>4° N-14° N</u>
<u>L'Atalante GEOMAR 4 (Feb-Mar 2008)</u>	<u>23° W section, moorings</u>	<u>2° S-14° N</u>
<u>Maria S. Merian 08/1 (Apr-May 2008)</u>	<u>23° W section, GUTRE tracer release</u>	<u>7.5° N-14° N, 23° W, 8° N at 330 m</u>
<u>Maria S. Merian 10/1 (Nov-Dec 2008)</u>	<u>GUTRE tracer survey</u>	<u>4° N-14° N / 27.5° W- 17.5° W</u>
<u>Polarstern Ant XXV/5 (May 2009)</u>	<u>23° W section</u>	<u>5° S-14° N</u>
<u>Endeavor 463 (May-Jun 2009)</u>	<u>23° W section</u>	<u>4° S-3° N</u>
<u>Ron Brown (Jul-Aug 2009)</u>	<u>23° W section</u>	<u>0-14° N</u>
<u>Meteor 80/1 (Oct-Nov 2009)</u>	<u>23° W section, moorings</u>	<u>5° S-14° N</u>
<u>Polarstern Ant XXVI/1 (Nov 2009)</u>	<u>23° W section</u>	<u>5° S-14° N</u>
<u>Meteor 80/2 (Dec 2009)</u>	<u>GUTRE tracer survey</u>	<u>4° N-14° N / 31° W-15° W</u>
<u>Meteor 81/1 (Feb-Mar 2010)</u>	<u>22° W section</u>	<u>5° S-13° N</u>
<u>Polarstern Ant XXVI/4 (May 2010)</u>	<u>23° W section</u>	<u>5° S-13.5° N</u>
<u>Meteor 83/1 (Oct-Nov 2010)</u>	<u>GUTRE tracer survey</u>	<u>2° N-15° N / 28° W-15° W</u>
<u>Maria S. Merian 18/2 (May-Jun 2011)</u>	<u>23° W section, moorings</u>	<u>5° S-14° N</u>
<u>Maria S. Merian 18/3 (Jun-Jul 2011)</u>	<u>23° W section</u>	<u>4° N-14° N</u>
<u>Ron Brown (Jul-Aug 2011)</u>	<u>23° W section</u>	<u>0-14° N</u>
<u>Maria S. Merian 22 (Oct-Nov 2012)</u>	<u>23° W section, moorings</u>	<u>5° S-14° N</u>
<u>Maria S. Merian 23 (Dec 2012)</u>	<u>23° W section, OSTRE tracer release</u>	<u>4° S-5° N, 21° W, 11° N at 500 m</u>

Meteor 97 (May-Jun 2013)	OSTRE tracer survey	8° N-12° N / 23° W-19° W
Meteor 106 (Apr-May 2014)	23° W section, moorings	5° S-14° N
<b>Tropical Atlantic, 26° W-16° W / 18° N</b>		
P320/1 (Mar-Apr 2005)	18° N section	19°W-16.4°W
Meteor M68/3 (Jul-Aug 2006)	18° N section	26° W-16.3° W
P347 (Jan-Feb 2007)	18° N section	17.5° W-16.3° W
P348 (Mar 2007)	18° N section	23.2° W-16.4° W
L'Atalante GEOMAR 3 (Feb 2008)	18° N section	24.3° W-16.3° W
P399/2 (Jun 2010)	18° N section	21° W-16.5° W
Maria S. Merian 22 (Nov 2012)	18° N section	26° W-20° W
<b>Tropical Pacific, 22° S-2° N / ~86° W and continental slope</b>		
Knorr (Mar-Apr 1993)	~86°W section	22° S-2° N
Meteor 77/3 (Jan 2009)	Continental slope	18° S-10° S
Meteor 77/4 (Feb 2009)	~86° W section	14° S-2° N
Meteor 90 (Nov 2012)	~86° W section	22° S-2° N
Meteor 91 (Dec 2012)	Continental slope	17° S-5° S
Meteor 92 (Jan 2013)	Continental slope	13° S-10° S
Meteor 93 (Feb 2013)	Continental slope	14° S-10° S

1466  
1467  
1468

- Peter Brandt 14.11.2014 17:17  
**Gelöscht:** Main Work ... [4]
- Peter Brandt 4.11.2014 11:19  
**Formatierte Tabelle**
- Peter Brandt 4.11.2014 11:32  
**Formatierte Tabelle**
- Peter Brandt 4.11.2014 11:38  
**Formatierte Tabelle**
- Peter Brandt 4.11.2014 11:46  
**Formatierte Tabelle**
- Peter Brandt 4.11.2014 11:44  
**Formatierte Tabelle**

1471 | Table 2. Moored oxygen observations in the eastern tropical Atlantic along 23°W.

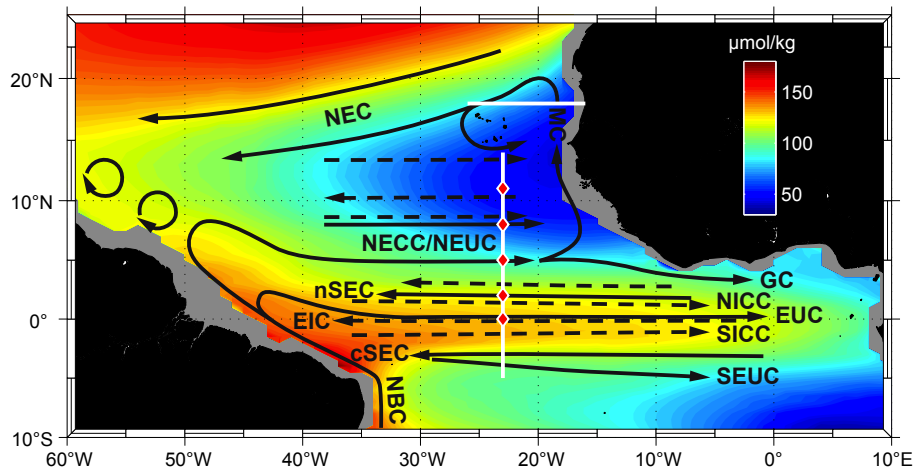
<u>Position</u>	<u>Period</u>	<u>Mooring type</u>	<u>Depth [m]</u>
<u>0° / 23° W</u>	<u>May 2011 - Oct 2012</u>	<u>Subsurface</u>	<u>300, 500</u>
<u>2° / 23° W</u>	<u>Feb 2008 - May 2011</u>	<u>Subsurface</u>	<u>300, 500</u>
<u>4° / 23° W</u>	<u>Jul 2009 - Jan 2013</u>	<u>PIRATA</u>	<u>300, 500</u>
<u>5° N / 23° W</u>	<u>Nov 2009 - Oct 2012</u>	<u>Subsurface</u>	<u>100 – 800</u>
<u>8° N / 23° W</u>	<u>Nov 2009 - Oct 2012</u>	<u>Subsurface</u>	<u>100 – 800</u>
<u>11.5° / 23° W</u>	<u>Jul 2009 - Jan 2013</u>	<u>PIRATA</u>	<u>300, 500</u>

1472 |  
1473 |

Peter Brandt 14.11.2014 17:18

**Gelöscht:** SFB 754 subsurface moorings in the eastern tropical Atlantic. -  
**Period** ... [5]

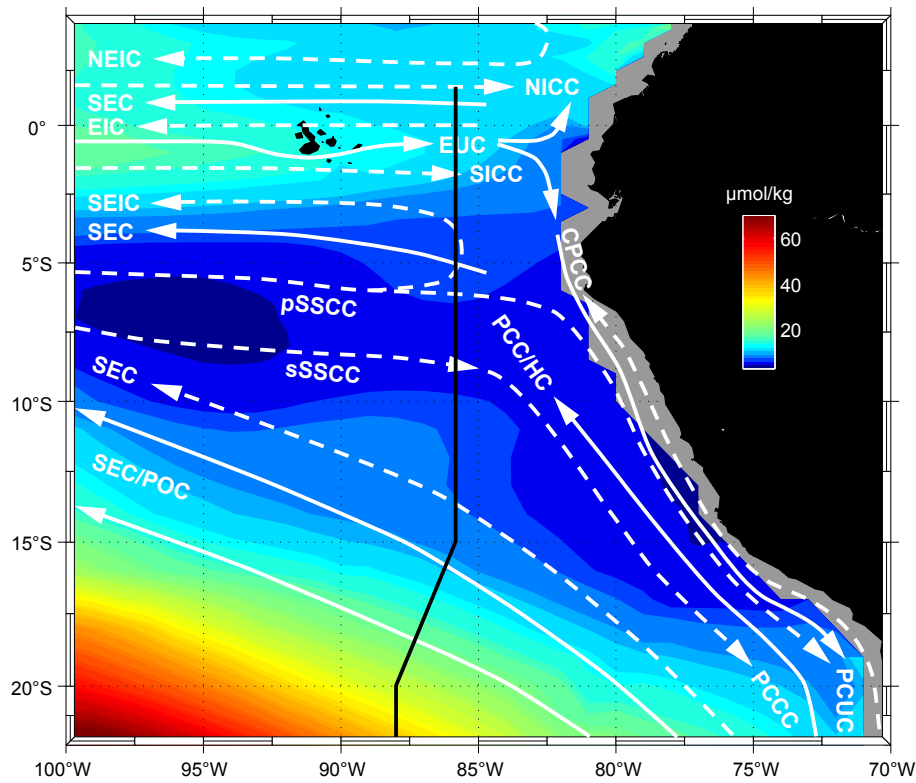




1477

1478 **Figure 1.** Oxygen concentration [ $\mu\text{mol/kg}$ ] in the tropical Atlantic at  $\sigma_\theta=27.1 \text{ kg m}^{-3}$  (close to  
 1479 the deep oxygen minimum) as obtained from the MIMOC climatology (Schmidtko et al.,  
 1480 2013) with circulation schematic superimposed. Surface and thermocline current branches  
 1481 shown (black solid arrows) are the North Equatorial Current (NEC), the Mauritania Current  
 1482 (MC), the northern and central branch of the South Equatorial Current (nSEC and cSEC), the  
 1483 North Equatorial Countercurrent (NECC), the Guinea Current (GC), the North Brazil Current  
 1484 (NBC), the North and South Equatorial Undercurrent (NEUC and SEUC), and the Equatorial  
 1485 Undercurrent (EUC). Intermediate current branches shown (black dashed arrows) are North  
 1486 and South Intermediate Countercurrents (NICC and SICC) or “flanking jets”, and the  
 1487 Equatorial Intermediate Current (EIC). The 23° W and 18° N repeat sections are marked by  
 1488 white lines, mooring positions by red diamonds.

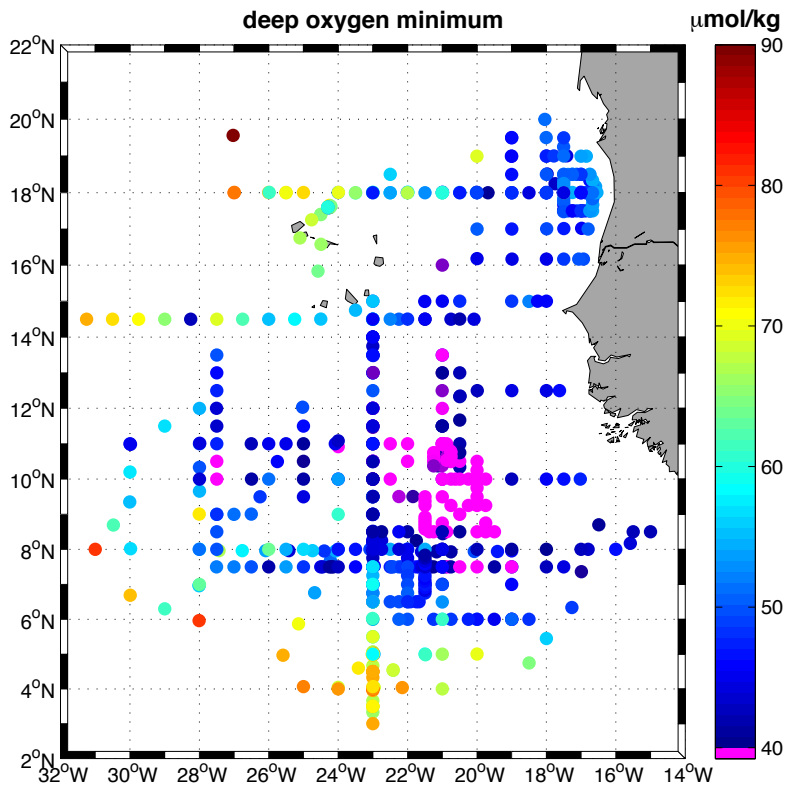
1489



1490

1491 **Figure 2.** Oxygen concentration [ $\mu\text{mol kg}^{-1}$ ] in the eastern tropical Pacific at  $\sigma_{\theta}=26.8 \text{ kg m}^{-3}$   
 1492 (close to the deep oxygen minimum) as obtained from the MIMOC climatology (Schmidtko et  
 1493 al., 2013) with circulation schematic superimposed. Current bands displayed are for the  
 1494 surface layer (white solid arrows) the South Equatorial Current (SEC), the Equatorial  
 1495 Undercurrent (EUC), the Peru-Chile or Humboldt Current (PCC/HC), the Peru Oceanic  
 1496 Current (POC) and for the thermocline layer (white dashed arrows) the North Equatorial  
 1497 Intermediate Current (NEIC), the North Intermediate Countercurrent (NICC), the Equatorial  
 1498 Intermediate Current (EIC), the South Intermediate Countercurrent (SICC), the primary and  
 1499 secondary Southern Subsurface Countercurrent (pSSCC, sSSCC), the deeper layer of the  
 1500 SEC, the Chile-Peru Coastal Current (CPCC), the Peru-Chile Undercurrent (PCUC) and the  
 1501 Peru-Chile Countercurrent (PCCC). The location of the  $\sim 86^{\circ}$  W section is marked as black  
 1502 line.

1503



1504

1505 **Figure 3.** Minimum oxygen concentration below 200 m (representing the deep oxygen  
 1506 minimum) as obtained from CTD station data taken during the period 2006 to 2013. Oxygen  
 1507 concentration at the deep oxygen minimum below 40  $\mu\text{mol kg}^{-1}$  is marked by purple dots.

Peter Brandt 27.10.2014 19:15

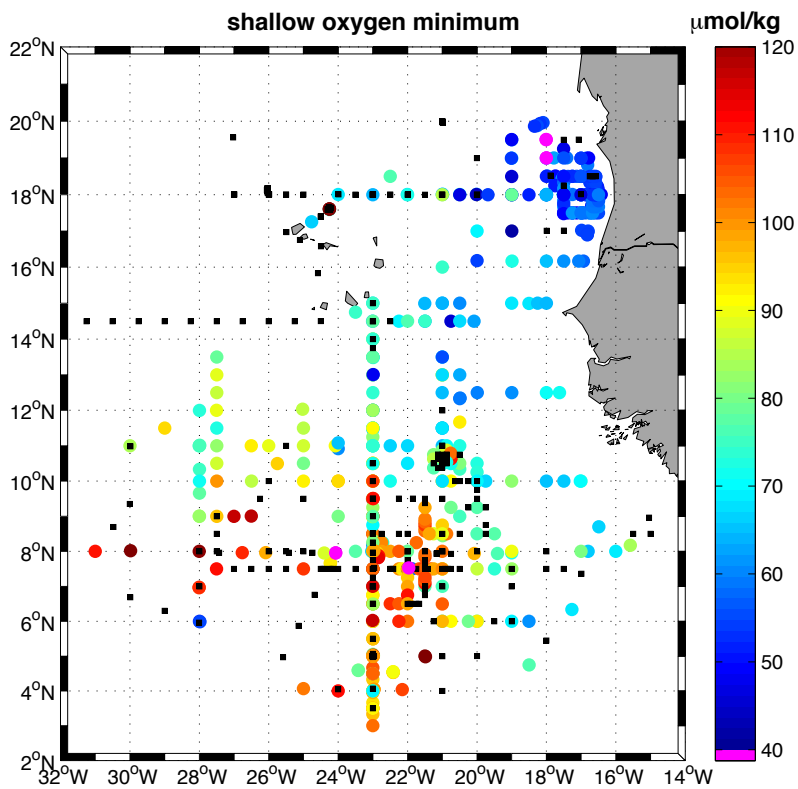
Gelöscht: 0

Peter Brandt 27.10.2014 19:15

Gelöscht: at the deep oxygen minimum (

Peter Brandt 27.10.2014 19:15

Gelöscht: )

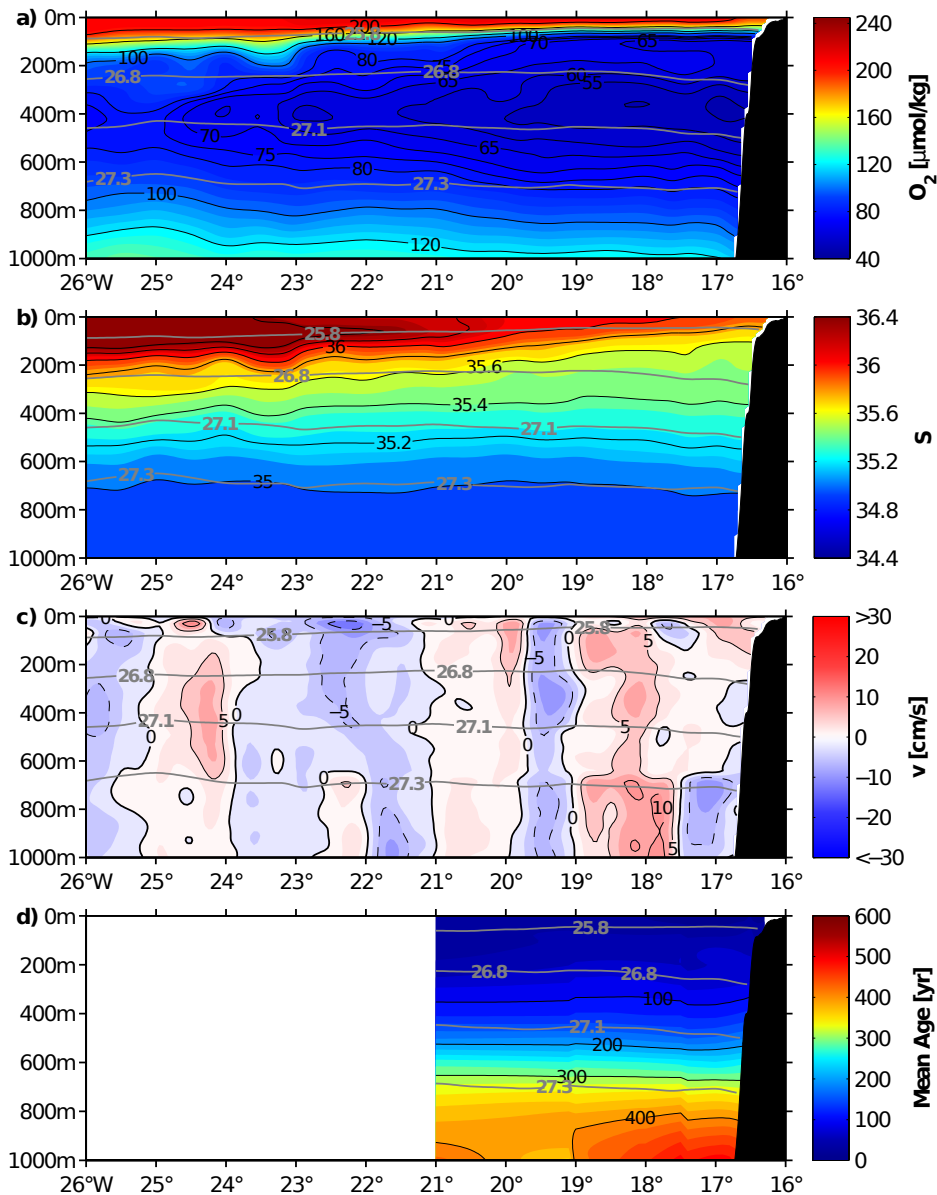


1511

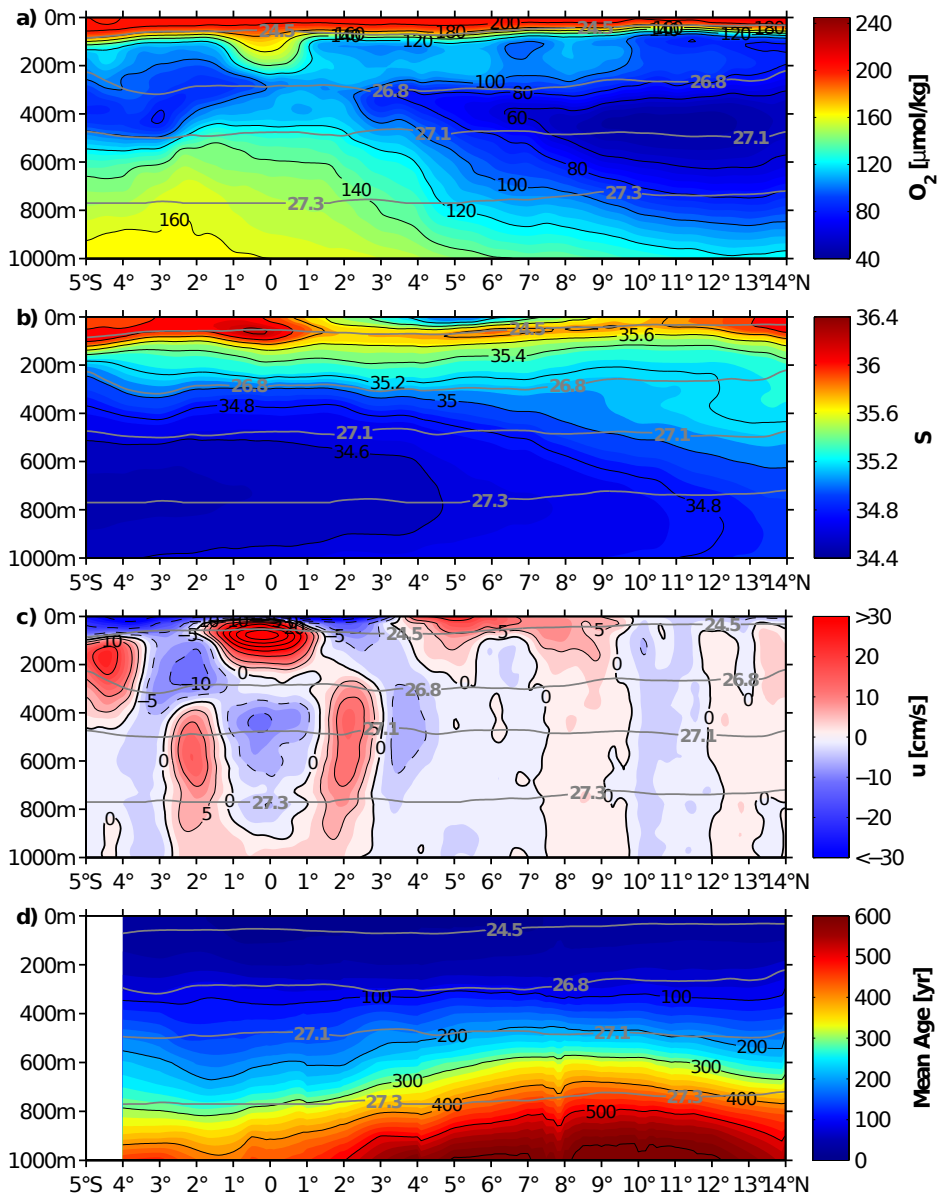
1512 **Figure 4.** Minimum oxygen concentration above 200 m (representing the shallow oxygen  
 1513 minimum) as obtained from CTD station data taken during the period 2006 to 2013. Black  
 1514 squares indicate profiles without a shallow oxygen minimum (i.e. minimum oxygen  
 1515 concentration was found at the lower boundary of the chosen depth range that is 200 m).  
 1516 Oxygen concentration at the shallow oxygen minimum below  $40 \mu\text{mol kg}^{-1}$  is marked by  
 1517 purple dots.

1518

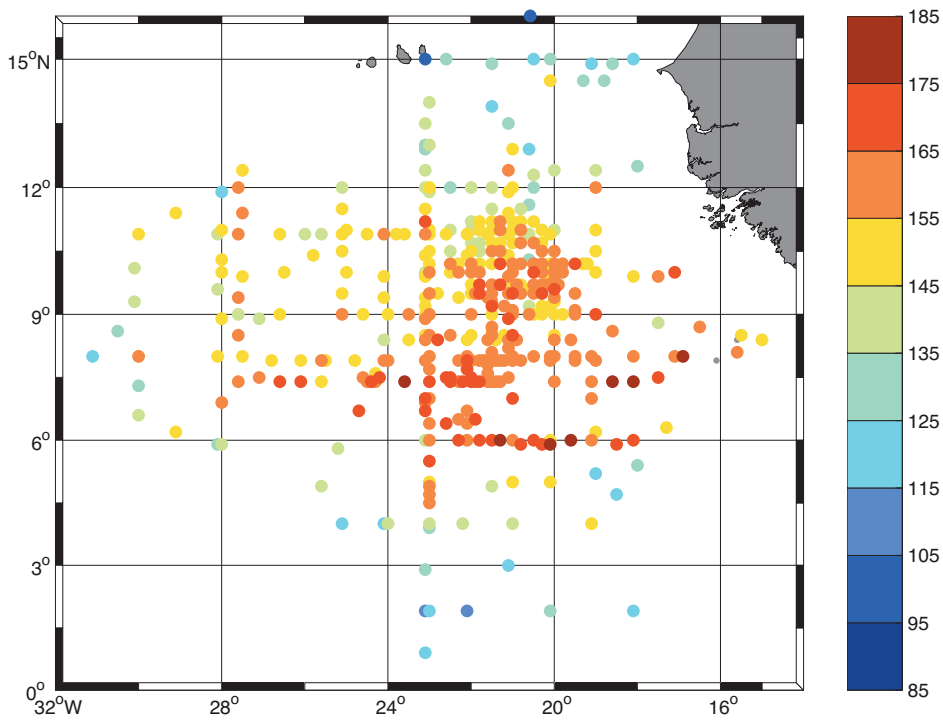
- Peter Brandt 27.10.2014 19:17  
**Gelöscht:** 0
- Peter Brandt 27.10.2014 19:18  
**Gelöscht:** at
- Peter Brandt 27.10.2014 19:18  
**Gelöscht:** (above 200 m)
- Peter Brandt 14.11.2014 17:20  
**Gelöscht:** of the upper 200 m was at about 200 m



1523  
 1524 **Figure 5.** (a) Mean oxygen content, (b) salinity, (c) meridional velocity (positive northward),  
 1525 and (d) mean age as obtained from zonal ship sections taken along 18° N during 2005-2012.  
 1526 Grey contours mark potential density [ $\text{kg m}^{-3}$ ]. Besides the deep oxygen minimum at about  
 1527 400 m depth there is a shallow oxygen minimum at about 100 m in proximity to the shelf (a).  
 1528



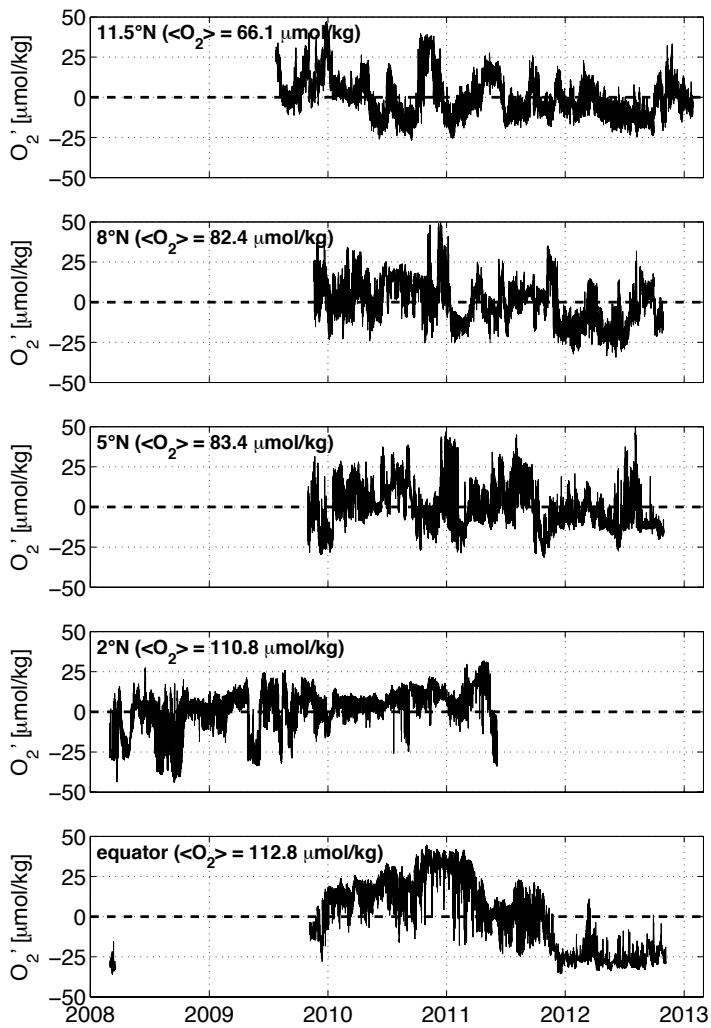
1529  
 1530 **Figure 6.** (a) Mean oxygen content, (b) salinity, (c) zonal velocity (positive eastward), and  
 1531 (d) mean age as obtained from meridional ship sections taken along 23° W during 1999-2012.  
 1532 Grey contours mark potential density [ $\text{kg m}^{-3}$ ]. Eastward current bands, marked by reddish  
 1533 colours, are generally associated with elevated oxygen content.  
 1534



1535

1536 **Figure 7.** Mean age [yr] at  $\sigma_{\theta}=27.0 \text{ kg m}^{-3}$  which corresponds approximately to the depth of  
 1537 the deep oxygen minimum.

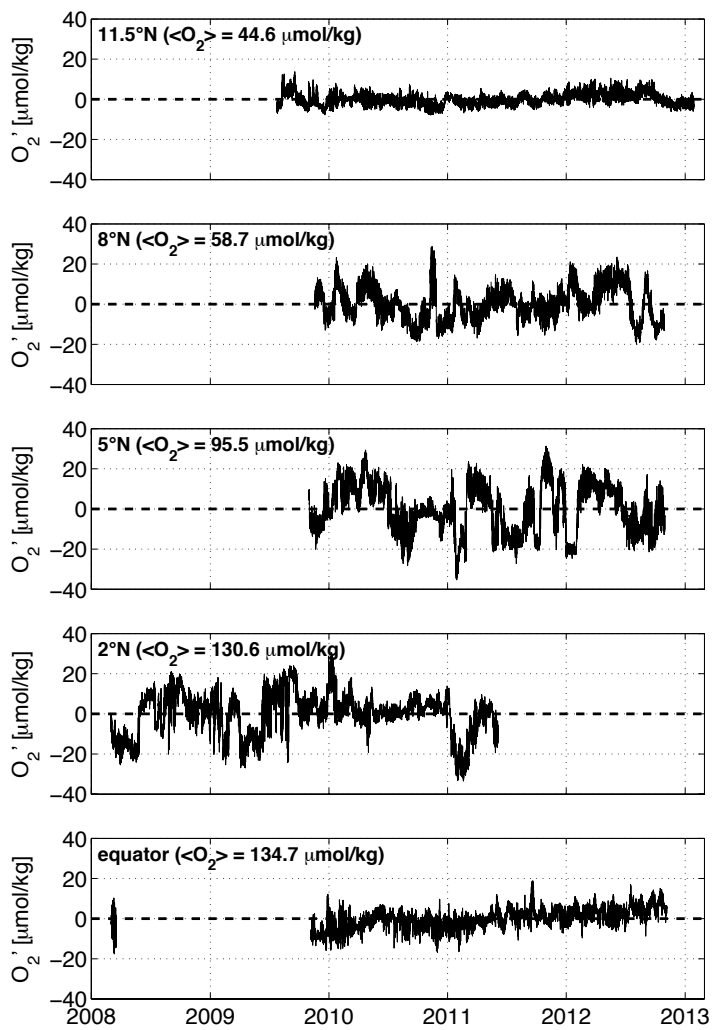
1538



1539

1540 **Figure 8.** Time series of oxygen anomaly at about 300 m depth from moored observations  
 1541 along 23° W at different latitudes. Mean oxygen values at the different mooring locations are  
 1542 given in brackets.

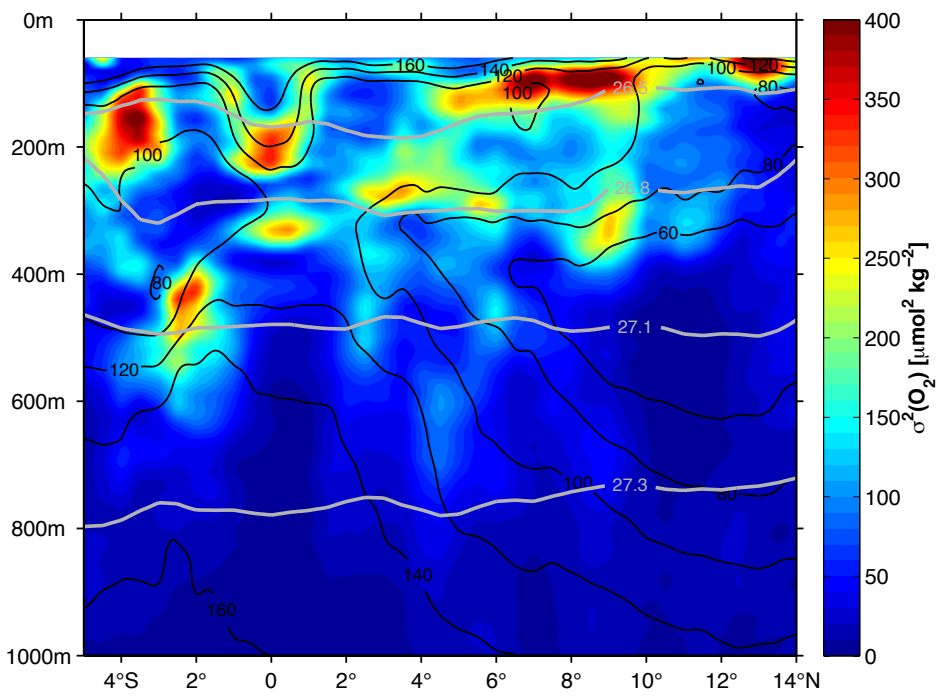




1543

1544 **Figure 9.** As Fig. 8, but at about 500 m depth.

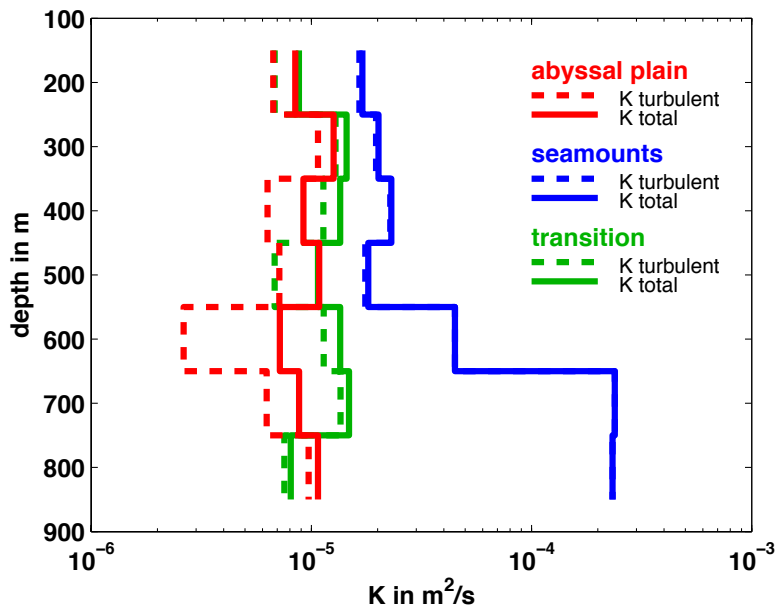
1545



1546

1547 **Figure 10.** Oxygen variance along 23° W from repeat ship sections. The analysis was done on  
 1548 isopycnal surfaces and the results were projected back onto depth coordinates. Grey contours  
 1549 mark potential density [ $\text{kg m}^{-3}$ ], black contours mark mean oxygen [ $\mu\text{mol kg}^{-1}$ ].

1550



1551

1552 **Figure 11.** Profiles of the diapycnal eddy diffusivity as estimated from microstructure  
 1553 measurements (dashed lines) and by accounting for the effect of double diffusion (solid lines)  
 1554 for different regions: (red) abyssal plain, (blue) seamount region, and (green) transition  
 1555 region.

1556

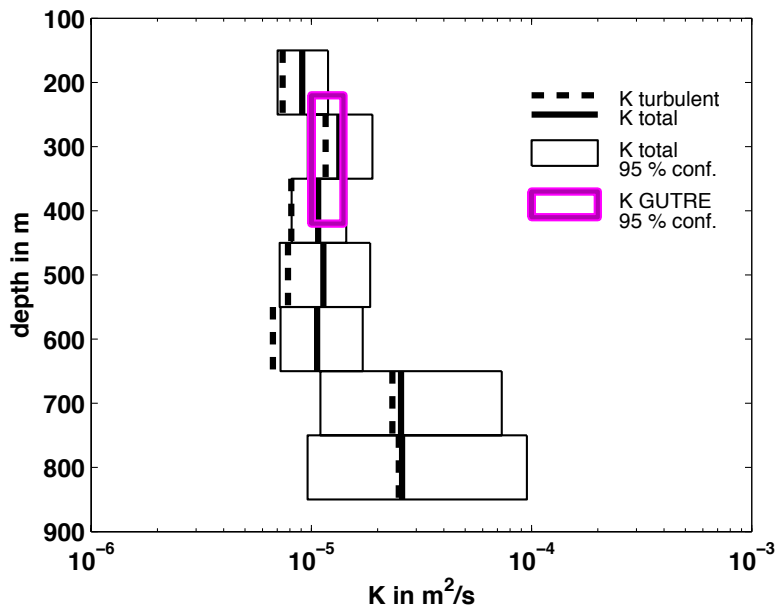
Unknown

Formatiert: Schriftart:Fett

Peter Brandt 2.11.2014 18:33

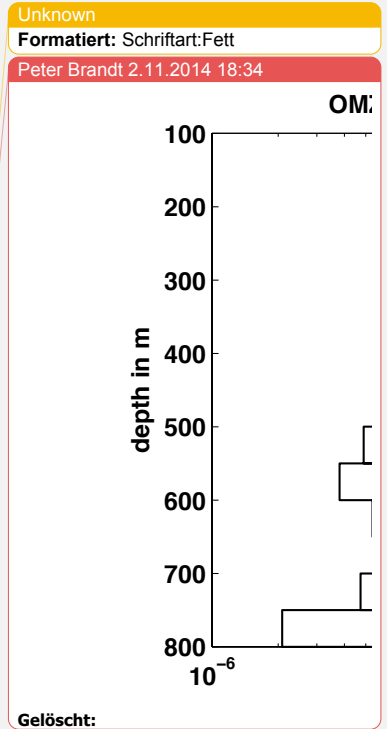
regio

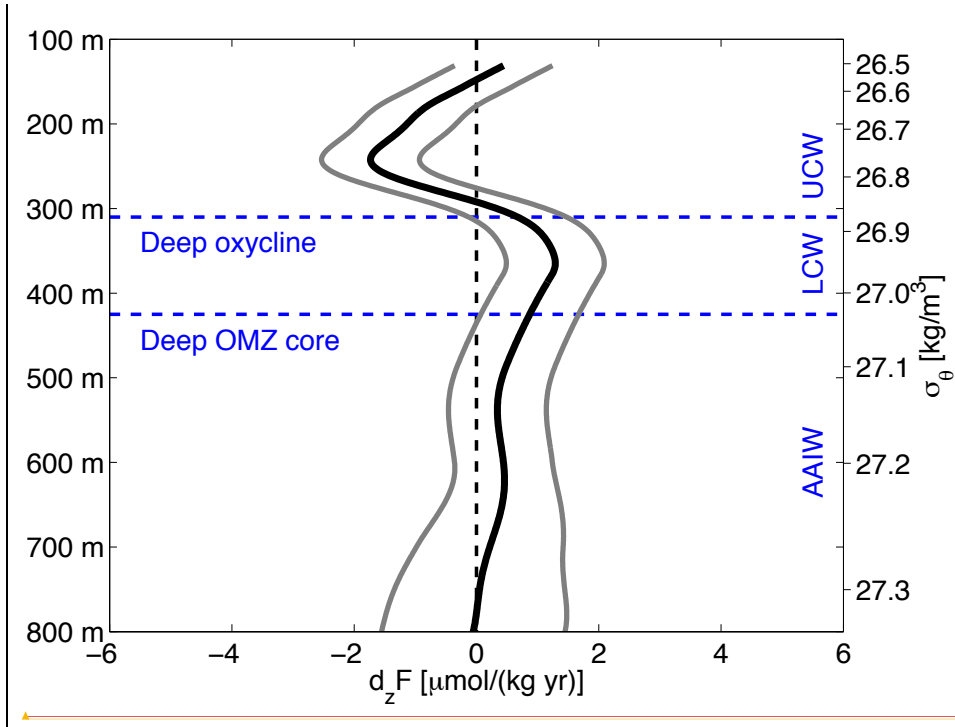
Gelöscht:



1558

1559 **Figure 12.** Diapycnal eddy diffusivity as estimated from microstructure measurements  
 1560 (dashed black line) and the tracer release experiment (purple box representing 95 %  
 1561 confidence error level). The profile of total diapycnal eddy diffusivity is obtained by  
 1562 accounting for the effect of double diffusion (solid black line with 95 % confidence  
 1563 error level).  
 1564





1566

1567 **Figure 13.** Mean oxygen supply due to diapycnal mixing (solid black line) for the open ocean  
 1568 ETNA OMZ and 95 % confidence error level (solid grey lines) as function of depth (left axis)  
 1569 or potential density (right axis). Blue dashed lines mark the depths of the deep oxycline and of  
 1570 the core of the deep OMZ that separate layers of upper and lower CW, and AAIW.

1571

1572

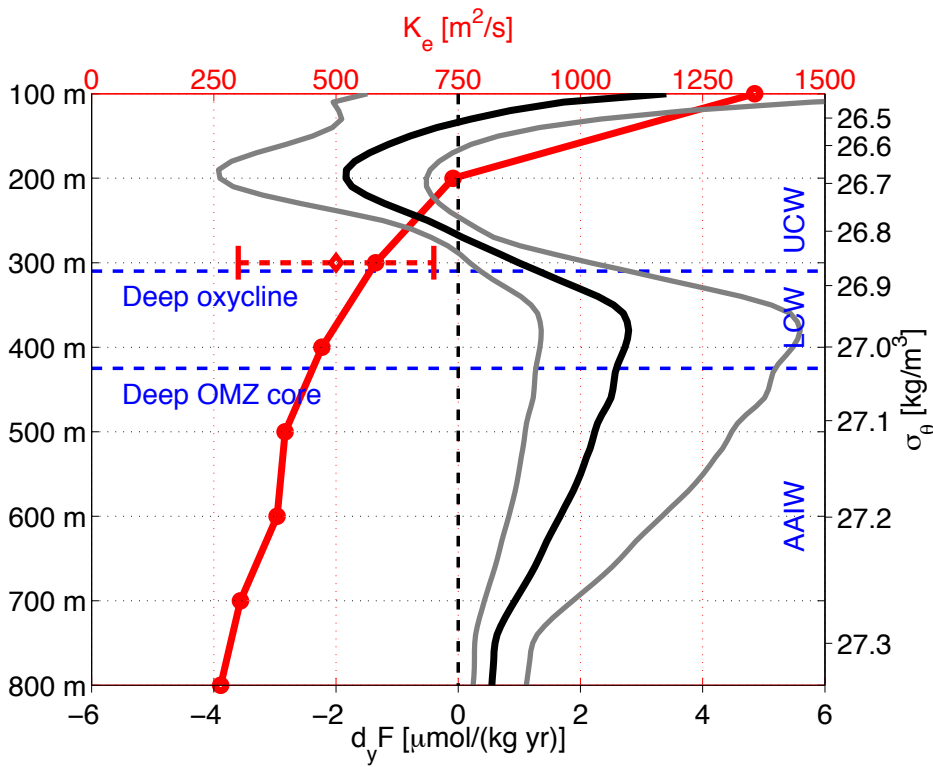
1573

Unknown

Formatiert: Schriftart:Fett

Peter Brandt 2.11.2014 18:34

Gelöscht:

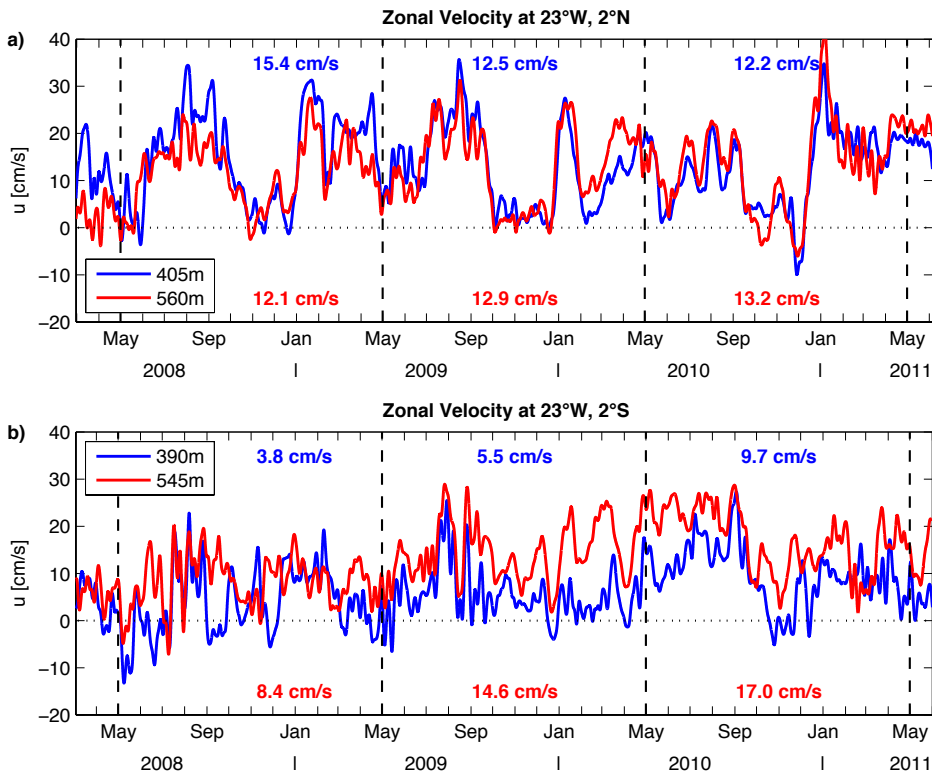


1575

1576 **Figure 14.** Eddy diffusivity as estimated from moored and shipboard observations (red  
 1577 circles, red line, upper axis) and from the tracer release experiment (red diamond with error  
 1578 bar, upper axis) as function of depth (left axis) or potential density (right axis). Also shown is  
 1579 the mean isopycnal meridional eddy-driven oxygen supply (black line, lower axis) for the  
 1580 open ocean ETNA OMZ with error levels (grey lines, lower axis) that were calculated from  
 1581 both the error of the curvature of the meridional oxygen distribution (95% confidence) and the  
 1582 error of the eddy diffusivity (factor 2 assumed). Blue dashed lines mark the depths of the deep  
 1583 oxycline and of the core of the deep OMZ that separate layers of upper and lower CW, and  
 1584 AAIW.

1585

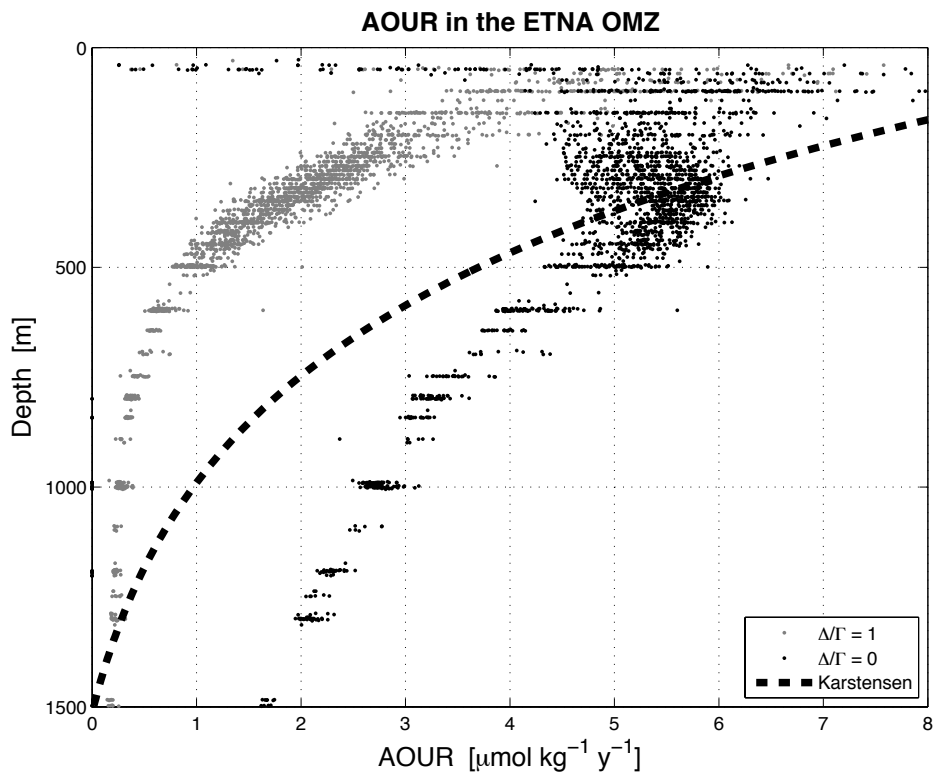
Peter Brandt 2.11.2014 19:48  
**Gelöscht:** 95 % confidence  
 Peter Brandt 2.11.2014 19:48  
**Gelöscht:** ; see further details in text and in Hahn et al. (2014)



1589

1590 **Figure 15.** Zonal velocity from moored observations at 23° W, 2° N (a) and 23° W, 2° S (b)  
 1591 at about 400 m (blue lines) and 550 m (red lines). Blue and red numbers represent annual  
 1592 mean velocities at about 400 m and 550 m depth, respectively. Dashed vertical lines mark  
 1593 time periods used for the calculation of annual means; dotted horizontal line marks zero  
 1594 velocity.

1595



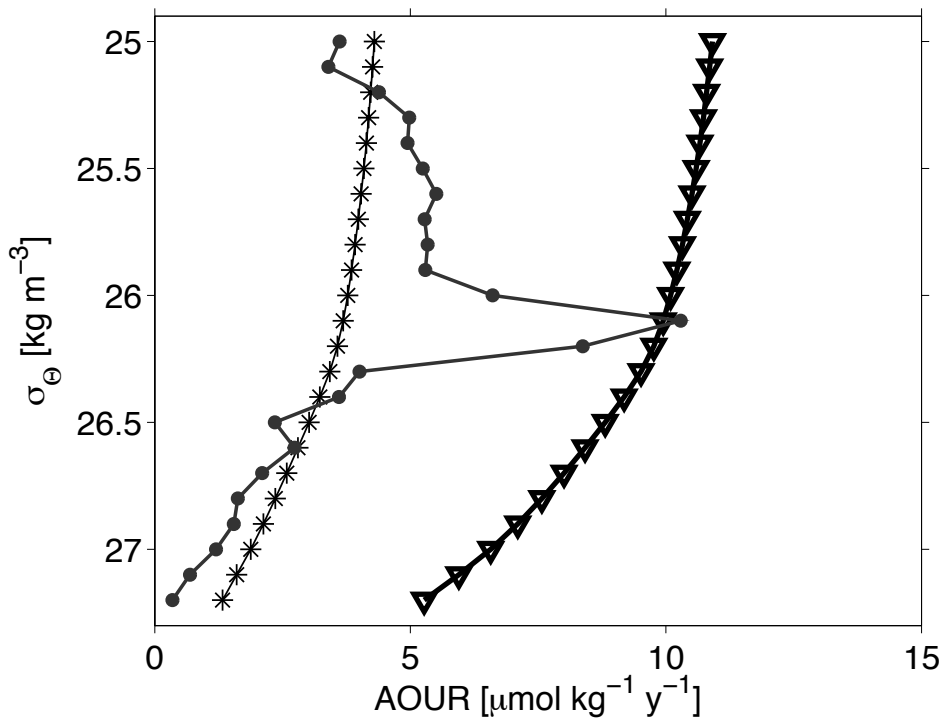
1596

1597 **Figure 16.** AOUR in the ETNA OMZ (between 4° N and 14° N and east of 32° W). The  
 1598 AOUR was calculated using the TTD approach with two different assumptions about mixing:  
 1599 Black dots corresponds to no mixing,  $\Delta\Gamma=0$ ; grey dots to moderate mixing,  $\Delta\Gamma=1$ . The  
 1600 dashed line marks AOUR as obtained by Karstensen et al. (2008) using CFC-11 ages from the  
 1601 ventilated gyre.

1602

1603





1604

1605 **Figure 17.** Three estimates of AOUR as function of density: Schneider et al. (2012) used the  
 1606 TTD approach for the ETNA (stars), Karstensen et al. (2008) used CFC-11 water ages from  
 1607 the ventilated gyre only (triangles), and based on the ratio of North Atlantic mean AOU for  
 1608 isopycnal volumes and the corresponding reservoir ages (black dots, see further details, e.g.  
 1609 reservoir ages and volumes, in Karstensen et al. (2008) Figs. 9 and 10).

1610

1611

Peter Brandt 27.10.2014 18:53

Gelöscht: as obtained by

Peter Brandt 27.10.2014 18:53

Gelöscht: ing

Peter Brandt 27.10.2014 18:54

Gelöscht: and by

Peter Brandt 27.10.2014 18:54

Gelöscht: ing

Peter Brandt 27.10.2014 18:57

Gelöscht: using

Peter Brandt 27.10.2014 18:58

Gelöscht: (0-60° N) basin scale

Peter Brandt 27.10.2014 19:01

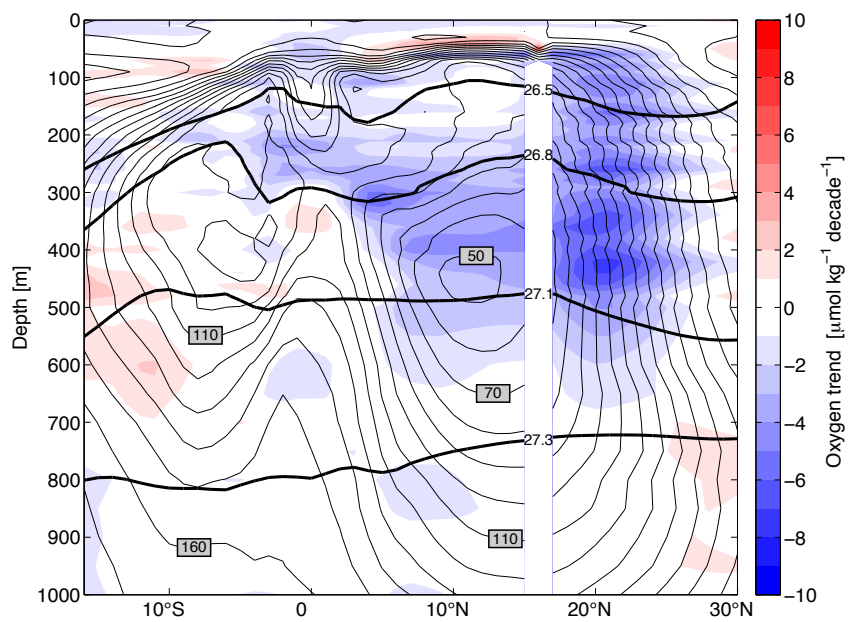
Gelöscht: discrete density increments of 0.1 kg m<sup>-3</sup> and

Peter Brandt 27.10.2014 19:03

Gelöscht: respective

Peter Brandt 27.10.2014 19:03

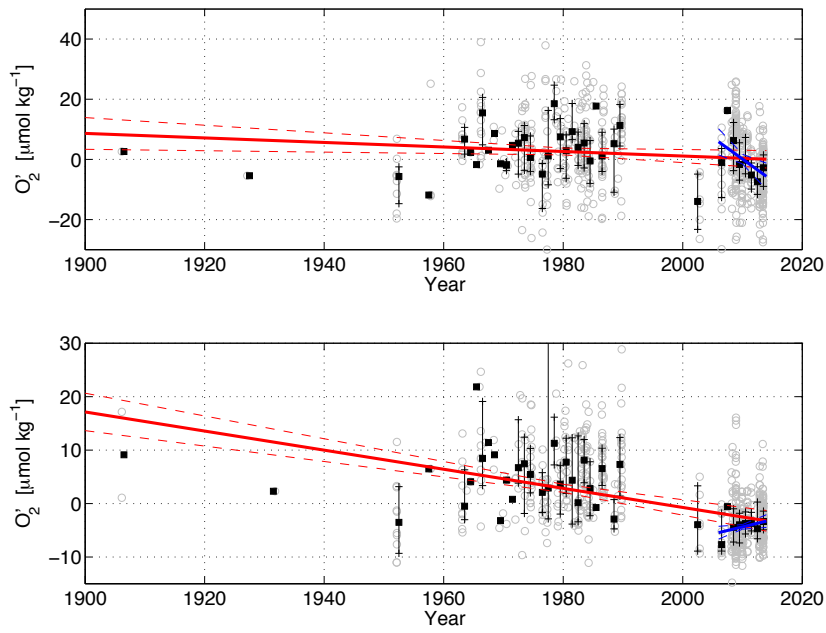
Gelöscht:



1622

1623 **Figure 18.** Oxygen trend along 23° W between 20° W and 26° W and between 1972 and  
 1624 2013 as obtained from the MIMOC climatology (Schmidtko et al., 2013). The trend was  
 1625 calculated on depth coordinates using oxygen anomalies relative to mean oxygen. Thin black  
 1626 contours mark mean oxygen [ $\mu\text{mol kg}^{-1}$ ], thick black contours mark potential density [ $\text{kg m}^{-3}$ ],  
 1627 both from the MIMOC climatology.

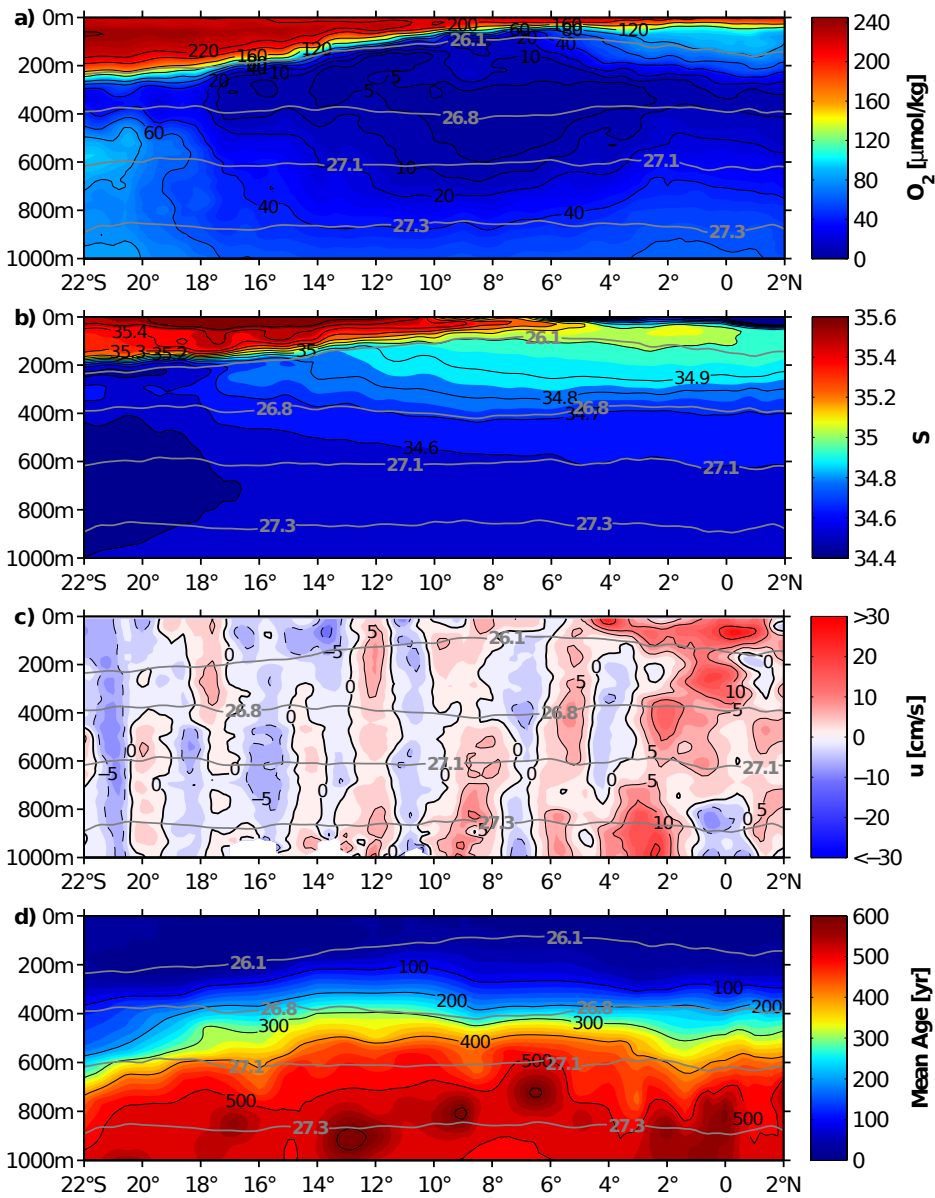
1628



1629

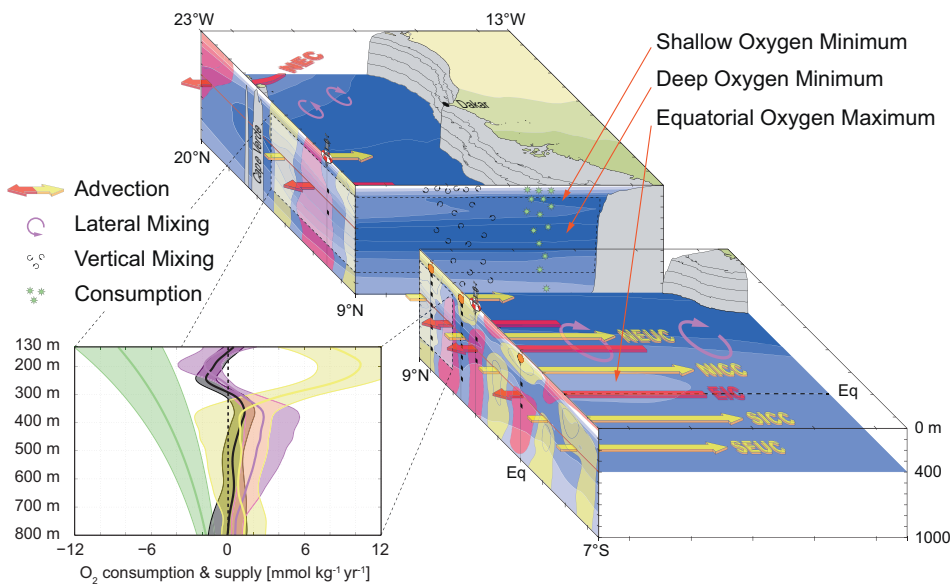
1630 **Figure 19.** Oxygen anomalies for the region 9-15° N, 20-26° W and 150-300 m (intermediate  
 1631 oxygen maximum, upper panel) and 350-700 m (deep oxygen minimum, lower panel). Grey  
 1632 circles represent all available data, whiskers show interquartile range of data within each year  
 1633 and the black squares annual medians. Trends are calculated using annual medians weighted  
 1634 by the square root of available data within each year for the period 1900-2013 (solid red line)  
 1635 and 2006-2013 (solid blue line). The dashed lines mark the standard errors of the trends.

1636



1637  
 1638 **Figure 20.** (a) Mean oxygen content, (b) salinity, (c) zonal velocity (positive eastward), and  
 1639 (d) mean age as obtained from meridional ship sections taken on three Pacific surveys along  
 1640  $\sim 86^\circ$  W during 1993-2012. Grey contours mark potential density [ $\text{kg m}^{-3}$ ]. The mean age is  
 1641 solely based on data from 1993. Eastward current bands, marked by reddish colours, are  
 1642 generally associated with elevated oxygen content.

1643



1644

1645 **Figure 21.** Schematic of the functioning of the ETNA OMZ and its oxygen budget. In the  
 1646 upper box, the oxygen distribution (bluish colours with dark/light blue corresponding to  
 1647 low/high oxygen) is shown at the sections along 23° W and 9° N and at the depth of 400 m; in  
 1648 the lower right box it is shown at the section along 23° W and at the depth of 400 m. Red and  
 1649 yellow areas at the 23° W section correspond to westward and eastward flow also marked by  
 1650 red and yellow arrows, respectively. The oxygen budget (lower left panel) includes physical  
 1651 supply by meridional (violet curve) and vertical mixing (black curve) as well as consumption  
 1652 after Karstensen et al. (2008) (green curve). The yellow curve in the lower left panel is the  
 1653 residual of the other 3 terms, which is dominated by zonal advection. All error estimates  
 1654 (coloured shadings) are referred to a 95 % confidence [except the isopycnal meridional eddy  
 1655 supply, where the error was estimated from both the error of the oxygen curvature (95 %  
 1656 confidence) and the error of the eddy diffusivity (factor 2 assumed)] (see further details in text  
 1657 and in Hahn et al. (2014)).

1658

